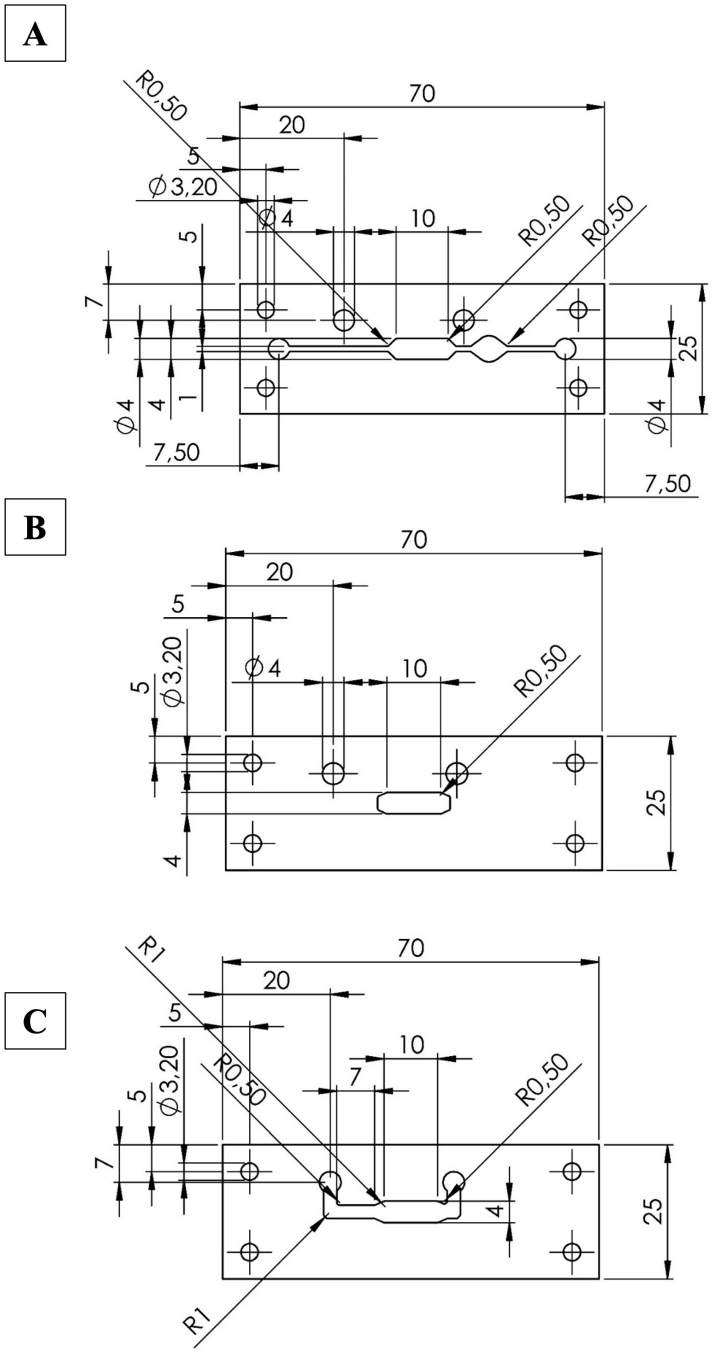

Figure 64. A) Upper vinyl layout dimensioned, B) Intermediate viniyl layout dimensioned, C) Lower vinyl layout dimensioned. Units are expressed in mm.

The final chip structure comprises seven different layers illustrated in Figure 65:

a) Bottom glass layer

b) Lower microfluidic chamber vinyl layer

c) Intermediate vinyl layer

d) PET membrane with a pore size of 0.4 μm

e) Second intermediate vinyl layer

f) Upper microfluidic chamber vinyl layer

g) Top layer consisting of a PDMS block including a PTFE plug.

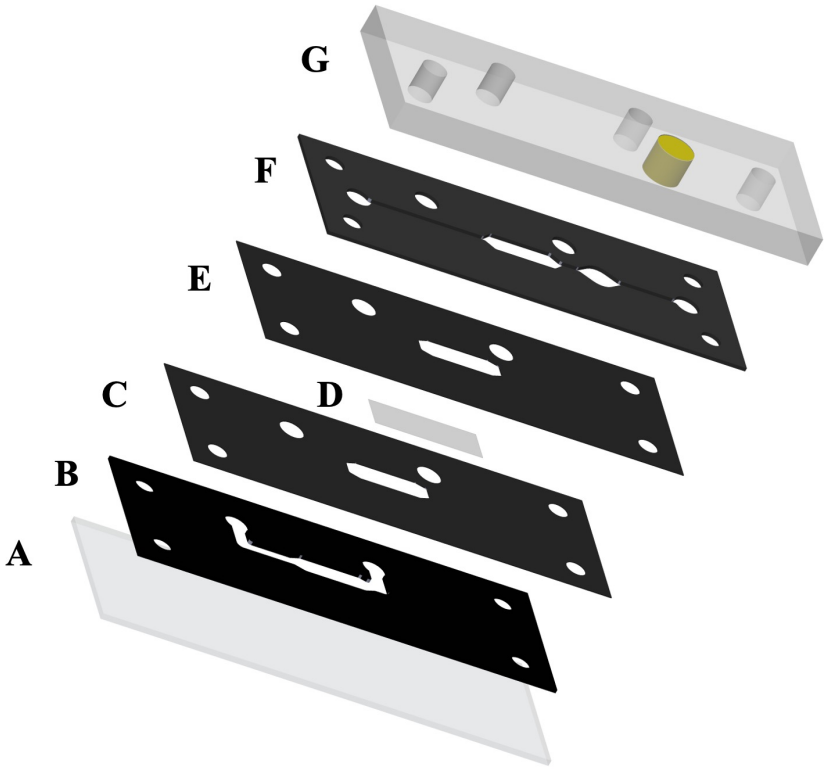

Figure 65. Exploded view of the skin-on-a-chip. Letters are referred to the chips structure explained in section 6.1.

6.1.1 Skin-on-a-chip fabrication procedure.

The SOC devices have a different structure compared to the previously manufactured OOC devices, with modifications that have significantly impacted the manufacturing process, necessitating further adjustments. The critical element responsible for these protocol changes is the replacement of the PC membrane with the PET membrane, as explained in the previous section. The increased membrane thickness implies a risk of potential leakage points on the chip. Photoresist SU8 is utilized as an adhesive to seal these sensitive areas of the chip to address this issue.

Another significant difference from the brain-slice-on-chip manufacturing process is that the entire assembly process can be completed without the need to seed the biological sample before the final sealing step since the cells can be pipetted through the entry ports of the compartments or injected as needed.

The final difference lies in using a third vinyl layout with a design that only includes the common area shared by the microfluidic chambers, which enhances the compartmentalization of the chip. As a result, the fabrication protocol is the following (illustrated in Figure 66):

1. A protective paper is positioned on the aligner tool base, where the first vinyl cut's adhesive side will be stuck.
2. Four lower vinyl cuts are overlapped.
3. A first intermediate cut is affixed above the lower vinyl cuts.
4. A double-sided vinyl with the intermediate design is placed to secure the membrane.
5. A liquid sample of SU8 resin is lightly spread before placing the PET membrane to reinforce its fixation and minimize potential leakage points. After that, the membrane is then placed over the area covered by SU8.
6. A second intermediate vinyl is placed on top of the membrane to trap it.
7. Three upper vinyl cuts are overlaid.
8. A final double-sided vinyl is placed to facilitate the twisting of the last vinyl.
9. The final vinyl piece is removed from the aligner tool and adhered to a glass slide.
10. The glass-vinyl assembly undergoes temperature and pressure treatment (5 kg, 80°C).

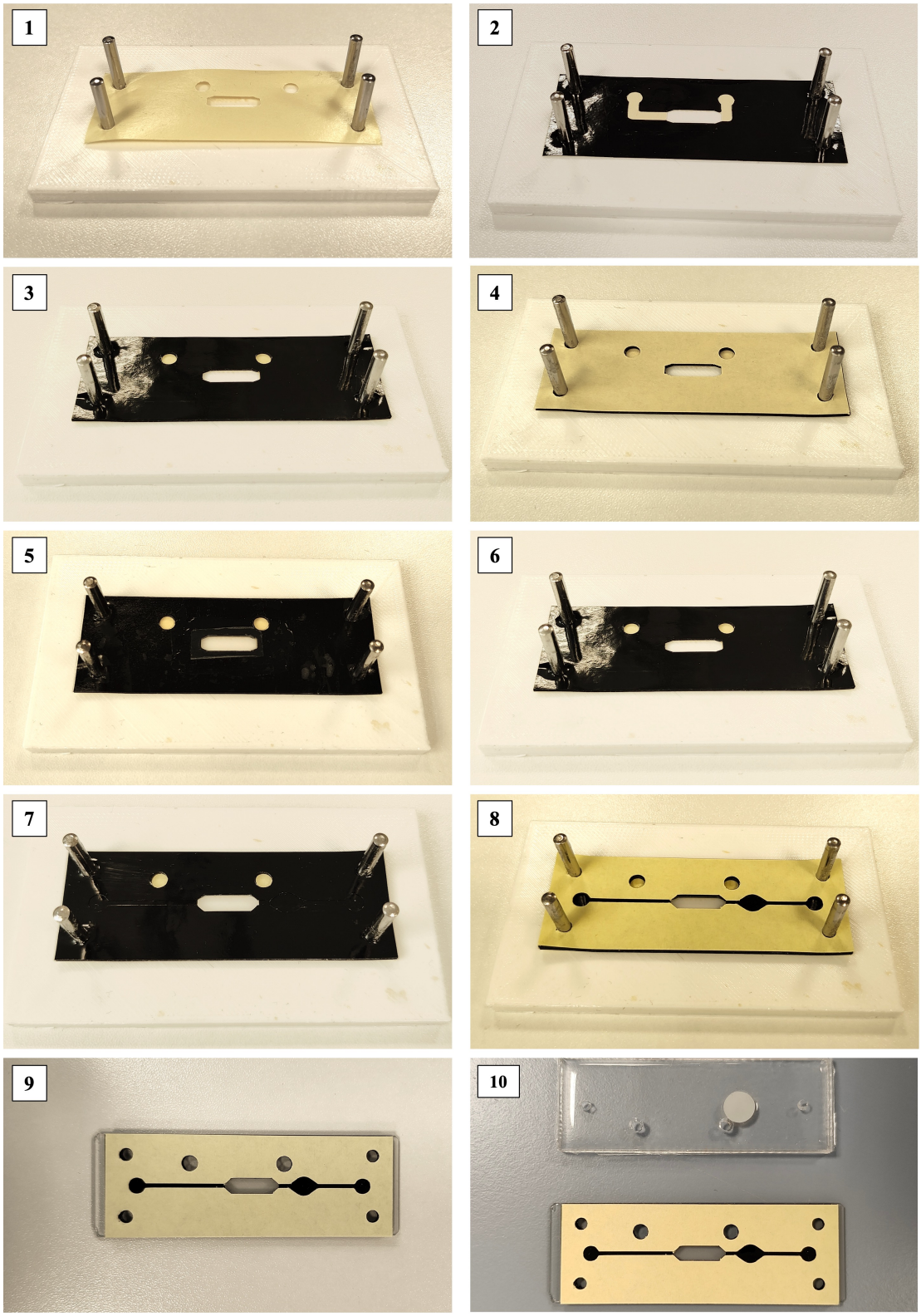

Figure 66. Skin-on-a-chip fabrication procedure. Each image represents the indicated steps in section 6.1.1.

6.1.2 Design optimization stage.

The chip design underwent several changes from the initial prototype to the final version, primarily to address issues related to leaks that occurred during the development of cell cultures within the chips.

Initially, leakage tests were conducted before any cell or biological sample culturing. These tests involved priming both microfluidic compartments of the chip and perfusing distilled water for 2 hours at a flow rate of 1 µL/min, followed by an additional 2 hours at a lower flow rate of 0.2 µL/min. The first detectable problem in prototype 1 was the leakage between the vinyl layers when applying flow rates to the chips. These leaks were evident along the long sides of the chips, occurring between the vinyls adhered to the membrane. This issue had not been found in the brain slice-on-a-chip; because of that, it was suspected that it might be related to the characteristics of the membrane. A sealing process using SU8 was applied as a glue to prevent leaks between the vinyl layers. This solution reduced significantly the number of leaks in the chips.

Another problem arose at the same time as the leakage between vinyls: new leaks around the outlet tubing port. Up to this point, the tubes were inserted into the chip through the PDMS blocks, held in place by the pressure exerted by the PDMS itself. When there was an overpressure in the chip or the inside of the tubing was blocked, the perfused liquid could escape to the outside through the blocks. To mitigate this, it was decided to seal the tubing once it was inserted into the chip using acid silicone around the tubing chip entries to reinforce that specific point and prevent leakage.

After exploring solutions such as using SU8 for membrane bonding and acid silicone for tubing insertion reinforcement, a new chip design (prototype 2) was created. This design included resizing the lower layout to widen the microfluidic channels. Once the dual flow was infused in the new device, the PDMS block bordering to the bottom outlet began to deform, causing the PDMS block to bend. This problem occurred in approximately 25 percent of the chips. The bottom layout was redesigned one more time to address this issue, relocating the positions of the inlet and outlet to a more internal area within the 70 x 25 mm region of the vinyl cutouts. Additionally, the microfluidic channels of the bottom compartment were widened to reduce internal pressure within the chip. This configuration is the one used by the final prototype 3 (Figure 67).

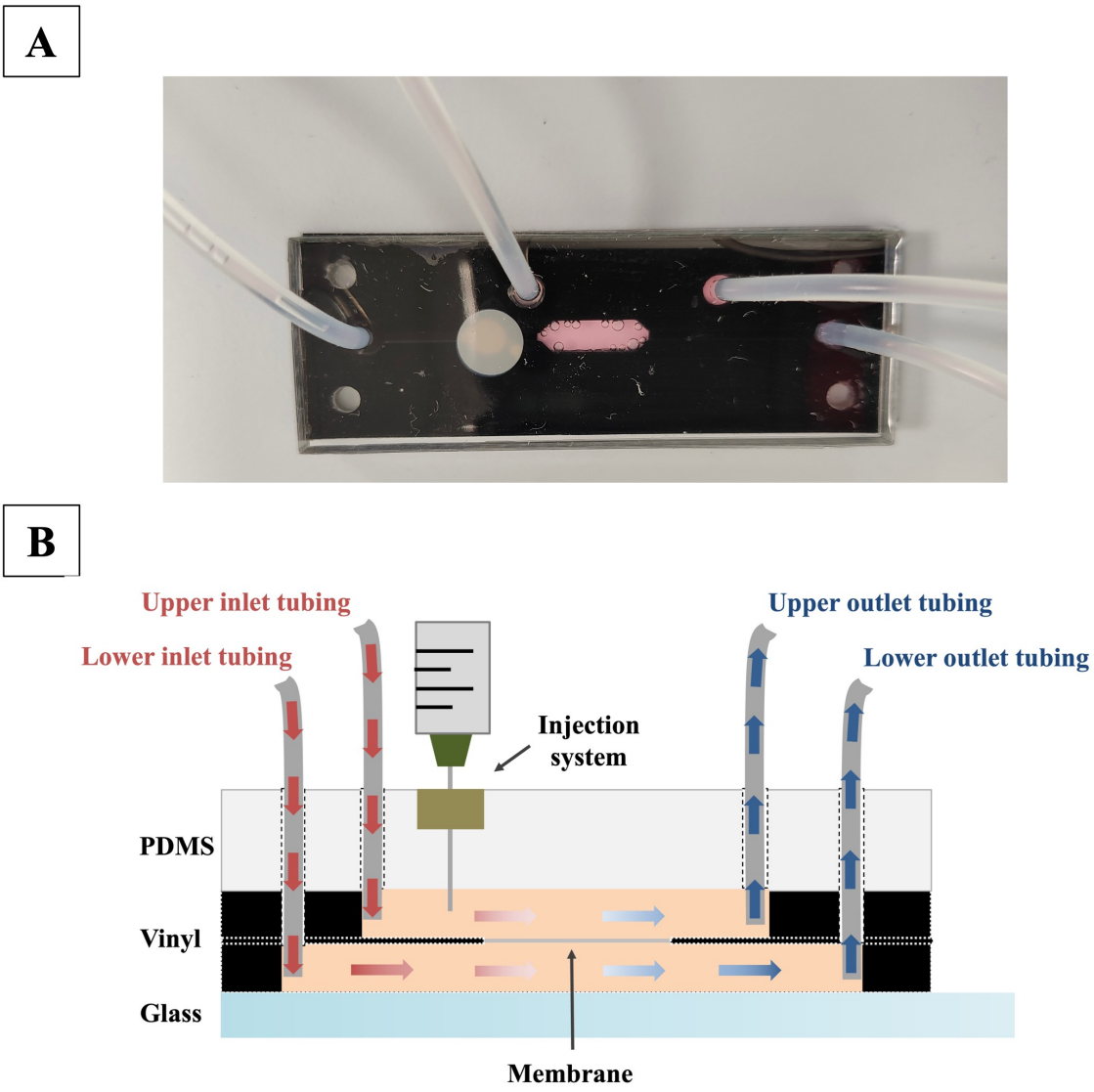

Figure 67. A) Picture of the final skin-on-a-chip prototype. B) Cross-sectional diagram depicting the dual flow within the chip.

After implementing these solutions, there were no leaks between the vinyl layers. Despite this improvement, there was a noticeable emptying of the microfluidic chamber. Since no external leakage was observed, the cause of this phenomenon was attributed to pressure drop within the chip and variations in the heights of the outlet tubing relative to the chip.

6.1.3 Chip microfluidic characterization

The issue of chamber emptying was traced back to the differing heights of the outlet tubes. This issue can be masked by the SOC's two interconnected microfluidic compartments separated by the PET membrane, which enables volume exchange. This complexity interferes with the evaluation of chip functionality, making it challenging to determine if chamber-filling issues stem

from manufacturing or microfluidic factors. To address this challenge, two microfluidic characterization tests were conducted to assess flow behavior under controlled conditions.

The first test involves the perfusion of two parallel flows simultaneously in the SOCs. A NE-1600 multi-syringe pump was employed for the test, with the capability to connect four microfluidic chips simultaneously, each operating at a flow rate of 1 µL/min, the maximum flow rate used in all skin-on-a-chip culture tests (Figure 68). Distilled water was chosen as the test fluid. This choice was made to prevent potential precipitation and blockages in the microfluidic connections and within the chip. Additionally, as the measurements would be based on weight, using distilled water facilitated precise mathematical calculations, as the inclusion of soluble dyes could alter the fluid density and result in less accurate calculations.

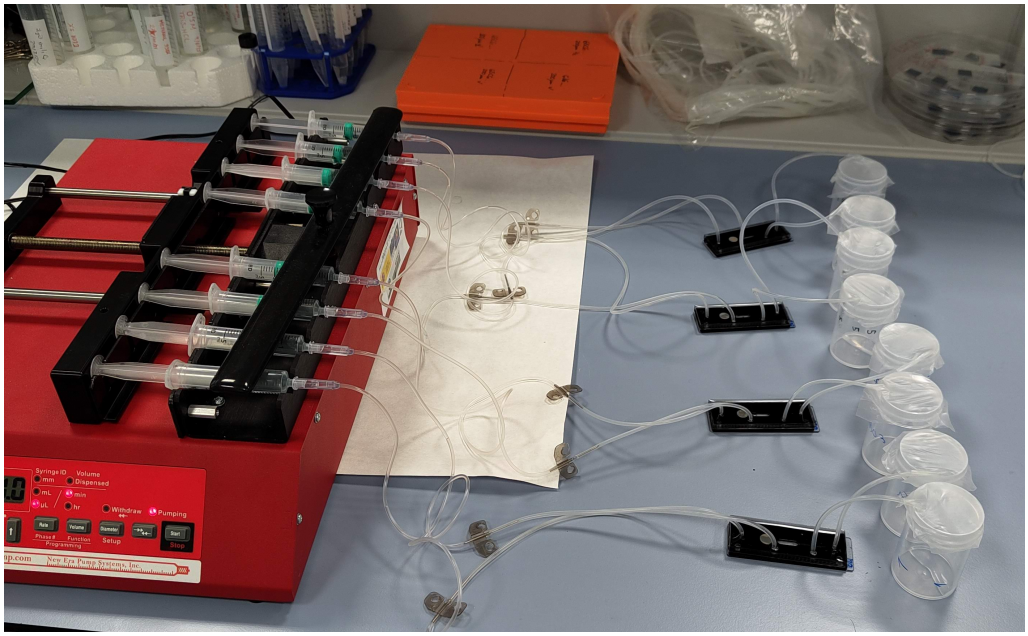

Figure 68. Microfluidic set up employed for the microfluidic characterization.

Eight plastic cups were initially weighed to quantify the volume of liquid evacuated from each chip outlet. After weighing, the chips, inlet, and outlet tubing were primed with distilled water. Each outlet was then individually placed into one of the plastic cups, ensuring that the outlet tubing ends were at the same height to avoid preferential flow through lower outlets, which could invalidate the characterization test. This test was conducted on 16 chips for at least 1000 minutes per chip, with three exhibiting leaks and being subsequently discarded.

The result of this test is shown in Figure 69. In this graph, the bars represent the ratio between the experimental flow rate and the theoretical flow rate. It displays each compartment's mean performance ratio and error bars representing the standard deviation. The performance values exceed 95%, suggesting no significant volume exchange occurs between the microfluidic compartments under dual parallel flow conditions.

Nonetheless, there was a desire to calculate a specific value that could be associate to each geometry. To achieve this, a second test was performed to determine the pressure drop of each microfluidic compartment.

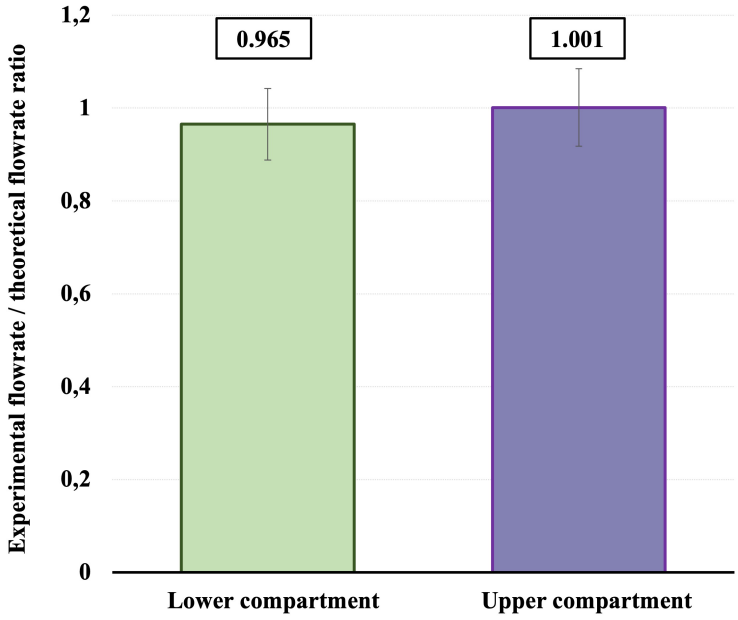

Figure 69. Graph depicting the results of fluidic characterization tests. The yield has been determined based on the experimental quantities of distilled water perfused through the microfluidic compartments and the anticipated theoretical value.

Pressure drop concept in microfluidics refers to the phenomenon where the electrical charge carried by particles, molecules, or ions within a microfluidic system is reduced or neutralized due to interactions with microchannel surfaces, collisions with oppositely charged entities, electrochemical reactions, and other factors. Calculating the pressure drop in a fluidic system requires consideration of two physical principles: the law of conservation of mechanical energy and Bernoulli's law.

The conservation of mechanical energy is a specific application of the broader law of conservation of energy. It pertains to mechanical systems in which only conservative forces (those that do not dissipate energy, such as gravitational forces) are at play. In such systems, the total mechanical energy remains constant as long as there are no non-conservative forces (like friction or air resistance) doing work on the system. In a fluidic system this principle can be expressed as:

$$W_{F_1} + E_{C_1} + E_{P_1} = W_{F_2} + E_{C_2} + E_{P_2} + E_{losses}$$

Where:

- W_{F_1} = Work done by external forces in the initial state
- E_{C_1} = Internal or kinetic energy of the system in the initial state
- E_{P_1} = Potential energy of the system in the initial state

- W_{F_2} = Work done by external forces in the final state
- E_{C_2} = Internal or kinetic energy of the system in the final state
- E_{P_2} = Potential energy of the system in the final state
- E_{losses} = Energy losses, which could include energy lost due to friction, heat, or other non-conservative forces.

Bernoulli's equation relates the pressure (P), velocity (v), and elevation (h) of a fluid in a steady, incompressible flow. This equation states that the sum of the pressure, kinetic, and potential energy per unit volume remains constant along a streamline. The equation can be simplified to:

$$P_1+\frac{1}{2}\rho v_1^2+\rho g h_1=P_2+\frac{1}{2}\rho v_2^2+\rho g h_2$$

Where:

- P_1 = pressure at point 1 along the streamline
- $\frac{1}{2}\rho v_1^2$= kinetic energy per unit volume, where ρ is the density of the fluid and v is the velocity of the fluid at that point
- $\rho g h_1$ = potential energy per unit volume due to elevation, where ρ is the density, g is the acceleration due to gravity, and h_1 is the height above a reference point at point 1
- P_2 = pressure at point 2 along the streamline
- $\frac{1}{2}\rho v_2^2$= The kinetic energy per unit volume at point 2
- $\rho g h_2$ = potential energy per unit volume due to elevation at point 2

According to Bernoulli's equation, the sum of these terms at point 1 is equal to the sum at point 2, assuming no significant external forces are acting on the fluid along the streamline.

These two principles can be applied in a fluidic system composed of the microfluidic chip, as depicted in Figure 70. In this system, the inlet is positioned at a higher elevation (h_1) compared to the outlet (h_2).

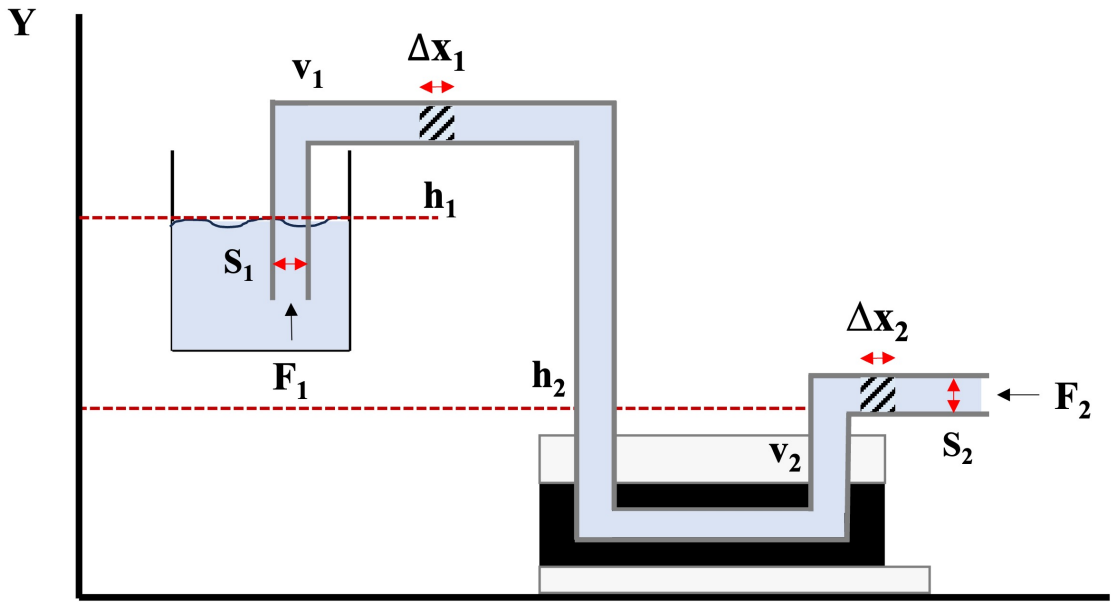

Figure 70. Diagram of the microfluidic set up prepared for the pressure drop trials. v represents the velocity, h the height, S the area section, Δx the difference in x value, and F the forces acting in the system.

The first consideration to calculate the pressure drop is the principle of continuity in fluid dynamics:

$$Q_1 = Q_2 \rightarrow \frac{V_1}{\Delta t} = \frac{V_2}{\Delta t} \rightarrow \frac{S_1 \Delta x_1}{\Delta t} = \frac{S_2 \Delta x_2}{\Delta t} \rightarrow S_1 v_1 = S_2 v_2$$

The conservation of energy equation can be represented as follows, associating the height and flow velocity parameters with energy:

$$F_1 \Delta x_1 + \frac{1}{2} m v_1^2 + mgh_1 = F_2 \Delta x_2 + \frac{1}{2} m v_2^2 + mgh_2 + E_{losses}$$

This equation can be adapted to integrate the Bernoulli principle with the conservation of energy:

$$\frac{F_1 \Delta x_1}{V} + \frac{1}{2}\frac{m v_1^2}{V} + \frac{mgh_1}{V} = \frac{F_2 \Delta X_2}{V} + \frac{1}{2}\frac{m v_2^2}{V} + \frac{mgh_2}{V} + \frac{E_{losses}}{V}$$

$$\frac{P_1 S_1 \Delta x_1}{S_1 \Delta x_1} + \frac{1}{2}\rho v_1^2 + \rho g h_1 = \frac{P_2 S_2 \Delta x_2}{S_2 \Delta x_2} + \frac{1}{2}\rho v_2^2 + \rho g h_2 + \Delta P_d$$

$$P_1 + \rho g h_1 = P_2 + \Delta P_d$$

$$\text{If } \; P_1 = P_2 \rightarrow \mathbf{\rho g h_1 = \Delta P_d}$$

With this last equation, the pressure drop of the microfluidic chips can be calculated experimentally as a function of the relative height between the inlet and outlet.

The protocol performed to calculate experimentally the pressure drop values of the SOC devices is the following:

1. The microfluidic compartment of the chip to be characterized and its inlet and outlet tubing are primed.
2. Once the system is primed, the end of the outlet tubing of the chip is placed onto a surface exposed to air.
3. The end of the inlet tubing is immersed into a beaker filled with distilled water, and the glass container is gradually lifted until water begins to flow out from the outlet tubing.
4. At this point, the height from the base of the glass to the ground surface is measured. With this value, it is possible to calculate the pressure drop.

The pressure drop tests have been conducted with a small number of chips (N=9) in which no specific correlation with each microfluidic compartment could be discerned from the results, yet it is possible to extract from the combined data a correlation with the generation of leaks: if one of the compartments of a chip has a pressure drop value exceeding 900 Pa, that chip has present leaks. Figure 71 displays the pressure drop values obtained from the nine tested chips. Only chips 8 and 9 (with values of 931 and 901.6 Pa) exceeded this threshold in one of their fluidic compartments; both experienced volume losses due to structural leaks in the chip.

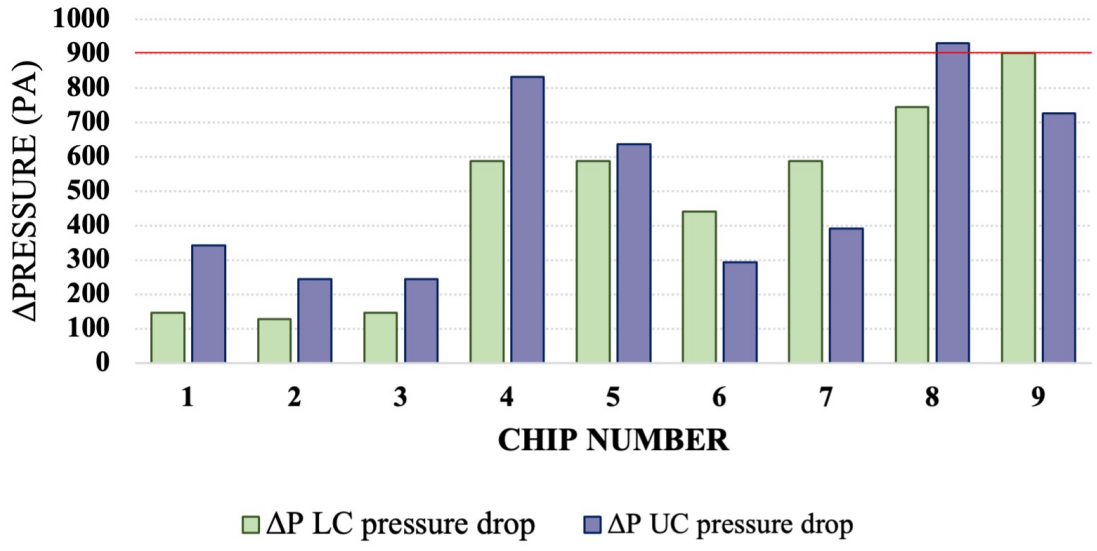

Figure 71. Bar graph representing the pressure drop values of the lower compartments (green) and upper compartments (violet) of the 9 SOCs tested.

Pressure drop value could be and indicator of potential manufacturing defect on the device. This procedure must be performed with a more significant number of chips to establish a more reliable reference value to assess the proper functioning of the devices and obtain specific values for each type of geometry.

After performing the two fluidic characterization tests, it was determined that the vinyl layouts of prototype 3 were not the cause of the microfluidic chamber emptying. Instead, this phenomenon was induced by the elevated positioning of the outlet tubing ends relative to the chip. Therefore, the characterization tests confirmed the proper functionality of the prototype, establishing it as the final chip design.

6.2 RESULTS

The objective of this chapter is to develop a SOC model that replicates a three-dimensional skin structure on a microfluidic platform. Skin models, whether in static plate cultures or microfluidic systems, typically utilize two primary cell types: fibroblasts and keratinocytes, which constitute different layers of the skin (Figure 72). These cells are adherent, meaning they require a surface for attachment, and they possess a natural affinity for plastic materials, eliminating the need for biofunctionalization to promote cell adhesion.

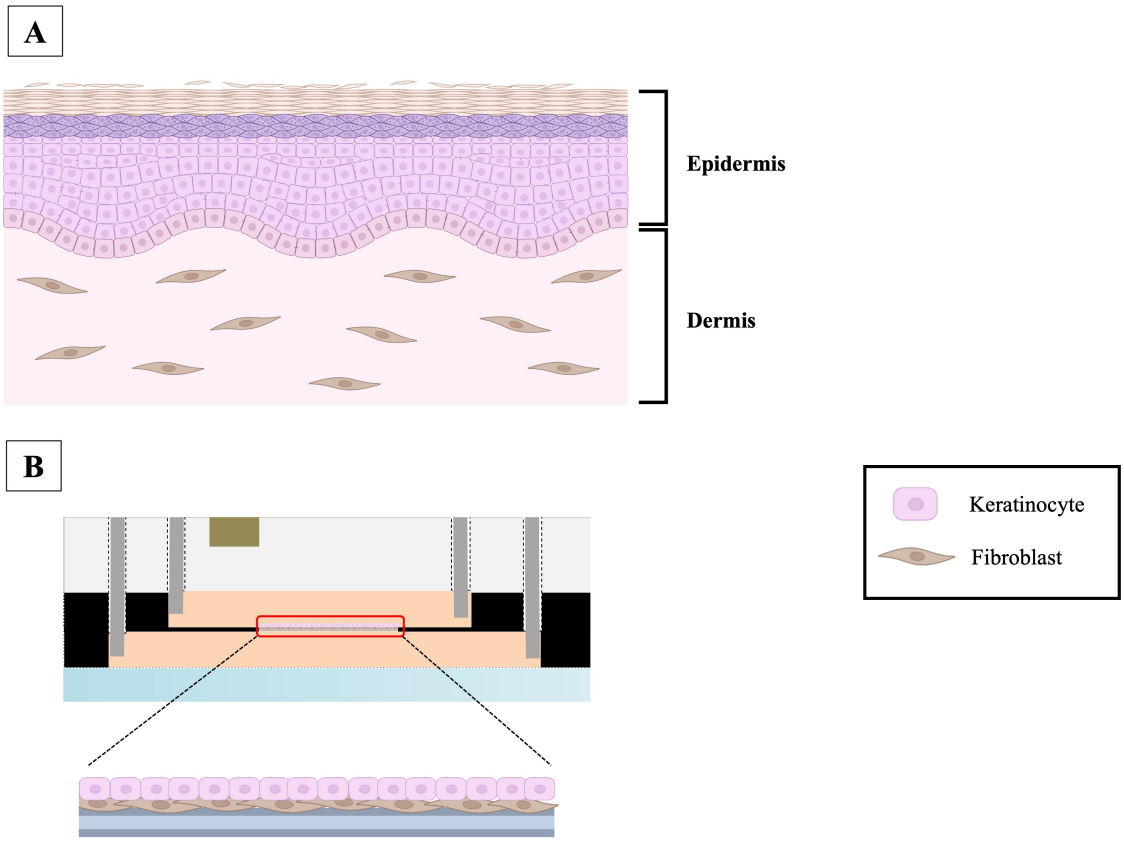

Figure 72. A) Simplified representation of skin composition. B) Basic skin-on-a-chip model proposed in Chapter 6. Created with Biorender.com

The results section of this chapter will present the culture of various cell types, including fibroblasts, keratinocytes, and immune cells. Each cell type has undergone individual culture both on plates and on-chip to assess their compatibility with the membrane and observe cell behavior under flow conditions. Following these monocultures, co-culture experiments have been fulfilled on-chip to replicate a complex skin model. In contrast to the brain slice-on-a-chip device discussed in the previous chapter, the microfluidic chips employed for the skin model do not require an open configuration for introducing biological samples. In this case, cells can be introduced via pipetting or injection. This characteristic allows the chips to undergo autoclaving. It is worth noting that the PET membrane included in this new microfluidic chip cannot withstand the high temperature of 124ºC required for autoclaving, rendering the chips incompatible with this sterilization method, and it was essential to modify the sterilization and assembly process for the microfluidic setup. For all experiments conducted with this new chip, the following sterilization protocol was adhered for cell monoculture tests:

1. The microfluidic chip compartments were washed with 500 µL of 70% ethanol, followed by a rinse with 500 µL of sterile distilled water.
2. The silicon tubing (0.5 mm ID, 2.5 mm ED) was autoclaved.

3. The tubing was then cut into 70 cm sections for the inlet tubes and 20 cm sections for the outlet tubes.
4. The tubing was inserted into the inlet and outlet ports of the chips.
5. Syringes were filled with culture medium.
6. The syringes were connected to the inlet tubes.
7. The entire microfluidic system, from the inlet tubes to the end of the outlet tubes, was primed.
8. A 100 µL volume of the corresponding cell solution was injected through the PTFE plug.
9. Tubings were sealed with acid silicone to prevent leakage and evaporation losses.
10. Depending on the cells added, an incubation period must be done, where the chips were not subjected to any flow to allow cell adhesion.
11. After the incubation period (if applicable), the syringes were connected to the perfusion pumps to initiate flow application on the chips. The pumps are located outside the incubator (Figure 73).

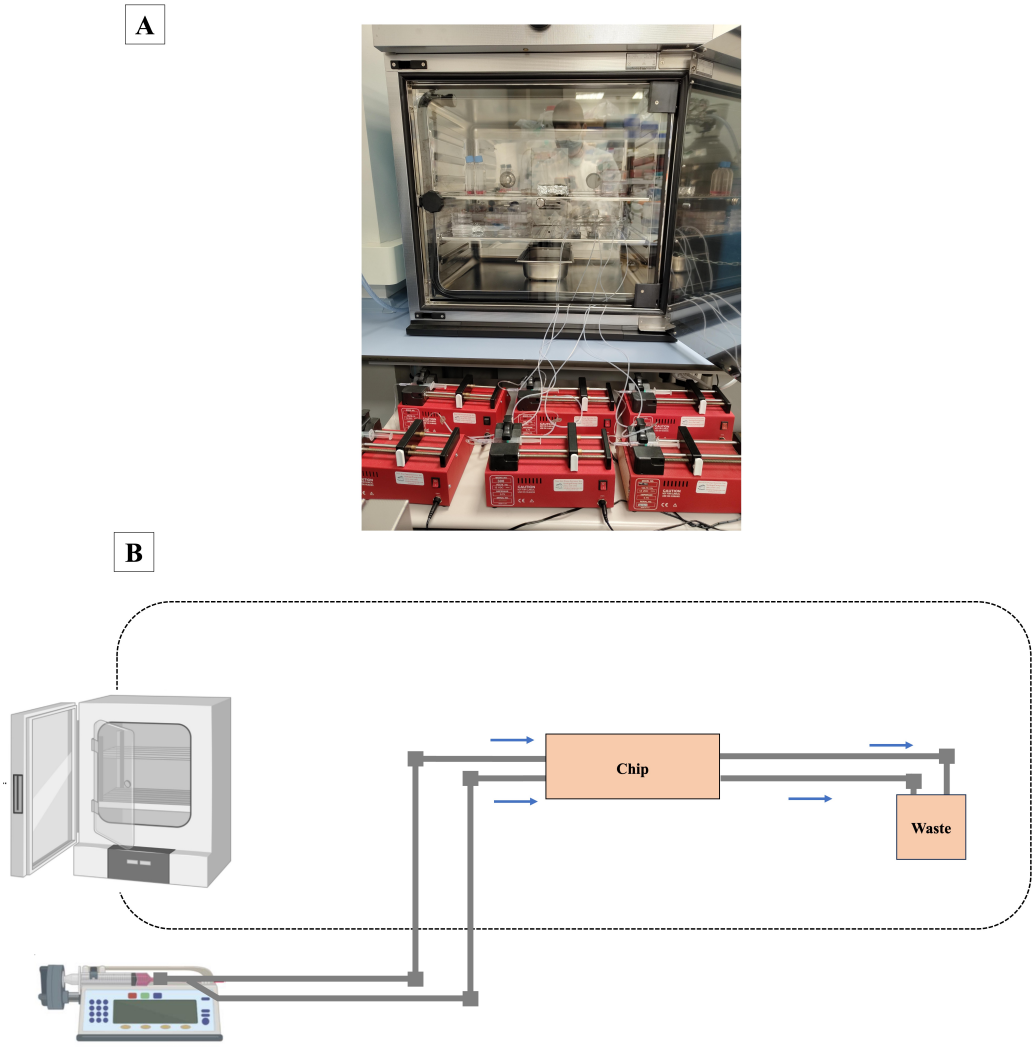

Figure 73. A) Picture of the microfluidic set up for the skin-on-a-chip cultures. B) Schematic view of the set up.

The flow rate of the pumps and the culture medium used varies according to the cells that have been seeded. To compile all this information, Table 11 presents the flow conditions used for each culture medium for each of the cell lines.

Cell line	Culture medium	Type of flow	Flow rate
CV-1	DMEM	Dual flow	0.2 µL/min
HaCaT	DMEM F12	Dual flow	1 µL/min
U937	RPMI	Single and dual flow	0.4-0.6-0.8-1-2 µL/min
HPF	DMEM F12	Dual flow	0.4 µL/min

Table 11. Microfluidic culture conditions of CV-1, HACAT, U937, HPF monocultures.

6.2.1 CV1 – fibroblast monoculture

While the skin model to be recreated in this thesis aimed to consist entirely of human cells, procuring an adequate and readily available supply of human fibroblasts presented certain challenges. Due to the fast availability of CV-1 cells by the GOFB research group, the initial experiments involving SOC devices were conducted using this cell line. The objective was to acquire insights into the adhesive properties of adherent cells when exposed to the potential membrane candidates intended for use in the chips.

The initial step involved assessing the in vitro adhesion capacity of fibroblasts on a 6-well plate housing the two candidate membranes: the hydrophilized PTFE membrane and a PET membrane, both possessing a pore size of 0.4 µm. As shown in Figure 74, this preliminary examination revealed distinct behaviors exhibited by the cells on each substrate: while the cells demonstrated an ability to adhere to the PET membrane (Figure 74A), they maintained a spherical configuration without adhering to the PTFE membrane (Figure 74B). Given the outcomes of these experiments, it was determined that the most suitable course of action was to proceed with the fabrication of the initial skin-on-a-chip devices, opting for the utilization of the PET membrane.

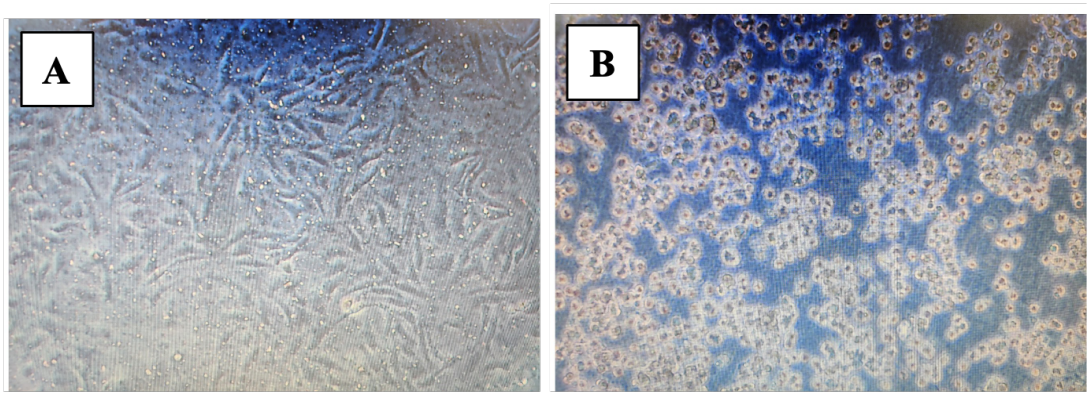

Figure 74. Qualitative CV-1 cell culture images in PET membrane insert (A) and PTFE membrane insert (B).

The next step in the development of the skin-on-a-chip was the introduction of CV-1 fibroblasts into the chip to assess their ability to maintain attachment under continuous flow conditions. Given the chip's configuration with two microfluidic compartments, the cells had the potential to adhere on both sides of the PET membrane. Four chips were employed for this experiment: in two of them, 3 x 10^4 cells were injected using the injection system, while in the other two, the lower inlet was removed, and the 100 µL containing the same quantity of cells was pipetted using a 1000 µL micropipette. The chips hosting cells in the lower compartment were flipped to facilitate cell settling on the membrane. In both scenarios, a 120-minute incubation period was allowed for cell adhesion, after which the chips were connected to the microfluidic system, subjecting them to a dual continuous parallel flow of 0.2 µL/min.

After 24 hours of continuous flow application, the chip cultures were evaluated, revealing successful fibroblast adhesion in both conditions, characterized by the typical morphology of healthy fibroblasts (Figure 75).

The images obtained from these chips validated the feasibility of culturing CV-1 fibroblasts on skin-on-a-chip devices within a continuous flow system. The chips exhibited culture media leakage between the vinyl that constitute the chip structure, primarily at the corners. 24 hours later, approximately one quarter of each microfluidic chamber had emptied. Under these conditions, the cell's state could deteriorate after the fourth day of culture.

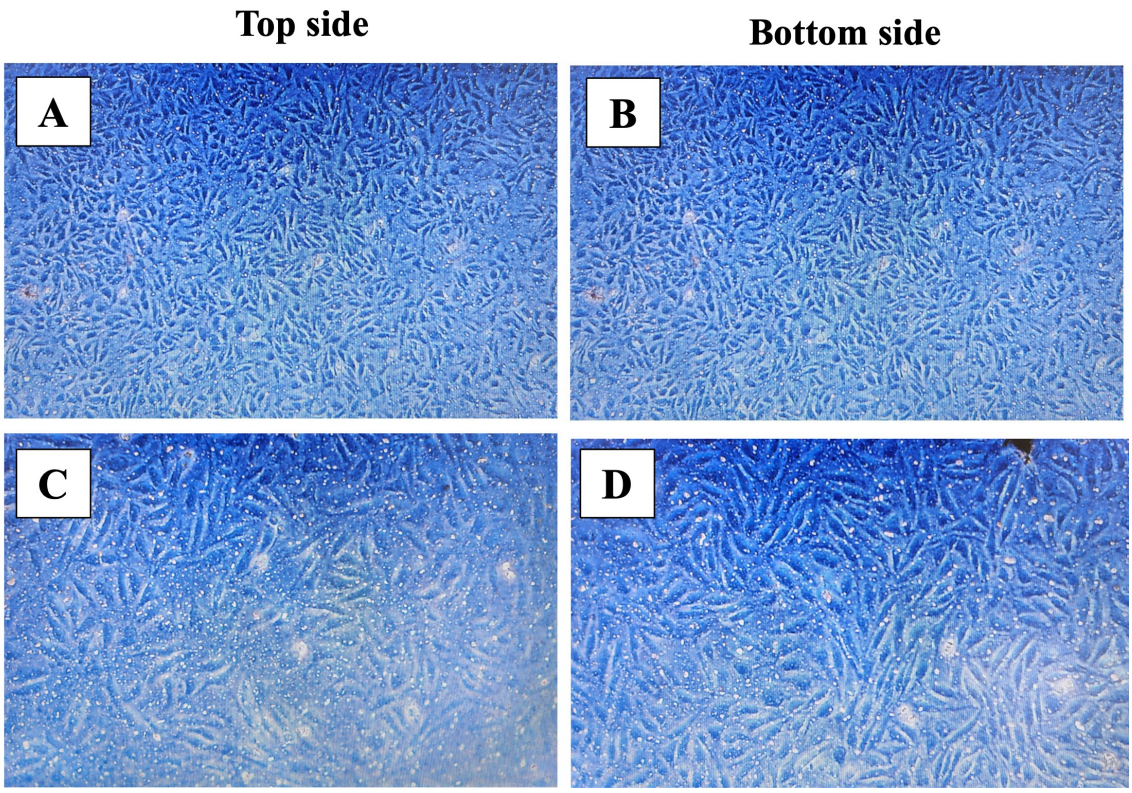

Figure 75. Qualitative CV-1 cell culture image on microfluidic chips. A and C show cells cultured on the upper side of the membrane. B and D show cells on the lower side of the membrane. Cells were cultured under dual parallel continuous flow of 0.2 µL/min for 24 hours.

6.2.2 HaCaT monoculture.

Following the successful attachment of CV-1 cells to the chips, a series of culture tests involving HaCaT cells was conducted using an identical approach for CV-1 cells. Consistent with the CV-1 cell experiments, the initial HaCaT cell test evaluated their adhesion to PET and PTFE membranes in an in vitro culture plate. The outcome was identical, with HaCaT cells demonstrating adhesion and growth on the PET membrane (Figure 76C,D). In contrast, the cells remained viable and capable of division on the PTFE membrane but failed to adhere to the substrate surface (Figure 76A,B).

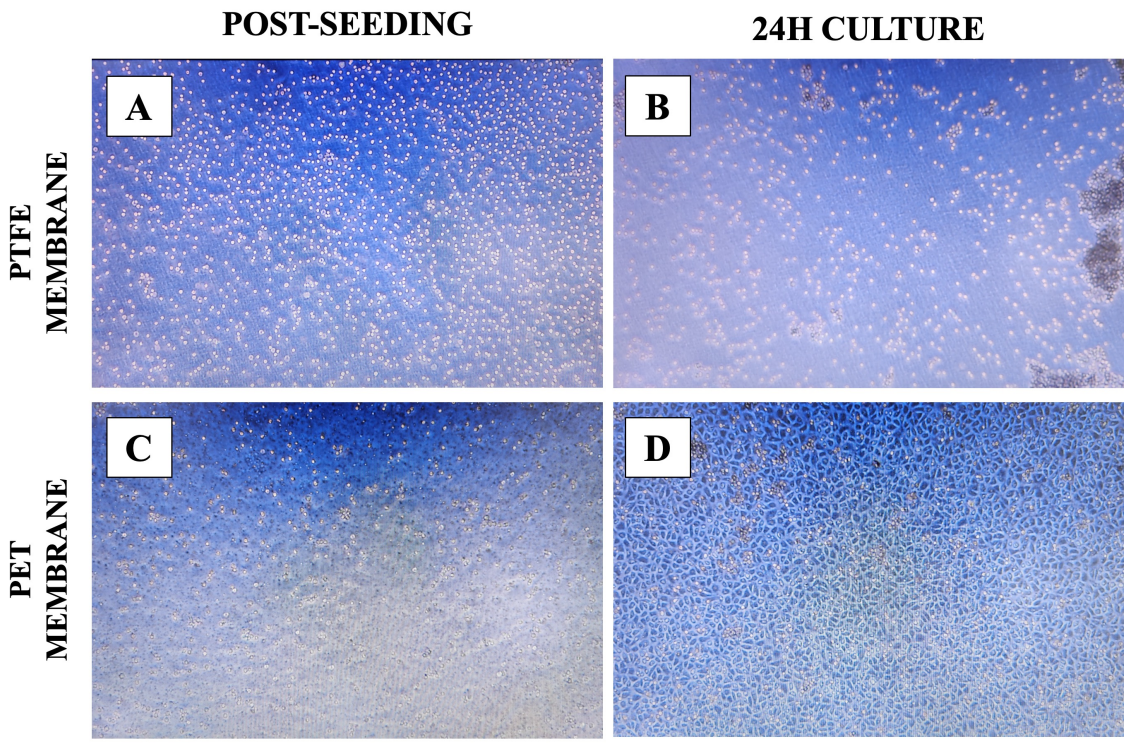

Figure 76. Qualitative image comparison of HaCaT cell cultures on two substrates: PTFE membrane (A, B) and PET membrane.

After this initial test, HaCaT cells were cultured on the microfluidic chips to determine the optimal cell density. HaCaT cultures on the PET membrane exhibited a faster proliferation rate than CV-1 cells. This circumstance leaded to the decision of seed 2 x 10^4 HaCaT cells instead of the previous 3 x 10^4 cells, along with fibroblasts, as the initial starting cell quantity.

Once again, it was imperative to assess the behavior of the cells under continuous flow conditions. In line with the protocol previously employed for CV-1 cells, 100 µL of culture medium containing 2 x 10^4 cells were injected into three chips. These chips remained without any flow for 2 hours, allowing for the adhesion of the keratinocytes to the membrane. Subsequently, the devices were connected to perfusion pumps.

To facilitate the monitoring of these cultures, Leica DMI3000 microscope was used. Unlike the traditional inverted culture microscope used to capture images of CV-1 cell cultures, this equipment possessed fluorescence capabilities, enabling cell labeling like the brain slice-on-a-chip devices. This round of experiments was the first interaction with this microscope. The chips were continuously connected to the microfluidic system for eight days at a 1 µL/min flow rate. The images obtained using the Leica DMI3000 microscope did not achieve the same degree of sharpness in depicting cell morphology due to the microscope's ability to focus on the granular texture of the membrane.

The contrast of the cells appeared lower, especially as the culture reached confluence towards the later stages. In order to demonstrate that the shapes observed in the images correspond to living cells, the OGB marker was introduced into the chip. Figure 77 illustrates the progression of the culture from day 3 to day 8, encompassing the intracellular calcium labeling of live cells on DIV 8. The presence of a green signal throughout the entire membrane area, combined with the visible cell morphology, provides solid evidence for the successful development and sustained existence of a HaCaT cell monolayer within the microfluidic chip, even under continuous flow conditions for a duration of up to 8 days.

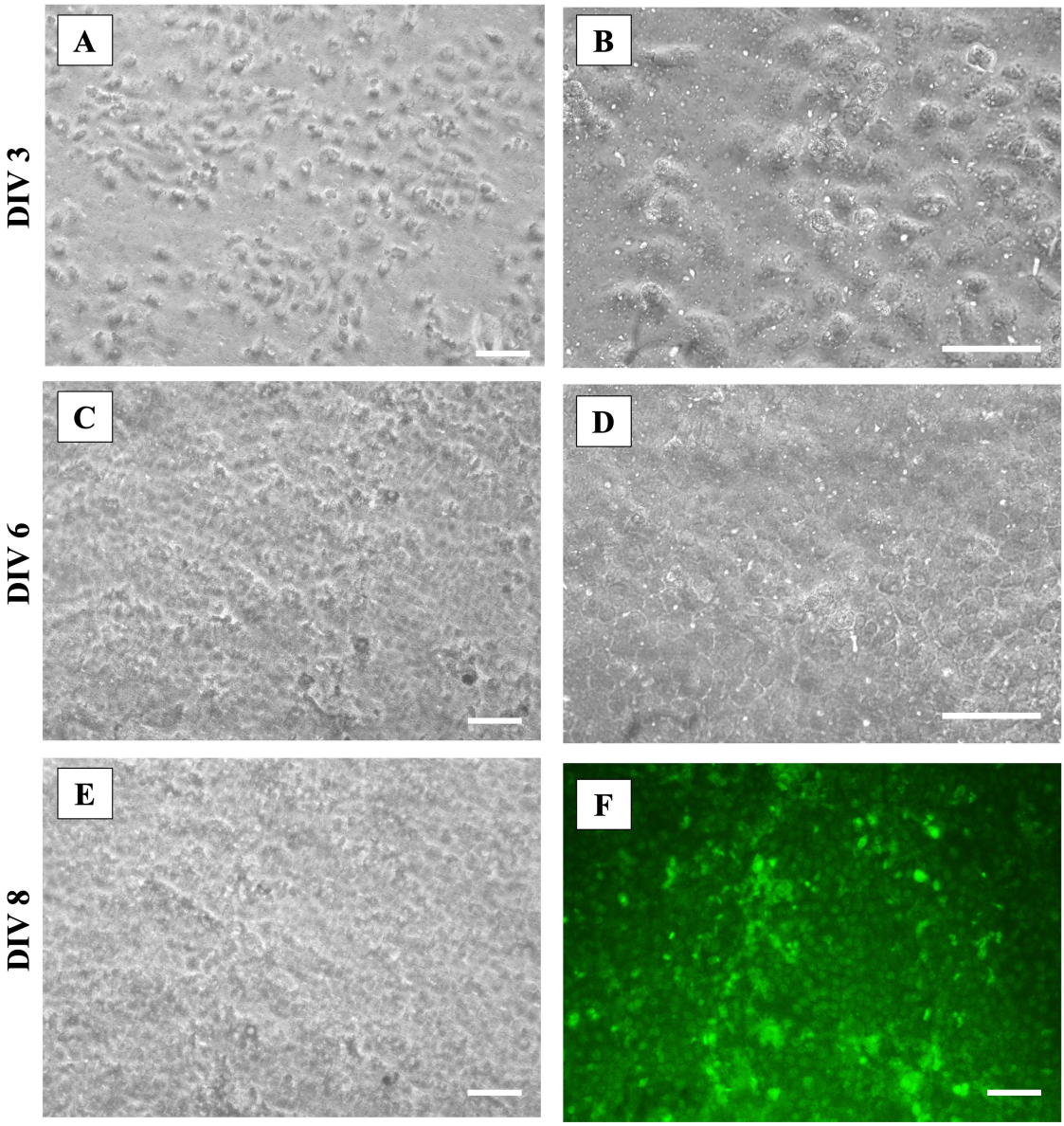

Figure 77. Evolution of HaCaT cell culture on-chip after 3, 6 and 8 days in vitro (DIV). Image F shows live HaCaT cells stained with OGB, highlighted in green. Cells were cultured under dual parallel continuous flow of 1 µL/min. Scale bars represent 200 µm.

Having successfully demonstrated the viability of maintaining cells within the SOC device, a conclusive experiment was conducted employing multiple chips in parallel. The objective was to determine the optimal flow rate for the sustained maintenance of keratinocytes. Experiments were carried out with a range of flow rates: 0.4; 0.6; 0.8; 1 and 1,2 µL/min, spanning seven days while maintaining the same initial cell quantity of 2 x 10^4 cells.

Initially, the cultures maintained a consistent condition for the first three days. As they reached confluence, noticeable differences in their appearance became evident. In particular, cultures exposed to flow rates below 1 µL/min displayed a significant decline in cell survivance. This study establishes a flow rate of 1 µL/min as the recommended rate for the long-term maintenance of HaCaT cells.

6.2.3 U937 monoculture

The skin model proposed in this chapter was conceived with a co-culture of fibroblasts and keratinocytes in the upper compartment. At the same time, the lower chamber was intended to host immune system cells. A challenge arose from U937 cells, which naturally grow in suspension and their lack the capacity to adhere to surfaces. This inherent characteristic posed an obstacle to achieving a stable skin model. Therefore, the model approach aimed to stimulate these cells to acquire adhesive properties.

Several studies have demonstrated that polymistrionic acid stimulation (PMA) can drive the differentiation of U937 cells into a macrophage-like phenotype (Song et al., 2015; Yang et al., 2017). This transformation equips the cells with the ability to adhere to culture surfaces. Considering this U937 cells' ability, the primary objective in the SOC model developed in this work was to seed U937 cells, stimulate their transition into a macrophage-like state, and facilitate their adhesion to the porous membrane on the chip's underside. The integration of U937 cells into a SOC, with their differentiation induced by PMA exposure, has been previously achieved in a detailed article, demonstrating the feasibility of the model (Ramadan & Ting, 2016).

The existing literature does not provide specific guidance regarding the concentration of the PMA reagent required for administration in microfluidic chips. The recommended PMA concentration range in culture plates varies from 10 ng/mL to 200 ng/mL. In order to know the optimal concentration for inducing differentiation of U937 cells, a series of tests were conducted using a P12 culture plate. Five different concentrations were tested: 5 ng/mL, 10 ng/mL, 20 ng/mL, 30 ng/mL, and 50 ng/mL.

The P12 culture plate was observed after 48 hours to check for any changes in cell morphology. The results revealed that a 5 ng/mL concentration yielded virtually no cell adhesion. In contrast, concentrations of 10 ng/mL and 20 ng/mL exhibited an adhesion rate of approximately 50% of

the cells, with noticeable alterations in cell morphology (Figure 78). These cells assumed a dendritic shape and adhered to the well's bottom. Although some cells exhibited adhesion at concentrations of 30 ng/mL and 50 ng/mL, the dendritic morphology was less pronounced. Based on these outcomes, concentrations of 10 ng/mL and 20 ng/mL were selected as reference concentrations for subsequent experiments.

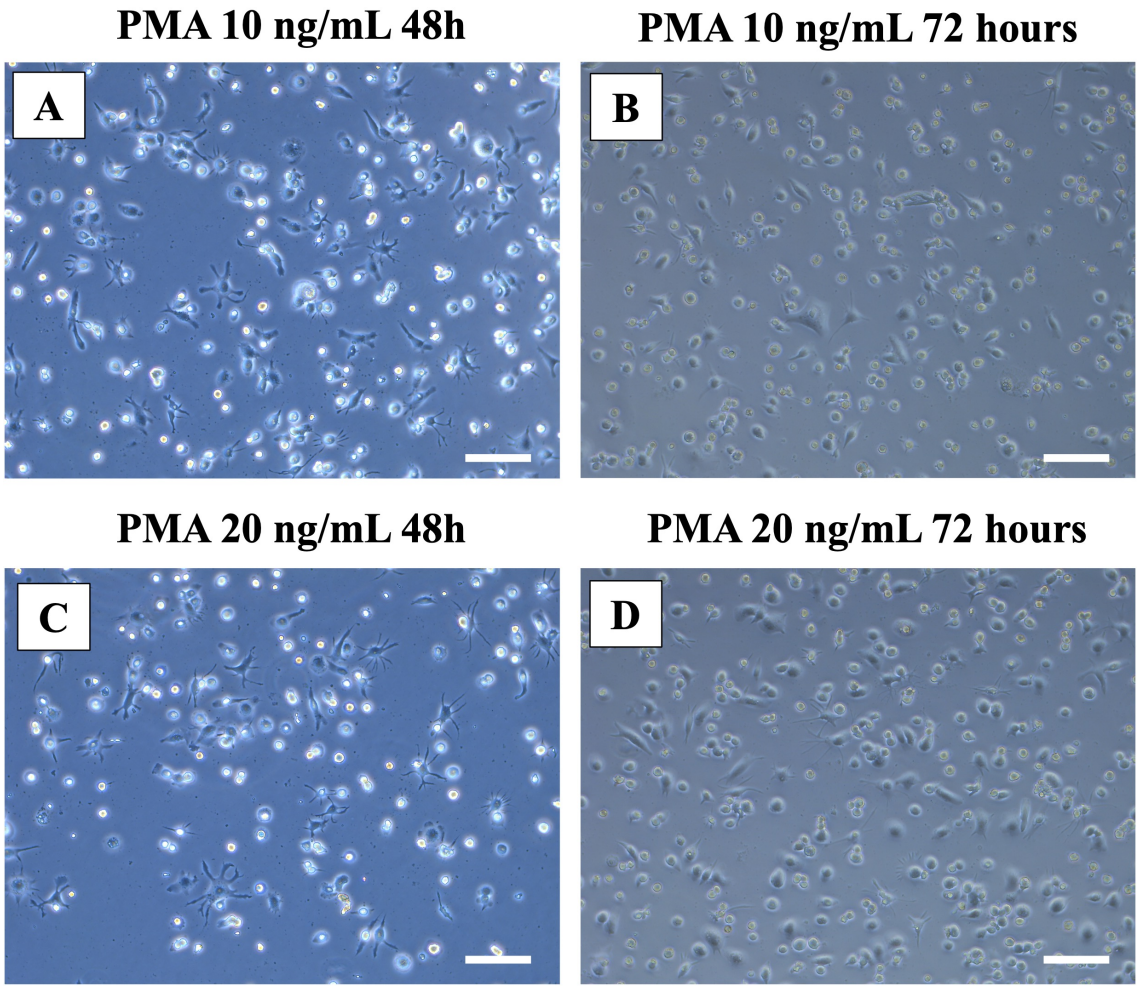

Figure 78. Differentiation of U937 cells into macrophage-like cells through stimulation with PMA at 48 hours (A,B) and 72 hours (C,D) post-administration. Scale bars represent 100 µm.

The next step was to validate whether the differentiation process could effectively occur on the PET membrane within the microfluidic chips. To minimize potential stress on the cells induced by the flow within the chips, which could hinder cell adhesion to the membrane, a preliminary evaluation was done in P6 culture plates using membrane inserts. Only culture medium was applied over the membrane, while the lower part of the membrane remained dry to prevent the culture medium from diffusing through the membrane (Figure 79).

500 µL of RPMI medium was pipetted into six membrane inserts, after which 1 x 10^4 cells were seeded per well. Then, a PMA was administered to achieve a final concentration of 10 ng/mL. After a 48-hour incubation period, the cultures were microscopically examined to assess cell

adhesion, following the same procedure as in the previous test. Due to the membrane's roughness and granularity, obtaining sharp cell images proved challenging.

Once the adhesion phenomenon on the PET membrane was demonstrated the cell attachment reproducibility, U937 had to be seeded in the SOC.

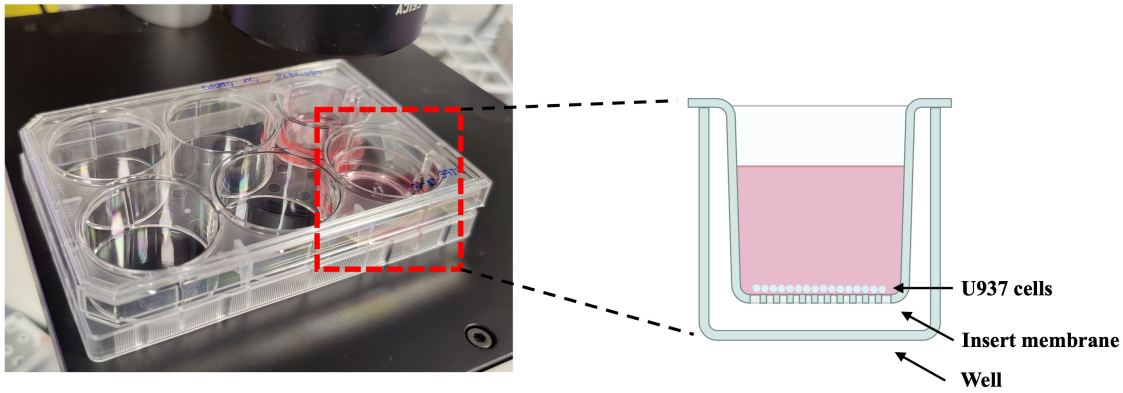

Figure 79. Schematic of the membrane insert culture procedure to test cell compatibility and cell differentiation with the membrane. Created with Biorender.com

During the evaluation phase of the U937 cell culture within the SOCs, a consistent observation was the cell viability, which sharply declined within the chip after 24 hours of culture. This outcome remained consistent across various flow conditions and cell quantities tested. Flow rates ranging from 0.2 µL/min to 2 µL/min were applied, including perfusion through either the upper fluidic compartment, the lower compartment, both compartments simultaneously, and static conditions. These tests encompassed a range of cell quantities, including 5 x 10^2, 1 x 10^3, 1,5 x 10^3, 3 x 10^3, 5 x 10^3, and 1 x 10^4 cells. Regardless of the flow rate or cell quantity, the cells were unable to survive beyond the 24-hours.

To elucidate the factors contributing to the failure of U937 cell culture on the chips, control plate cultures were employed to examine the potential link between cell viability and the membrane. Cells were seeded both on the well surfaces and membrane inserts to investigate whether membrane-related issues were responsible for the observed cell survival problems, even if the cells demonstrated previously the ability to get attached to de PET membrane with PMA stimulation

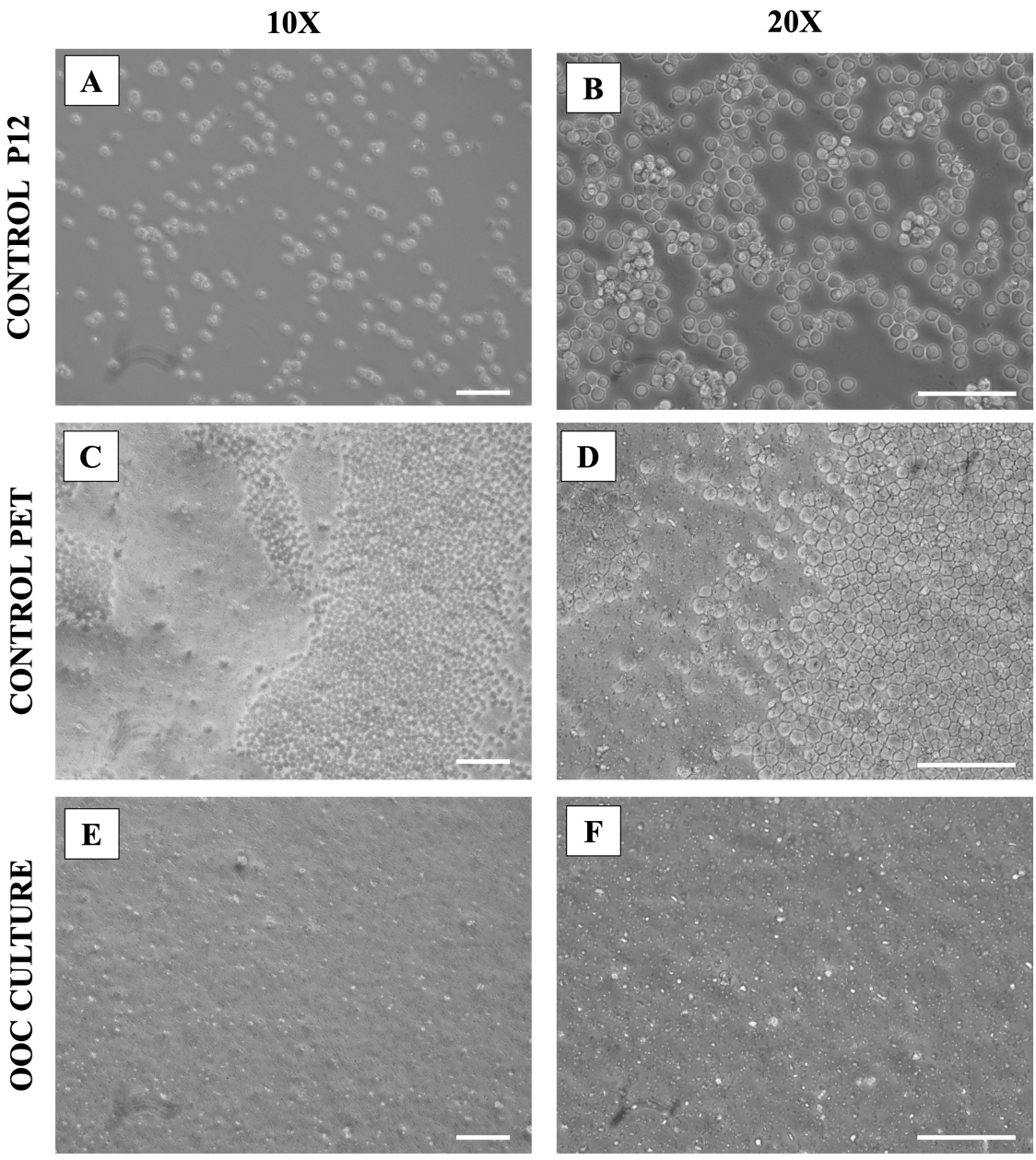

Figure 80. Comparison of U937 cell viability in plate culture (A,B), membrane insert plate (C,D) culture and on-chip culture. Scale bars represent 100 µm.

U937 cells exhibited optimal proliferation on the well surfaces and membrane insert surface, displaying healthy, spherical cells (Figure 80A-D). In contrast, within the microfluidic chips, there was an absence of spherical elements resembling viable cells (Figure 80E,F). This unexpected outcome was shocking because similar cell death issues had not been encountered with fibroblasts or keratinocytes seeded in the same microfluidic chip design and construction.

Following these results, the potential hypotheses explaining the challenges in culturing U937 cells were narrowed down to three possibilities:

1. Liquid-Air interface and O_2 demand: it was considered whether the liquid-air interface might have a critical impact on O_2 demand by the cells. This hypothesis appeared less

plausible because other studies involving U937 cell culture and differentiation via PMA stimulation had been successful in a traditional well-plate format, loading each well with culture media at maximum capacity.

2. Vinyl incompatibility with U937 cells: another possibility was the potential incompatibility of the vinyl material used in the microfluidic chips with U937 cells specifically.
3. Sterilization Protocol: The third hypothesis centered on the sterilization protocol, specifically the use of ethanol in the sterilization process. This hypothesis emerged due to the membrane's inability to endure the elevated temperatures required for autoclaving. Nonetheless, this hypothesis seemed to be less probable since other cell lines had verified no compatibility issues. Even so, ethanol washing as a sterilization technique must remained essential, even if it hypothetically contributed to the cell viability challenges encountered in chip cultures.

A final experiment was conducted to identify whether any of these three hypotheses were valid. Three different conditions were tested in a p12 culture plate:

- Condition 1: Culture of 5 x 10^3 U937 cells with 500 µL of RPMI medium in wells without any ethanol washing. This condition corresponded to the methodology employed in all prior plate cultures involving U937 cells.
- Condition 2: culture of 5 x 10^3 U937 cells with 500 µL of RPMI medium in wells following surface washing with ethanol and PBS.
- Condition 3: culture of 5 x 10^3 U937 cells with 500 µL of RPMI medium in wells where a circular vinyl cut stuck on the well base, and the well surface was pre-washed with ethanol and PBS before cell addition.

The outcomes were highly informative (Figure 81). Cells in the wells under condition 1 demonstrated continued viability and displayed an optimal division rate, starting with the same initial cell density and culture medium volume as the other conditions. Conversely, conditions 2 and 3 yielded identical, unfavorable results, characterized by cell degeneration and death across all wells. These results conclusively point to ethanol washing as the underlying cause of impaired cell survival in the culture, regardless of the presence or absence of vinyl in the cellular environment.

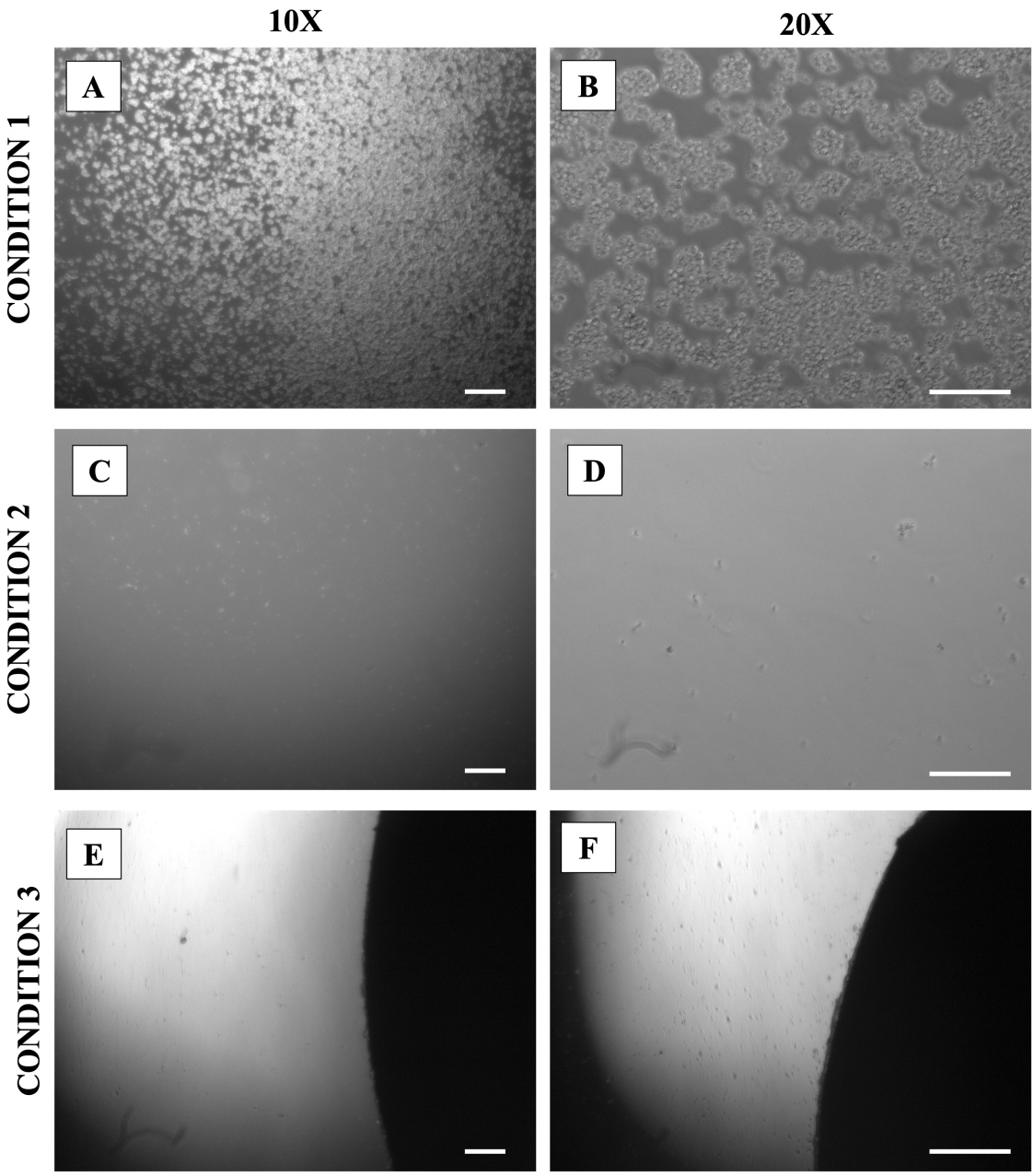

Figure 81. Images of the U937 culture in the three proposed conditions to compare the viability of the culture. Scale bars represent 200 µm.

With all the tests performed with this cell type, the use of the U937 cell line for the skin model under development was ruled out, given the inability to maintain a live U937 culture for 24 hours. Further testing of surface washes is necessary until a protocol is achieved to eliminate ethanol's detrimental effect on sterilized materials. One encouraging aspect arising from this study is that based on all the experiments conducted with these cells, both on chips and in vitro cultures, it can be concluded that the inability of U937 cells to survive is not attributed to the materials used in the chip.

6.2.4 Human primary fibroblasts monoculture

Due to the challenges encountered in culturing U937 cells within microfluidic chips, the skin model focus shifted towards developing a skin model comprised exclusively of human cell lines. In this regard, the animal-origin CV-1 cells were replaced with primary human fibroblasts (HPF), generously provided by the Tissue Engineering and Regenerative Medicine group of the Universidad Carlos III de Madrid.

Having previously assessed the behavior of fibroblasts on PTFE and PET membranes, as well as achieving successful cultures inside the chips, HPF cells were cultured immediately on the chips. During the initial experimentation phase, 2 x 10^4 cells were injected into each of the four microfluidic chips. A 2-hour incubation followed the seeding to facilitate cell adhesion to the PET membrane. Once this period was finished, a continuous flow rate of 0.4 µL/min was set for the chips. After observing the cultures 24 hours later, only 20% of the membrane exhibited cell coverage. Subsequent examinations at the 72-hour milestone showed no significant change in culture status, with minimal cell proliferation evident. This trend persisted throughout the first week of in vitro culture.

In response to these preliminary results, adjustments were made to the experimental design. First, the number of injected cells was increased to 3 x 10^4 to enhance membrane coverage, minimizing cell spacing to promote cell division. Second, it was determined that the chips should be connected to the microfluidic system 24 hours after seeding rather than the initial 2-hour period.

Due to the fragile nature of HPF cells as primary cells and the dual-chamber design of the SOC devices, an alternative culture protocol was explored to enhance cell adhesion and proliferation. This new approach involved replicating the new cell density and flow conditions using single upper flow, single lower flow, and double parallel flow configurations. Three chips were employed for each condition, priming the entire microfluidic system in each one of them. 3 x 10^4 cells were injected per chip, followed by a 24-hour incubation period and the initiation of flow at a rate of 0.4 µL/min, adjusted for each specific condition.

The chips were connected to the microfluidic platform for seven days. All the chips displayed an increase in cell population, covering approximately 80-90% of the membrane surface. A mild decline in cell condition was discernible in chips featuring single upper chamber flow, whereas chips with parallel flow and lower chamber flow exhibited optimal cell visual aspect. The differences were more evident in the tubing. In chips without flow in the top compartment, the upper inlet and outlet tubing were filled with air. When the tubes were re-primed to expel any remaining air from the microfluidic system, noticeable resistance was encountered after pushing the syringe plunger, akin to the sensation experienced during tube blockages. This phenomenon suggests the possible formation of solid residues within the tubing resulting from air intrusion.

This tubing filling issue did not occur in chips featuring laminar flow in the upper chamber. This discrepancy may be attributed to the upper compartment's upper material boundaries. The PDMS block allows for gas diffusion, while the lower compartment is made of glass, vinyl, and the PET membrane. This fact justify the absence of volume loss in the lower compartment due to evaporation, which may result in the inability to fill the tubing connected to this compartment.

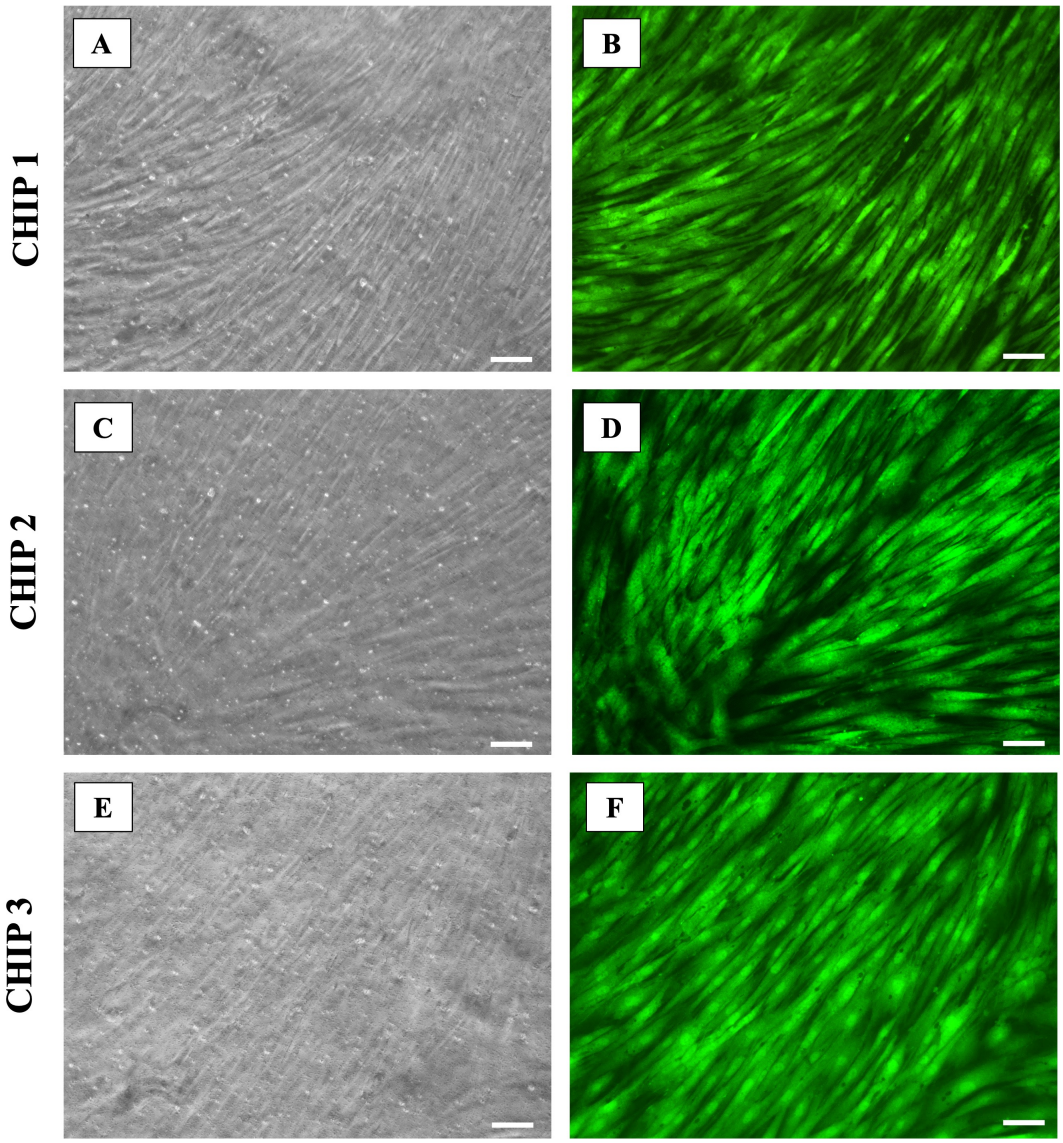

Figure 82. HPF cell culture in the upper side of the membrane of the SOCs in a monolayer distribution after 9 days in vitro (DIV). Cells were cultured under dual parallel continuous flow of 0.4 µL/min. Pictures B, D and F show the green, fluorescent signal of the CMFDA tracker that represents living cells. Scale bars represent 100 µm.

The chips with double parallel flow did not exhibit any issues, so the decision was made to use this type of flow for culturing the skin models. The next objective was to confirm the viability of fibroblasts attached to the membrane by fluorescent labeling of the cells, equally to previous monoculture experiments in skin-on-a-chip development. In the case of HPFs, a new reagent called CMFDA was employed as an alternative to OGB. CMFDA exhibits the unique

characteristic of being inherited by both daughter cells upon cell division, which is particularly significant in the context of the skin model in this chapter, where the proliferation and distribution of the cells must be evaluated.

A round of experiments was arranged involving five skin-on-a-chips, each initially containing 3 x 10^4 cells, and subjected to 24 hours of incubation with two parallel laminar flows at 0.4 µL/min to perform this analysis. On DIV 10, a 100 µL solution of the CDFDA reagent at 25 µM was injected, followed by a 30-minute incubation period before the microscope imaging of the cultures.

The results, depicted in Figure 82, illustrate the condition of the cultures after DIV 9. The images depict a complete monolayer of HPF cells exhibiting the characteristic morphology of fibroblasts. While this pattern can be distinguished in images captured in transmitted light, the fluorescence pictures truly reveal the distribution of cells on the membrane. This observation is intriguing as it hints at a direct influence of flow patterns on fibroblast morphology, seemingly causing cellular stretching with an orientation perpendicular to the flow direction. across all chips. It is important to highlight that, in contrast to neuron-on-a-chip prototypes, there was no evidence of cell dragging despite the impact of flow on the culture.

This conclusive round of on-chip fibroblast culture validates the long-term culture of HPF cells in the upper chamber of the chip. This accomplishment serves as the foundation for the development of a SOC model to sustain a co-culture of human fibroblasts and keratinocytes.

6.3 SKIN-ON-A-CHIP MODEL BASED ON FIBROBLAST-KERATINOCYTE CO-CULTURE

Once the culture tests of fibroblasts and keratinocytes cells were performed individually in OOCs, the next objective was to maintain a co-culture of both types simultaneously to replicate a simplified skin model on the microfluidic chip. Considering the challenges associated with U937 cells, the decision was made to prioritize the development of an initial skin model featuring a co-culture of human-origin fibroblasts and keratinocytes on the chips and enhance the model's complexity in the future by incorporating other cell types. Both fibroblasts and keratinocytes would be introduced into the upper compartment of the chip, aiming to emulate a bilayer skin model. Meanwhile, the lower compartment would remain cell-free to accommodate immune cells in future iterations of the SOC model.

After having previously optimized the culture conditions for both primary human fibroblasts and keratinocytes, the following methodology was used to reproduce the co-culture of these two cell types:

1. Sterilization of both the chip and tubing.
2. Connection of the chip and tubing within a laminar flow hood and their subsequent priming with DMEM F12 medium supplemented with 10% FBS and 1% Pen/Strep using 5 mL syringes until the outlet tubings are fully filled.
3. HPF cell seeding in the upper chamber of the chip by injecting a 100 µL solution of DMEM F12 containing 3 x 10^4 HPF cells.
4. 24-hour incubation period to allow cell adhesion.
5. Maintenance of fibroblasts with a parallel dual flow rate of 0.4 µL/min until DIV 7.
6. Injection of a 100 µL solution of the CDFDA reagent at 25 µM on DIV 8.
7. 30-minute incubation period, following by the reconnection of the chips to the microfluidic system with a parallel dual flow rate of 0.4 µL/min.
8. Injection of a 100 µL solution of DMEM-F12 with 2 x 10^4 prelabeled HaCaT cells with CMTPX on DIV 9.
9. 2-hour incubation period of HaCaT cells in the chip.
10. Sustaining the co-culture of HaCaT and HPF cells on the chip with a parallel dual flow rate of 1 µL/min.

The chip maintenance was carried out in a cell incubator at 37°C, 5% CO_2 atmosphere under humidified conditions, while the perfusion pumps remained outside the incubator. Viability and confluence assessments were conducted using optical microscopy with fluorescent labeling.

6.3.1 HPF-HaCaT co-culture results

As previously remarked in monocultures of various adherent cell lines, the clear visualization of cell position and morphology is challenging without the use of fluorescent labeling, and it is even more difficult to identify different cell lines over the same surface area.

To address this issue, two distinct cellular fluorescent markers were employed, each designed to label a specific cell type. This approach allowed for the acquisition of images where cell distribution of each cell type could be easily visualized. The markers used were CMFDA, previously utilized with HPF cells and the CMTPX marker. These markers had different signal wavelengths, enabling the acquisition of images without signal interference. The staining methods could be applied in two ways: labeling the cells after they are attached to a surface or pre-labeling the cells before seeding them.

HPF cells were pre-cultured in the SOC cultures for seven days to stabilize the culture and create a fibroblast monolayer. On DIV 8, a 100 µL solution of DMEM F12 containing CMFDA at a concentration of 25 µM was injected, followed by a 30-minute no-flow incubation. After incubation, 500 µL of culture medium was perfused through both compartments of the microfluidic chip to remove any residual staining.

The following day (DIV 9), 2 x 10^4 HaCaT cells pre-labeled with CMTPX were injected. To pre-stain the cells, a solution with the desired cell quantity was prepared in a 1.5 mL microtube. The tube was then centrifuged, and cells were resuspended in 200 µL of DMEM F12 culture medium with the addition of CMTPX cell tracker at 25 µM. After incubating the cells in the dark for 30 minutes, they were centrifuged again and resuspended in 100 µL to be injected into the chip.

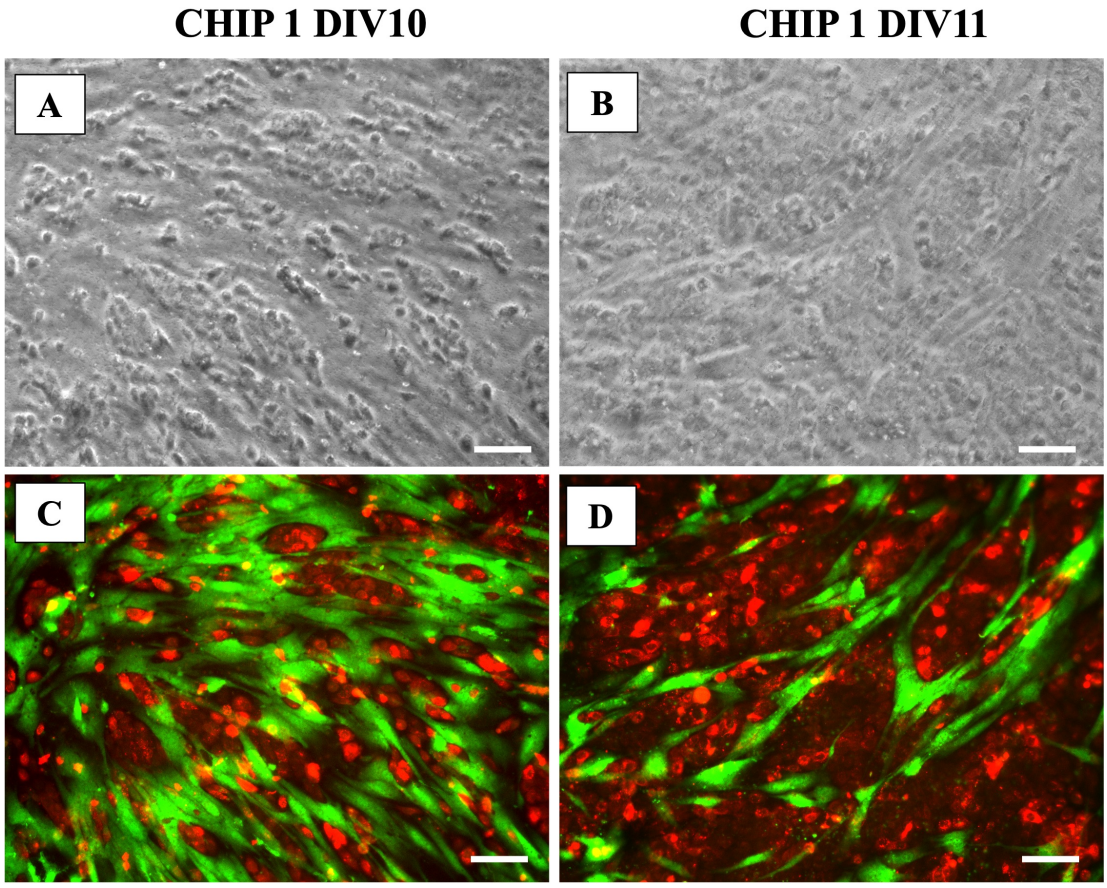

Figure 83. Images of HPF-HaCaT co-culture after 10, and 11 days in vitro (DIV) after connecting chip 1 to the microfluidic system for the first time. The co-culture was supplied with a dual parallel continuous flow of 1 µL/min. HaCaT cells are represented in red, HPF cells are represented in green. Scale bars represent 100 µm.

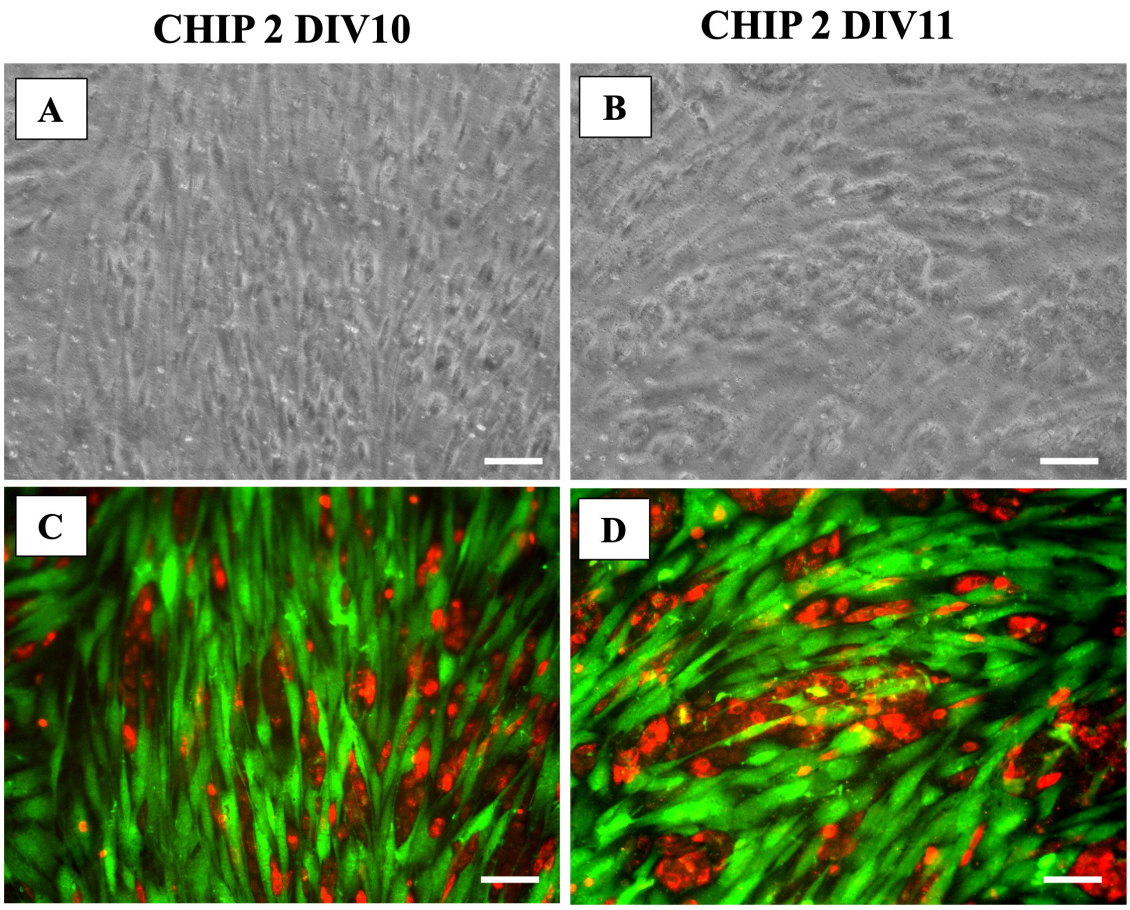

Figure 84. Images of HPF-HaCaT co-culture 10, and 11 days in vitro (DIV) after connecting chip 2 to the microfluidic system for the first time. The co-culture was supplied with a dual parallel continuous flow of 1 µL/min. HaCaT cells are represented in red, HPF are represented in green. Scale bars represent 100 µm.

Once the HaCaT cells' adhesion was achieved, microscopic images were captured to observe the cell distribution (Figures 83,84). The results indicate that while both cell types coexist inside the chip, the previously established fibroblast monolayer (green signal) before keratinocyte seeding is not maintained. Instead, the HaCaT cells (red signal) displace the previously attached fibroblasts and occupy their position on the membrane. Chip co-cultures were maintained until day 15 with an optimal fluorescent signal. A trend was observed in which Hacat cells proliferated on the membrane, gradually replacing the previously adhered HPF cells.

The results indicate that co-culturing HPFs and HaCaTs in the same microfluidic compartment did not generate a cell bilayer despite seeding each type of cells on different days. In both Figure 83 and 84, transmitted light images show distinct cell textures: one is flatter and elongated, corresponding to fibroblasts, while the other has a more compact appearance associated to keratinocytes. This pattern difference is also reflected in the fluorescence images, which reveal a lack of signal overlap between red and green. Instead, there is complementation in the fluorescence merge images, without areas in the fluorescence images devoid of red or green signals. Although the intended skin model was not achieved (Figure 85A), a stable co-culture in

the SOCs was established, with detectable fluorescence signals from both cell types in all the chips up to DIV15 (Figure 85B).

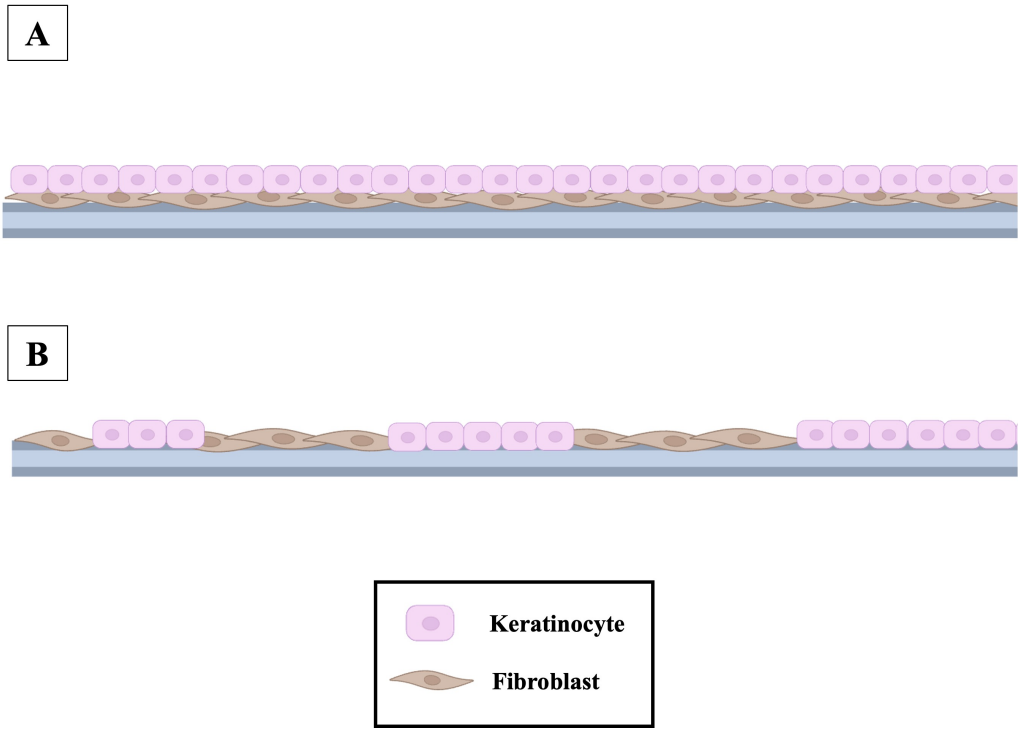

Figure 85. A) Expected fibroblast-keratinocyte co-culture model. B) Achieved fibroblast-keratinocyte co-culture model. Created with Biorender.com

6.3.2 Melanoma-on-a-chip concept

After having achieved a functional co-culture of fibroblasts and keratinocytes and having validated the distribution of the cells with the fluorescent trackers, the subsequent objective was to increase the complexity of the skin model by introducing an additional cell line. SK-MEL-28, consisting of melanoma cells, was chosen for this purpose. The selection of this cell line aligns with the primary applications of OOCs, their utility in drug testing, disease therapy development, and personalized medicine. Being able to replicate a melanoma model in an OOC would enable the testing of an anticancer drug, such as Gemcitabine, through the injection system present on the chip (Figure 86).

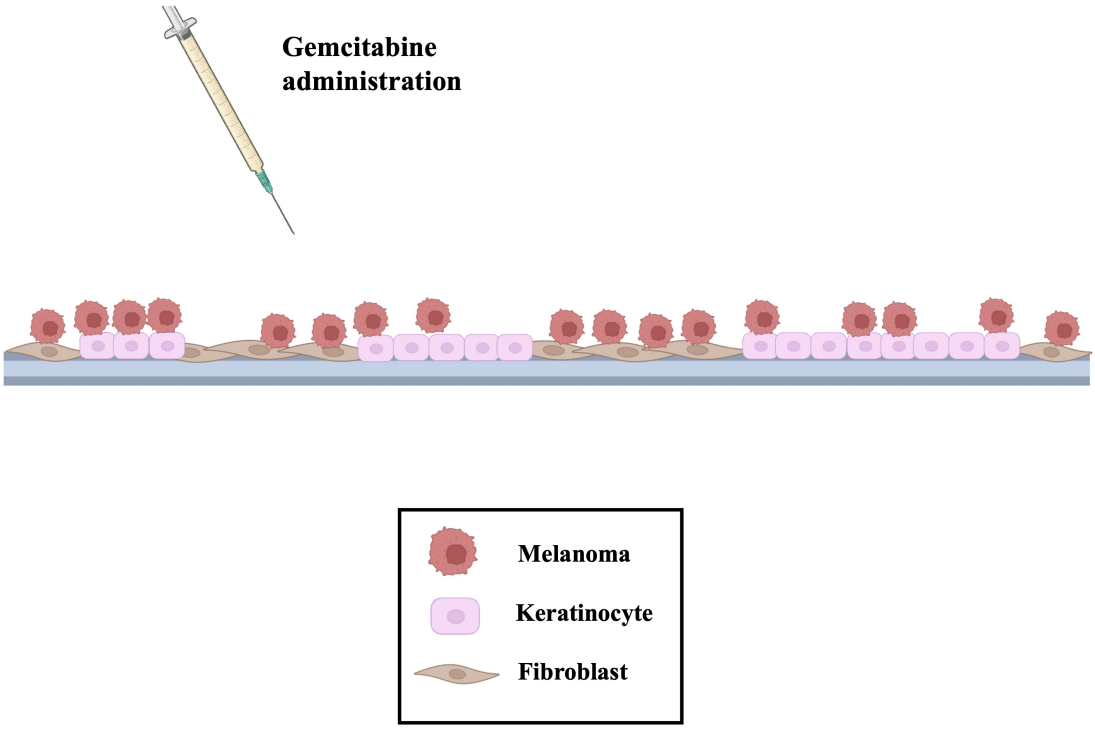

Figure 86. Schematic representation of the skin model discussed in section 6.3.2.

A melanoma-on-a-chip was developed, introducing a third cell line, SK-MEL-28, a human melanoma cell line, to create a triple cell co-culture, replicating a skin cancer-on-a-chip model suitable for drug development. The melanoma-on-a-chip concept has as its starting point the co-culture of HPT-HaCaT cells achieved in the previous section. Initially, a stable co-culture of keratinocytes and fibroblasts was established, followed by the seeding of melanoma cells. Regarding the methodology employed to assess co-culture viability, CMFDA and CDTPX trackers were employed, as they were the only options available capable of transmitting their signals to the daughter cells of labeled cells. HPF and HaCaT cells already seeded within the chips were co-stained with CMFDA, while SK-MEL-28 cells were specifically stained with CDTPX to differentiate the cell types. This approach was chosen in the context of the melanoma-on-a-chip to evaluate tumor cell proliferation and their subsequent response to drug administration. For the characterization of the melanoma model, the following procedure was implemented in two chips:

1. 2 x 10^4 HPF cells were seeded onto the PET membrane inside the upper chamber of the fluidic chip via the injection system.
2. After 24 hours, the chip was connected to the pumping system, and HPF cells were cultured under fluidic conditions at a flow rate of 0.4 µL/min.
3. Following three days, 3 x 10^4 HaCaT cells were seeded on the HPF monolayer formed inside the chip to establish a stable co-culture.

4. At DIV 5, fluorescence labeling was performed with the fluorescence CMFDA tracker to stain the HPF-HaCaT co-culture. A 100 µL solution of DMEM F12 containing CMFDA at a concentration of 25 µM was injected, followed by a 30-minute no-flow incubation.
5. After the incubation, 500 µL of culture medium was perfused through both compartments of the microfluidic chip to remove any residual staining.
6. In DIV 7, 1 x 10^4 SK-MEL-28 cells were previously labelled with CDTPX (25 µM) were introduced on the chip by injection.

The time required for fibroblast monolayer formation was reduced to two days, as the monolayer was achieved in that period. Subsequently, culture steps for HaCaTs, SK-MEL-28, and fluorescent staining were performed to prevent excessive proliferation of HaCaT cells. This precaution was taken to avoid negatively impacting the model by reducing the fibroblast population and to obtain images with a sufficient signal from the two fluorophores.

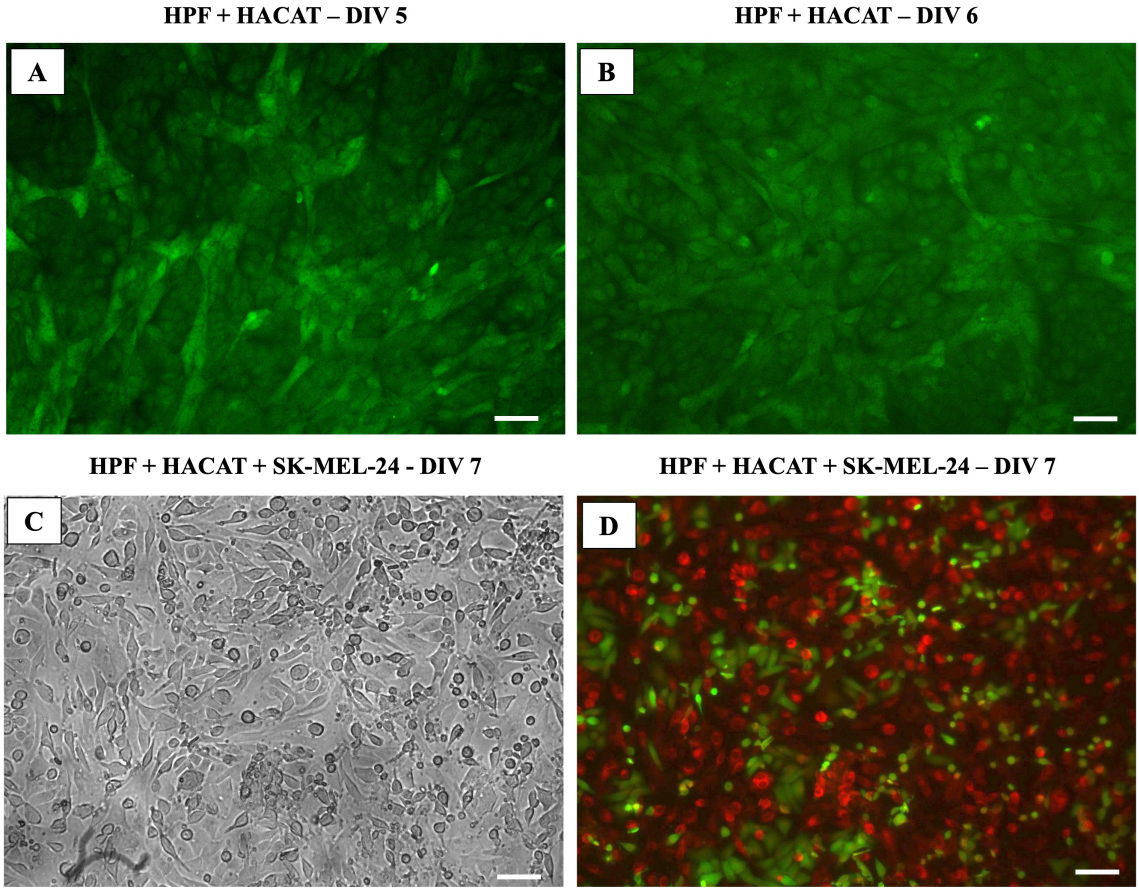

Figure 87. Images of a co-culture of fibroblasts, keratinocytes, and melanoma cells in a skin-on-a-chip model. Images A and B illustrate the co-culture of HPF and HaCaT cells. Image C shows the appearance of the culture after seeding SK-MEL-28 cells in bright field, and D presents the same image in fluorescence. HPF and HaCaT cells are represented in green, while SK-MEL-28 cells appear in red. Scale bars represent 100 µm.

Figure 87 illustrates the evolution of the cultures within the SOCs. The first image (Figure 87A), taken on DIV 5, shows the striated morphology of the fibroblasts, contrasting with the 'brick' morphology of the keratinocytes, which form clusters in the upper part of the image. Figure 87B, captured the following day, reveals increased HaCaT proliferation, making harder distinguish the fibroblasts. Finally, images C and D display the state of the triculture, with a predominance of SK-MEL28, even though they have been inside the microfluidic chip for only 24 hours (Figure 87D, red signal). While SK-MEL-28 cells are the dominant presence on the chip, the presence of a green signal in Figure 87D implies the coexistence of multiple cell types. At this point in the culture, a drug testing trial was performed on the two chips to compare the response of a chip exposed to an anticancer drug to that of one without this stimulus. In this context, Gemcitabine, a drug selected for its relevance and appropriateness, was chosen for experimentation.

Gemcitabine, an analog of deoxycytidine and an antimetabolite is a broad-spectrum anticancer medication that is commonly prescribed against ovarian, pancreatic cancer, lung and breast, among others (Beutel & Halbrook, 2023; Dent et al., 2008; Lorusso et al., 2005). To examine the potential impact of Gemcitabine on the co-culture, two melanoma-on-a-chip models were created, each containing a co-culture of HPF, HaCaT, and SK-MEL-28 cells. One of these models was subjected to Gemcitabine treatment, while the other served as a control without any treatment. The drug was administrated using the same method employed for cell seeding, involving the injection of 100 µL of Gemcitabine (6 µM) through the PTFE plug. A three-hour incubation period was performed, followed by perfusion of culture medium into both microfluidic compartments to eliminate the residual drug. After 24 hours, the control chip and the Gemcitabine-treated chip were examined under a microscope.

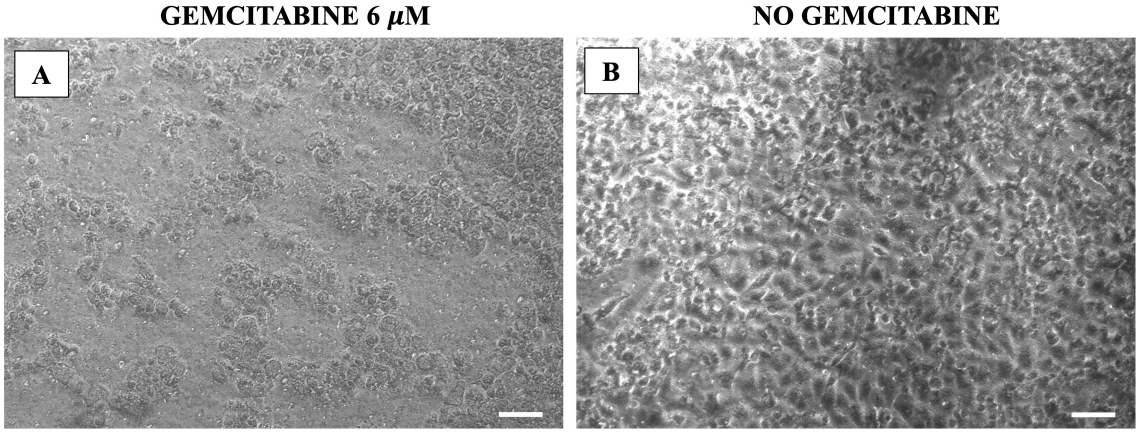

Figure 88. Co-culture of HPF, HaCaT, and SK-MEL-28 cells before treatment with Gemcitabine (A) and after treatment (B). Scale bars represent 100 µm.

The images revealed a more compromised culture and an increased occurrence of cellular death in the chip subjected to Gemcitabine treatment, in contrast to the untreated co-culture, which exhibited a healthy and stable appearance (Figure 88). Fluorescence microscopy was not

employed for image acquisition due to the diminishing intensity of cell trackers after 4 days, which could lead to potential misinterpretation of the fluorescent signal and consequently result in inaccurate conclusions regarding the behavior of the cells. Due to this, it is not possible to distinguish the cell type of the cells that remain viable on the Gemcitabine-treated chip.

With this proof of concept of 'melanoma on a chip,' it was possible to test an anticancer drug using the chip's injection system and compare the state of the triculture of fibroblasts, keratinocytes, and melanoma cells with and without Gemcitabine exposure. Noticeable differences exist between the cultures, indicating a direct impact of drug administration on the cell state. By optimizing this co-culture of three cell types and conducting a more detailed study on the effect of Gemcitabine on the culture, an alternative skin model with the potential to evaluate potential drugs for melanoma cancer could be achieved. By collecting biopsies from patients with this disease, melanoma-on-a-chip could become a tool for personalized medicine. These results, which demonstrate the construction of a skin-on-a-chip by injecting fibroblasts and keratinocytes, and the subsequent proof-of-concept of a melanoma-on-a-chip, have been used as the basis for a scientific article currently in the submission process.

6.3.3 International research collaboration with University of Hull

During the last year of the doctoral thesis, it was possible to carry out an international stay in collaboration with the University of Hull. This collaboration provided an excellent opportunity to test the microfluidic chips developed at UPM with new microfluidic systems and to evaluate the compatibility of these chips in a different working environment.

The specific objectives defined for this international stay were:

- To test new immune cell types that can be integrated into the SOC model using a recirculating microfluidic system based on a peristaltic flow system.
- To replicate the skin co-culture, which was initially performed at the CTB in the facilities of the University of Hull, demonstrating the reproducibility of the proposed methodology.
- To evaluate and compare the performance of PDMS-vinyl-glass microfluidic chips with a miniaturized peristaltic system developed by the host group at the University of Hull against a microfluidic setup composed of perfusion pumps.

6.3.3.1 Jurkat culture – peristaltic system

The first experiments performed in University of Hull facilities was the testing of a single-chamber chips made of PDMS, vinyl, and glass with Jurkat cell line, an immortalized T lymphocyte cell. This custom-designed chip comprises a single vinyl layout with microfluidic

geometry nearly identical to the SOC's lower compartment, including a pre-chamber injection (Figure 89).

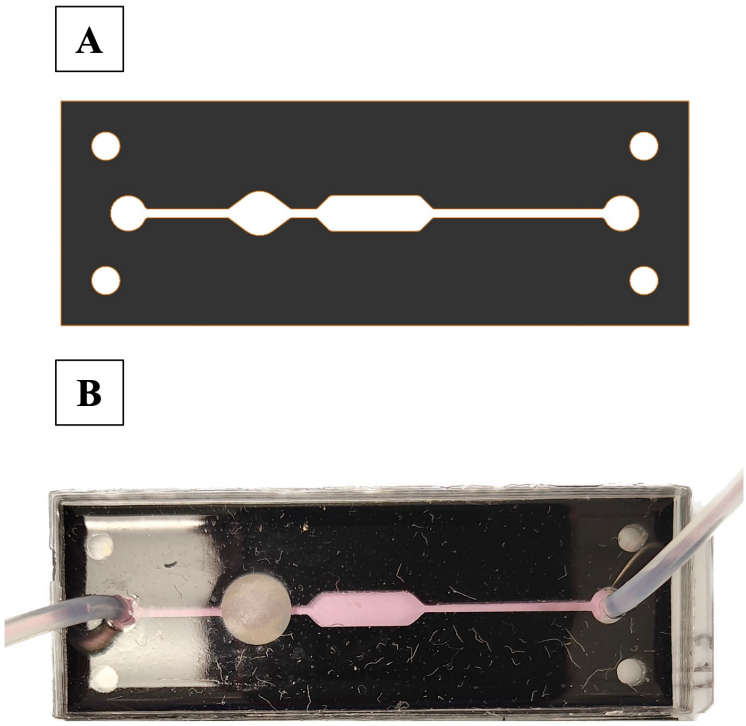

Figure 89. Layout (Design (A) and picture of the custom single-chamber OOC device (B) used to perform the peristaltic system and cell recirculation tests on microfluidic chips.

One of the biggest challenges in this thesis has been the integration of immune system cells into the skin model discussed in this chapter. Therefore, working with new cell types using the technology previously developed in the CTB was an ideal approach to initiate the collaboration between the two groups. Currently, the University of Hull group is working on developing a closed microfluidic platform to recirculate immune cells and simulate their in vivo behavior in the bloodstream. The microfluidic platform designed for this purpose includes a miniaturized peristaltic pump, which members of the group have developed. This choice was made because syringe perfusion pumps, commonly used in OOC systems, cannot be used when cells must be kept circulating in a closed system.

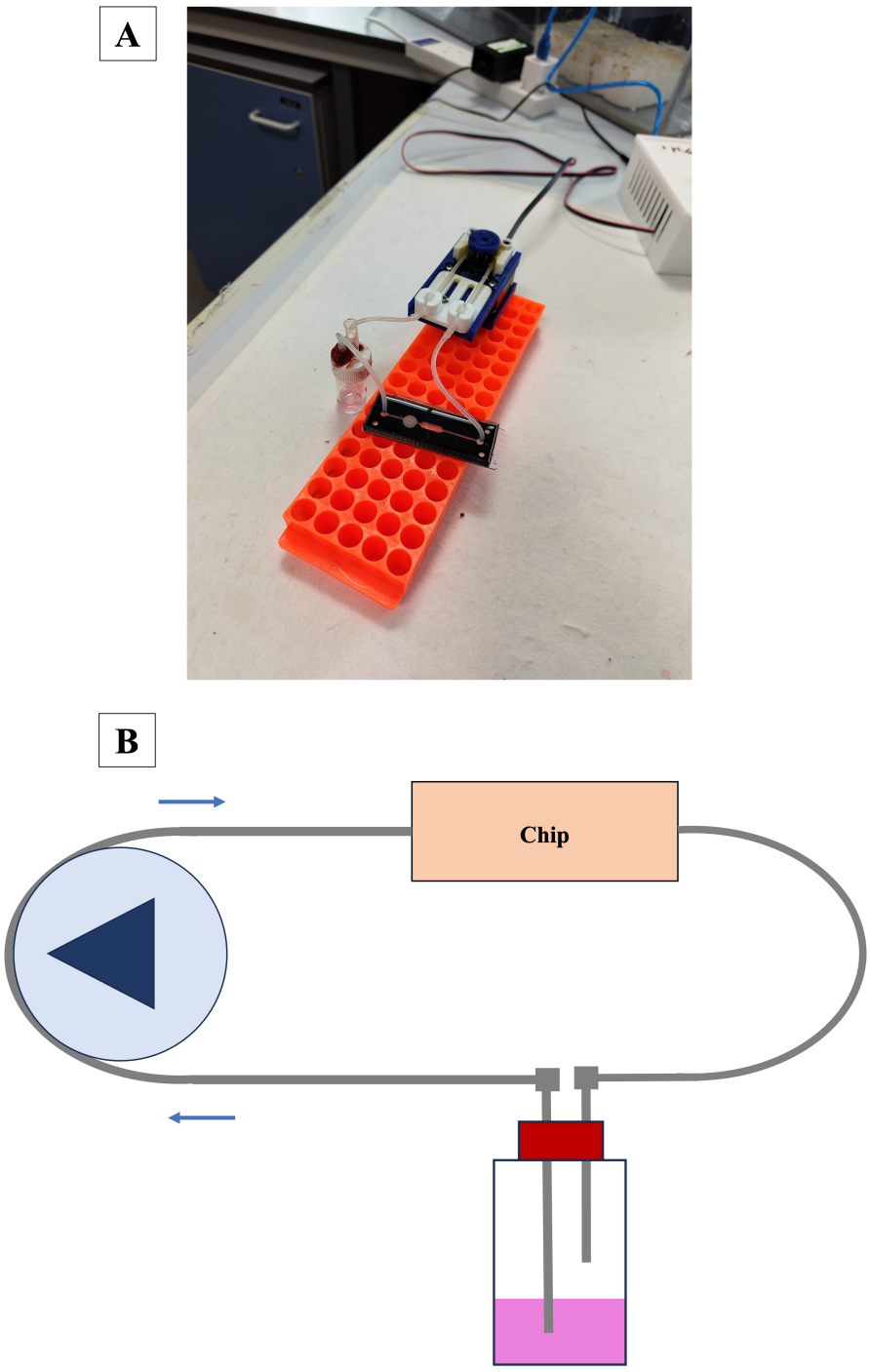

Figure 90. A) Alternative microfluidic setup using a peristaltic pump. B) Diagram of the microfluidic setup.

The microfluidic setup for the initial test, combining the vinyl microfluidic chip with the peristaltic pump, is illustrated in Figure 90. It consists of a glass reservoir containing 1 mL of cell solution with one million Jurkat cells. The diagram shows that the tube through which the cells are aspirated is completely submerged in the culture medium. The cells within the 1 mL of medium are aspirated using the force generated by the peristaltic pump, which was programmed to achieve a flow rate of 2 µL/min. After exiting the peristaltic pump, the tubing is connected to the vinyl chip, and the outlet tubing is directed back to the initial reservoir. It is worth noting that

the end of the outlet tubing is positioned above the level of the cell solution. This positioning was chosen to allow any air or bubbles generated along the microfluidic system to be eliminated without introducing potential microbubbles into the cell solution. The entire microfluidic setup was placed in an incubator at 37ºC without CO_2 supply and humidity. The choice to avoid maintaining a humid environment within the microfluidic platform was made to safeguard the electronic components of the peristaltic pump from potential damage or malfunctions.

The chip was observed 17 hours after connecting it to the microfluidic system. The device did not leak, but several bubbles were generated inside the microfluidic chamber. In Figure 91, cells could be observed inside the chip, effectively demonstrating cell aspiration with the peristaltic system. However, the size of the particles retained on the chip was smaller than that of cells cultured in a control reservoir without flow. This phenomenon was consistently observed in all tests using the peristaltic pump. A literature review was conducted to investigate whether a similar phenomenon occurred in similar studies using peristaltic pumps. Uesugi et al. reported that when cells pass through the tubing connected to a peristaltic pump with pins, cell crushing can occur, potentially explaining the reduction in cell size observed on the chip (Uesugi et al., 2020).

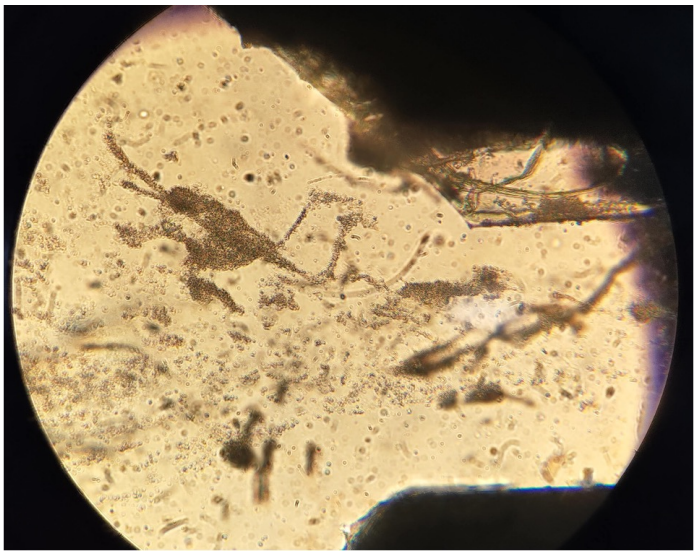

Figure 91. Qualitative image of the microfluidic chamber of the skin-on-a-chip after 17 hours under continuous flow conditions.

6.3.3.2 Cell distribution trial

As it was not feasible to guarantee the preservation of cell integrity within a closed system comprising peristaltic pumps, an alternative methodology was pursued to sustain Jurkat cells in suspension, replicating their conditions in an in vivo setting. Additionally, the objective was to

assess the consequences of resuspending cells within the reservoir from which they were drawn. Without any agitation, cells tended to settle at the vessel's base, resulting in challenging cell aspiration. To examine this phenomenon, an experiment was conducted employing two microfluidic chips: one chip underwent manual agitation in a15 mL Falcon tube for 10 seconds every 10 minutes, containing a 1 mL solution comprising one million Jurkat cells, while the other remained stationary.

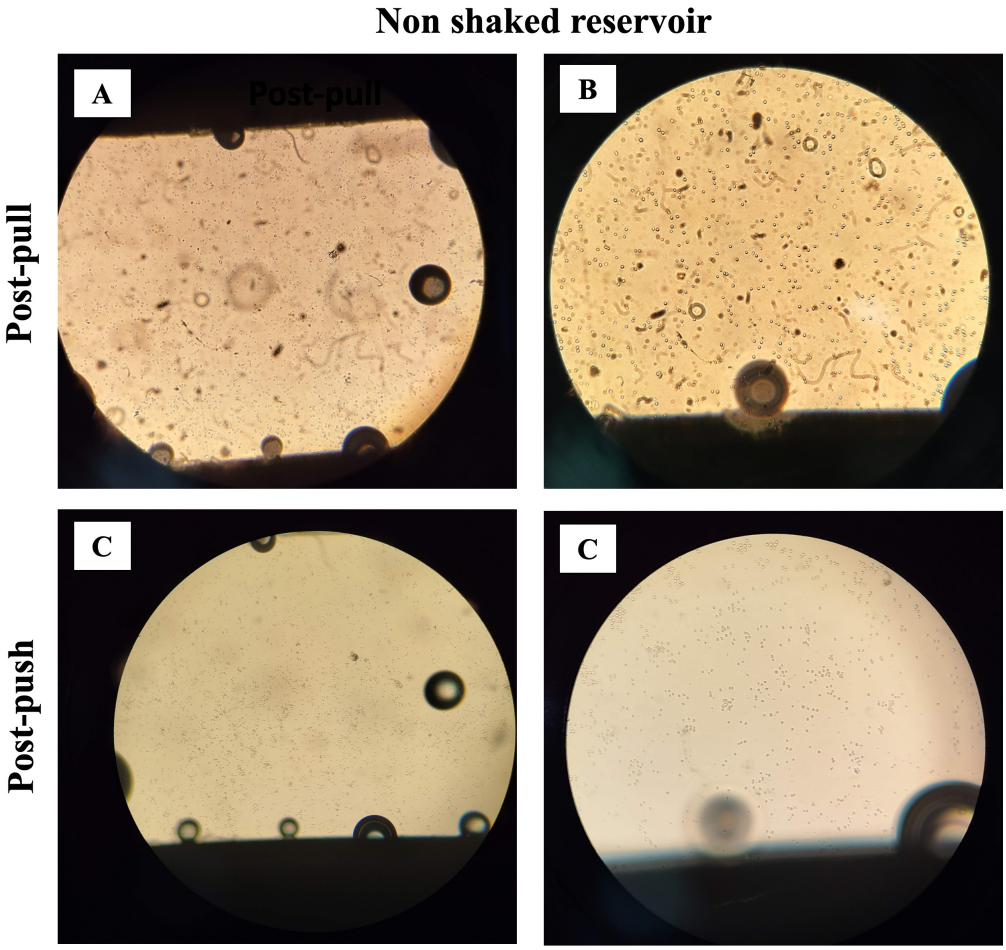

Figure 92. Qualitative pictures of a single-chamber chip during the cell aspiration experiment under non-shaking conditions. Images A and B show the microfluidic chamber after an aspiration process; images C and D show the state of the microfluidic chamber after the subsequent perfusion phase.

Following the setup, a half milliliter of each solution was aspirated using a perfusion pump set at a flow rate of 10 µL/min for 50 minutes. One hour after being connected to the equipment, the chips were examined under a microscope. A notable distinction became apparent between the chips subjected to varying conditions: chips with the agitated reservoir displayed a microfluidic chamber completely filled with cells, whereas chips without agitation exhibited only a minimal number of cells. Figures 92 and 93 illustrate images of the microfluidic chamber surfaces of the tested chips after the aspiration phase (post-pull) and the infusion phase (post-push). In both chips, the presence of cells is evident, but a significant disparity is noticeable between the chip without

reservoir agitation and the chip with continuous reservoir agitation. The latter exhibits a notably higher cell population.

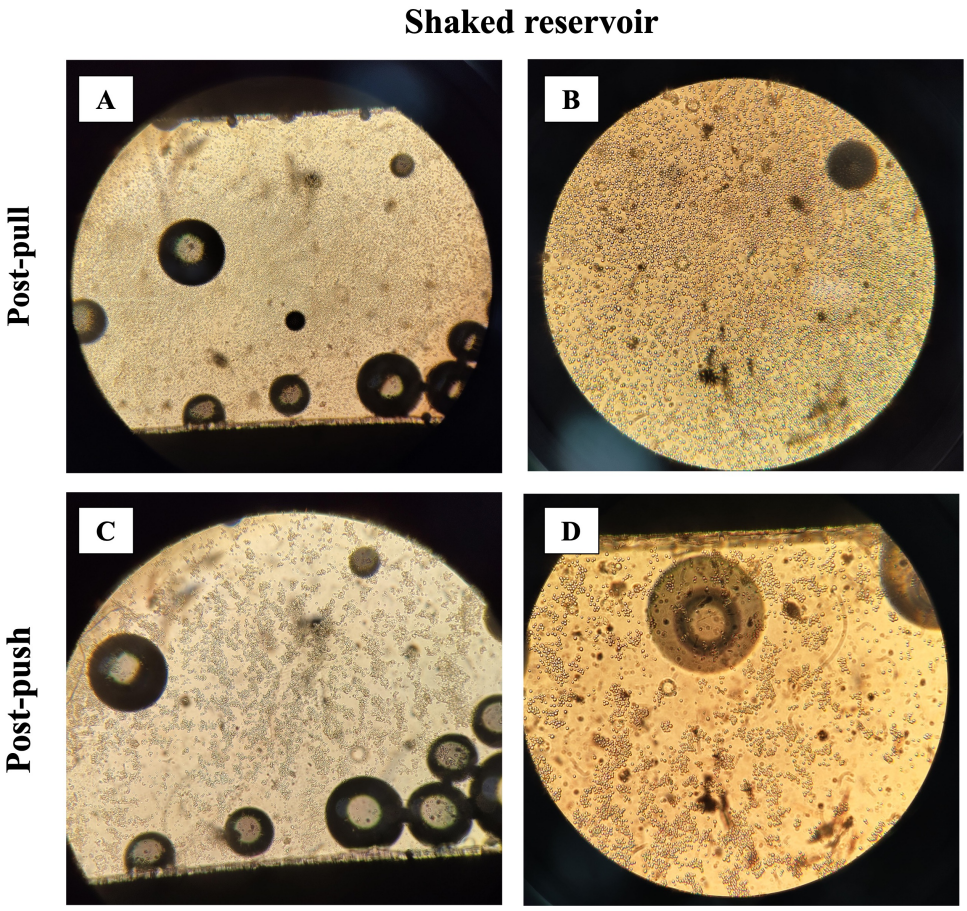

Figure 93. Qualitative pictures of a single-chamber chip during the cell aspiration experiment under shaking conditions. Images A and B show the microfluidic chamber after an aspiration process; images C and D show the state of the microfluidic chamber after the subsequent perfusion phase.

This test revealed several key findings. Firstly, subjecting the cell solution to agitation conditions increased the number of cells that can be aspirated and recirculated within a microfluidic system, potentially reducing the number of cells stored in the reservoir. Secondly, based on the chip geometry used in this test, it became evident that all cells remained trapped within the chip after the infusion step. Thus, redesigning the microfluidic chamber would be imperative to mitigate this effect if the objective of the microfluidic system is to facilitate cell recirculation. Lastly, in contrast to the test conducted with the peristaltic pump, the cells exhibited a more prominent appearance in this experiment, supporting the hypothesis that the pins of the peristaltic pump were indeed causing cell compression.

6.3.3.3 Fibroblast-HaCaT co-culture replication

Because of the cell viability issues encountered when using peristaltic pumps, a reorientation of the experiments was made toward replicating the skin model based on the co-culture of fibroblasts

and HaCaT cells. To achieve this, the HFF cell line was employed as an alternative to HPFs. This choice was motivated by the desire to investigate whether the displacement of fibroblasts observed in previous tests on PET membranes was attributable to the primary nature of the cells or if it could be mitigated by using a commercially available cell line.

Initially, for the fibroblast-keratinocyte co-culture tests conducted on dual-chamber microfluidic chips, a setup commonly used by the host group at the University of Hull. This setup included a multi-syringe perfusion pump and incubators capable of maintaining temperature without the need for additional carbon dioxide and humidity. This configuration without incubators with carbon dioxide supply offered improved accessibility and manageability for the cultures.

The same protocol employed in subsection 6.3 was replicated with slight modifications, including the use of DMEM medium (10% FBS, 1% Pen/Strep). The steps involved:

1. Sterilization of both the chip and tubing used for cell culture.
2. Connection of the chip and tubing within a laminar flow hood, followed by priming these components with DMEM medium using 20 mL syringes until the outlet tubing were completely filled.
3. Seeding of 100 µL of DMEM medium containing a total of 3 x 10^4 human fibroblast cells into the upper compartment of the chip through the upper inlet port.
4. A 24-hour incubation period without any flow to facilitate cell adhesion.
5. Connection of the perfusion pump with a flow rate of 0.4 µL/min.

The 24-hour incubation took place in incubators at 37°C with humidity but without CO_2 input. In the initial test, cell adhesion to the membrane was checked at 24 hours. No living cells were observed when the culture was re-examined at 72 hours after seeding. To address the lack of carbon dioxide in the incubators, the culture medium was supplemented with HEPES buffer (25 mM) to adjust the medium's pH. The experiment was subsequently repeated with two new chips, yielding virtually identical results, with isolated cells still attached to the membrane after 72 hours of culture.

Following the initial findings of null cell survival and adhesion in the dual-chamber chips, it was decided to replicate the experiment seeding only HaCaT cells. This particular cell line had previously shown success in the chips, in contrast to HFF cells, which represented a different type of fibroblast. By making this shift in cell type, the aim was to confirm that the lack of cell survival was indeed attributed to the absence of CO_2 supply.

Two chips were employed, each receiving an initial cell population of 2 x 10^4 cells. After 24 hours, microscopic observation revealed that the cells exhibited a spherical shape instead of their typical "brick-like" morphology. In response to these observations, the next 24 hours one chip was maintained in an incubator without CO_2 input, while the other was placed inside a cell

incubator with a 5% CO_2 supply, both chips with no flow supply. Upon inspection after this period, notable differences were observed. First, there was a noticeable change in the color of the culture medium, with the chip lacking CO_2 exhibiting a pinker appearance while the other chip had a more orange tint (Figure 94A). More significantly, there was a marked change in cell morphology in the chip that had been incubated in a 5% CO_2 environment, with the cells adhering to the membrane (Figure 94B). Conversely, in chip 2, the cells still failed to adhere to the membrane and appeared smaller than on the previous day (Figure 94C).

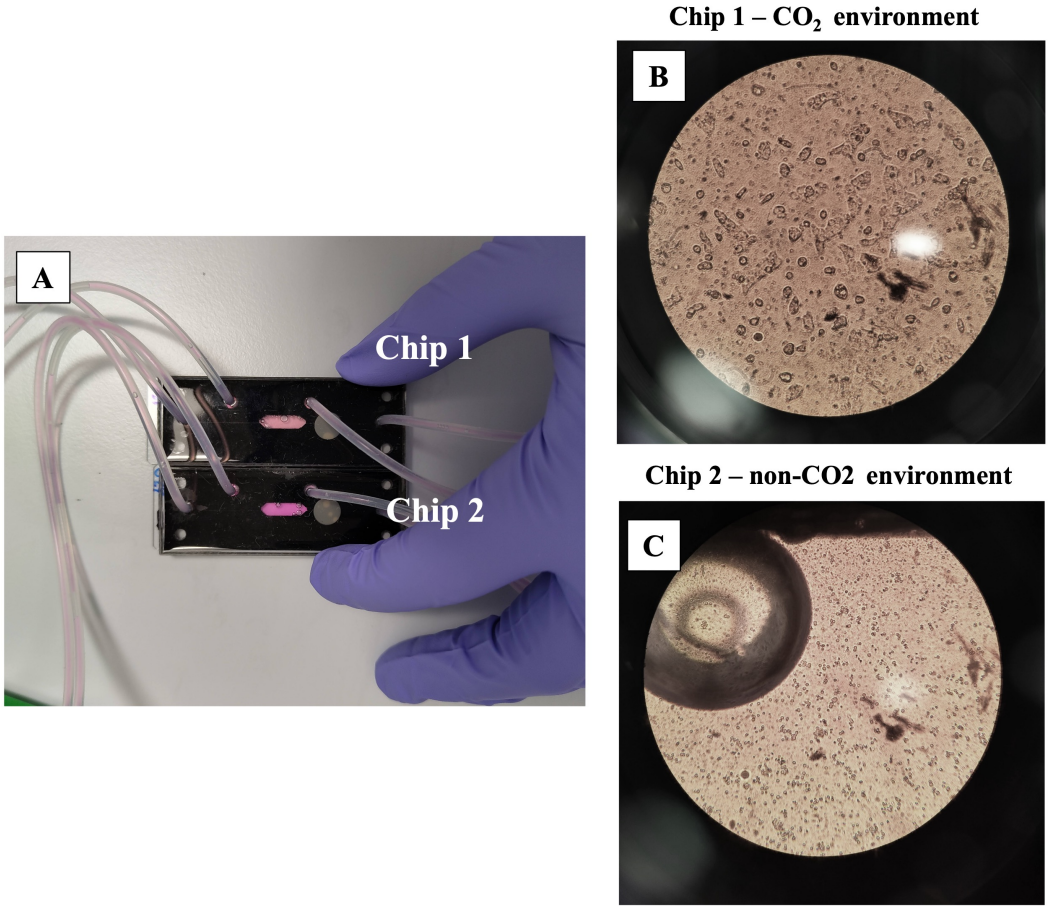

Figure 94. Qualitative HaCaT cells culture images. A) View of the culture medium in the microfluidic chip chamber. B) Chip 1 picture after been maintained 24 hours inside a gass incubator, C) Chip 2 picture after remained 48 hours.

Given these substantial disparities between the chips maintained under both conditions, the entire microfluidic system was relocated to an incubator at 37°C with a 5% CO_2 atmosphere to culture the HaCaT cells in an environment with 5% CO2 right from the start of the culture. Under these revised conditions, co-culturing was attempted on two new chips. Initial seeding involved HFF fibroblasts on both chips. These cells adhered correctly and remained viable in an optimal state until DIV 7. On this day, 2 x 10^4 HaCaT cells were introduced onto the chip. Figure 95 illustrates the condition of one of the chips on DIV 7 before the seeding of HaCaT cells and on DIV 8, after

one day of co-culture. The images depict a cell distribution equivalent to the HPF-HaCaT co-cultures performed in the CTB.

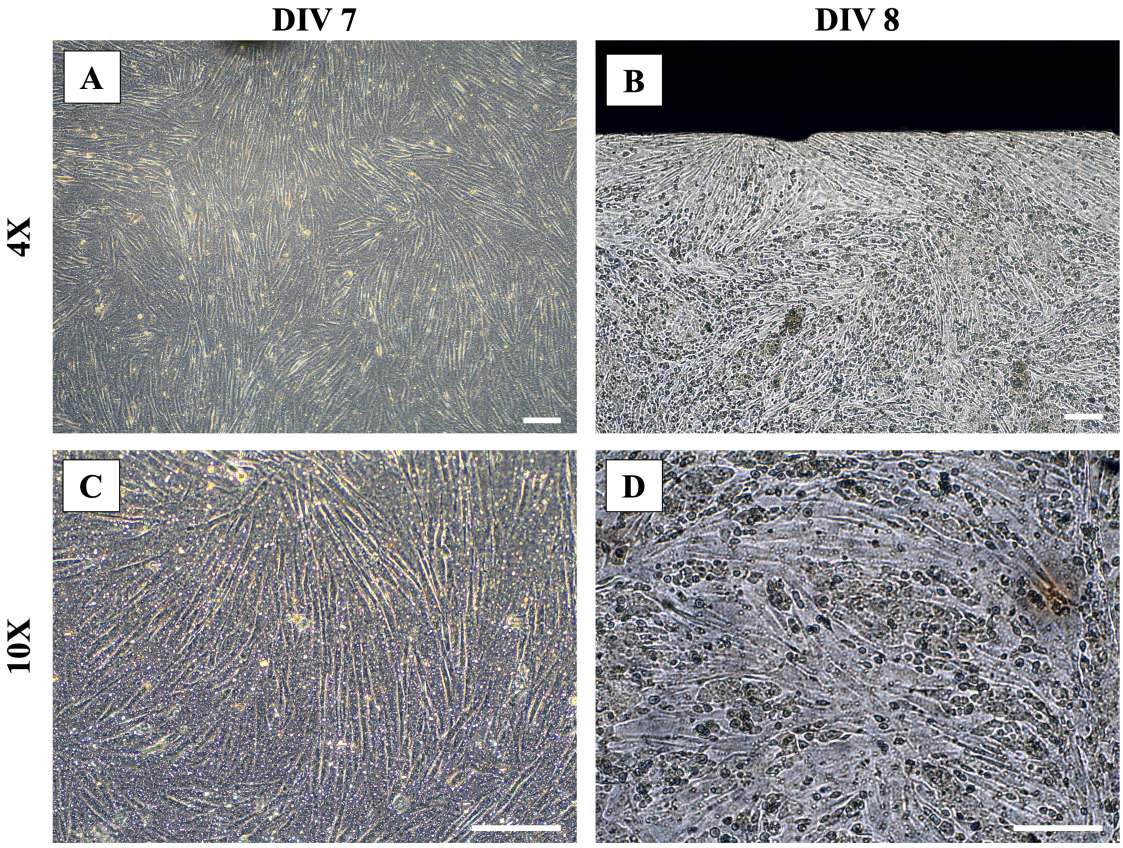

Figure 95. A, C) HFF cell culture in a double-chamber skin-on-a-chip inside a CO_2 cell incubator. B, D) Skin-on-a-chip culture 24 hours after HaCaT cell seeding on the fibroblast monolayer. Scale bars represent 100 µm.

6.3.3.4 Syringe pump culture vs peristaltic pump culture

Having successfully demonstrated the capability to co-culture fibroblasts and keratinocytes on the dual-chamber microfluidic chip within the University of Hull facility, a final in-house test was conducted. This experiment compared a chip connected to a multi-syringe perfusion pump and a chip connected to the miniaturized peristaltic pump. The chips were positioned within tip boxes filled with distilled water and securely sealed with Parafilm to prevent any potential degradation of the electronic components of the peristaltic pump, thereby maintaining a humidified environment during the culture phase. Figure 96 provides a diagram of the microfluidic setup featuring both microfluidic systems. The protocol executed in this experiment encompassed the following steps:

- Sterilization of both the chip and tubing designated for cell culture.

- Connection of the chip and tubing within a laminar flow hood, followed by priming of these components with DMEM medium supplemented with 10% FBS and 1% Pen/Strep using 20 mL syringes until the outlet tubings were completely filled.
- Seeding by pipetting through the upper inlet port of a 100 µL solution of DMEM, containing a total of 3 x 10^4 primary human fibroblasts, into the upper compartment of the chip.
- A 24-hour incubation period for the cells without any flow to facilitate cell adhesion.
- Sustaining the fibroblasts for two days under a parallel dual flow rate of 1 µL/min using the multi-syringe perfusion pump. It was necessary to set the flow rate to 1 µL/min as the chips from the previous experiment were still connected to the perfusion pump, and once HaCaT cells were introduced, a 1 µL/min flow rate was mandatory.
- Transitioning one of the chips from the perfusion pump to the peristaltic pump maintained a flow rate of 1 µL/min. This change included replacing the syringes with two glass reservoirs containing 8 mL of fresh culture media.
- Continuation of culture maintenance for both chips in the two microfluidic systems until day 6 of culture.

On DIV 6, an assessment of the chip conditions was conducted. Chip 3, which had been connected to the perfusion pump throughout the entire experiment, remained in excellent condition, with the microfluidic chambers containing an adequate amount of culture medium. In contrast, Chip 4, which had been connected to the peristaltic pump for four days after the microfluidic system change, had its lower compartment entirely emptied, along with the lower inlet and outlet tubes of the chip. Additionally, more air pockets were in the tubing section, extending from the peristaltic pump to the tubing inlet port inside the chip. Furthermore, the waste vessel contained only the eluted volume from the lower reservoir, indicating that no flow had occurred in the lower chamber since the peristaltic pump had been operational. Despite these circumstances, the fibroblasts remained viable on the membrane.

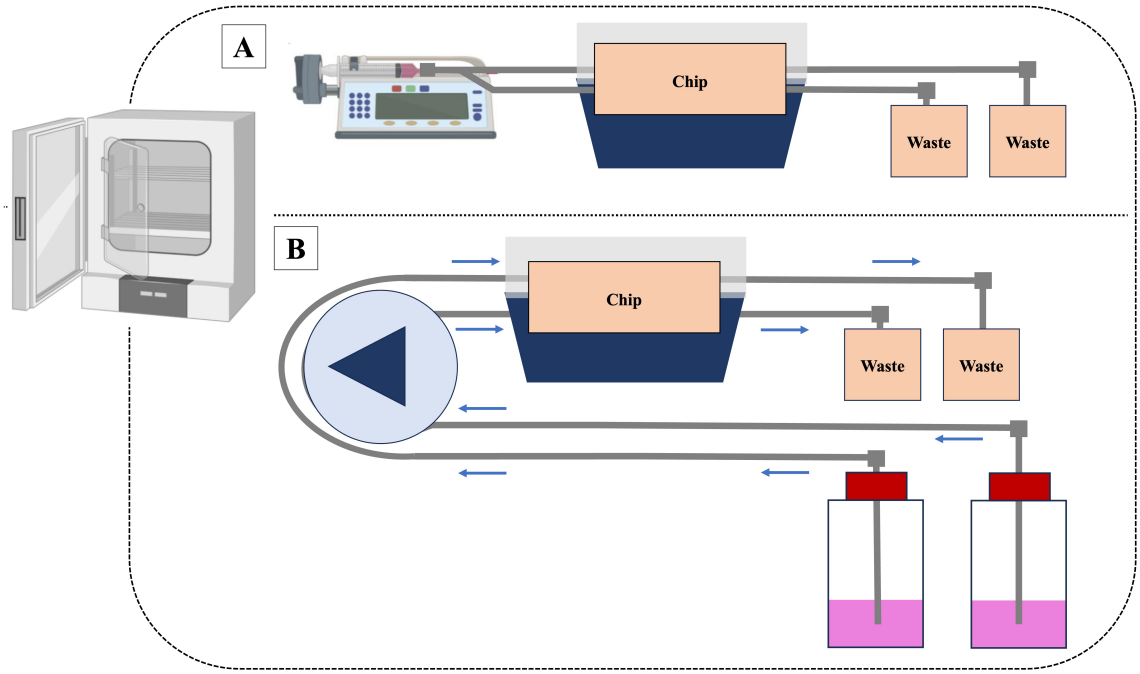

Figure 96. Schematic view of the microfluidic setups employed for the co-culture.

Figure 97 illustrates the cell status in both chips. While a similar condition was observed in both chips, there was a slight reduction in debris within the chip connected to the peristaltic pump, resulting in a clearer image of the membrane with the fibroblasts adhering to the surface.

A modification was made to the configuration of the peristaltic microfluidic set up to mitigate the potential formation of air bubbles within the tubing of Chip 4 (Figure 98). This alteration involved connecting the reservoirs containing fresh media directly to the chip and routing the outlet tubing through the peristaltic pump. Additionally, a replacement peristaltic pump with the same specifications was on standby in case of any malfunctions. The entire chip and tubing system were re-primed as part of this process.

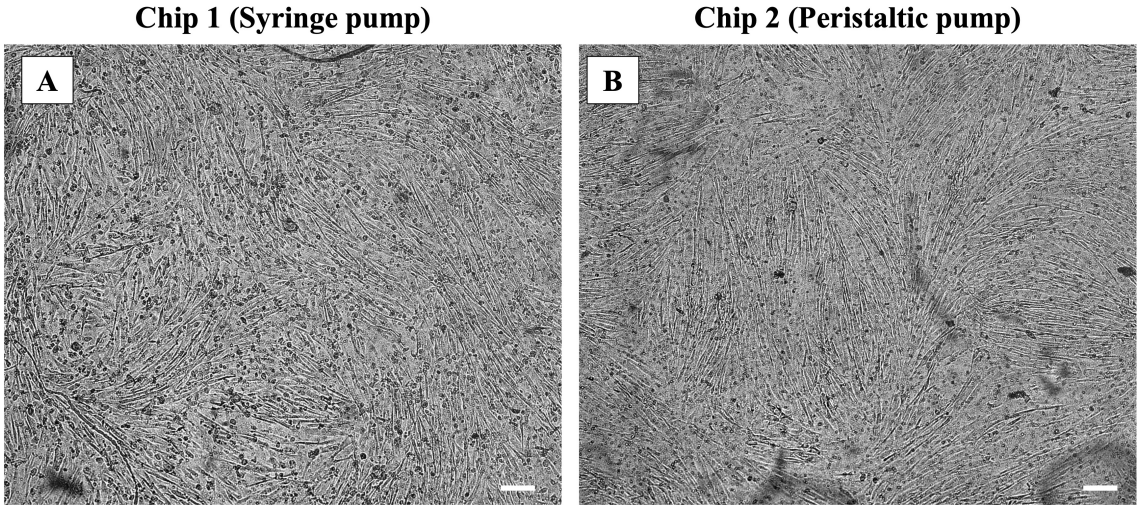

Figure 97. Comparison of HFF cell cultures in skin-on-a-chip devices with continuous flow delivered by a syringe pump (A) and a peristaltic pump (B). Scale bars represent 100 µm.

Upon comparing both setups, apart from the utilization of pumps employing different mechanisms, there was an additional distinction involving the container for storing fresh culture medium. The perfusion pump relied on syringes, which are closed and hermetically sealed containers, ensuring no pressure losses. Conversely, the peristaltic pump employed open reservoirs. This seemingly inconsequential difference held important implications: with the syringe, characterized by its closed and sealed nature, there were no pressure fluctuations, whereas the reservoirs, containing movable components like stoppers and air, were susceptible to inducing changes in the flow direction of the culture medium through the tubes, potentially altering the relative positioning of the reservoirs to the chip.

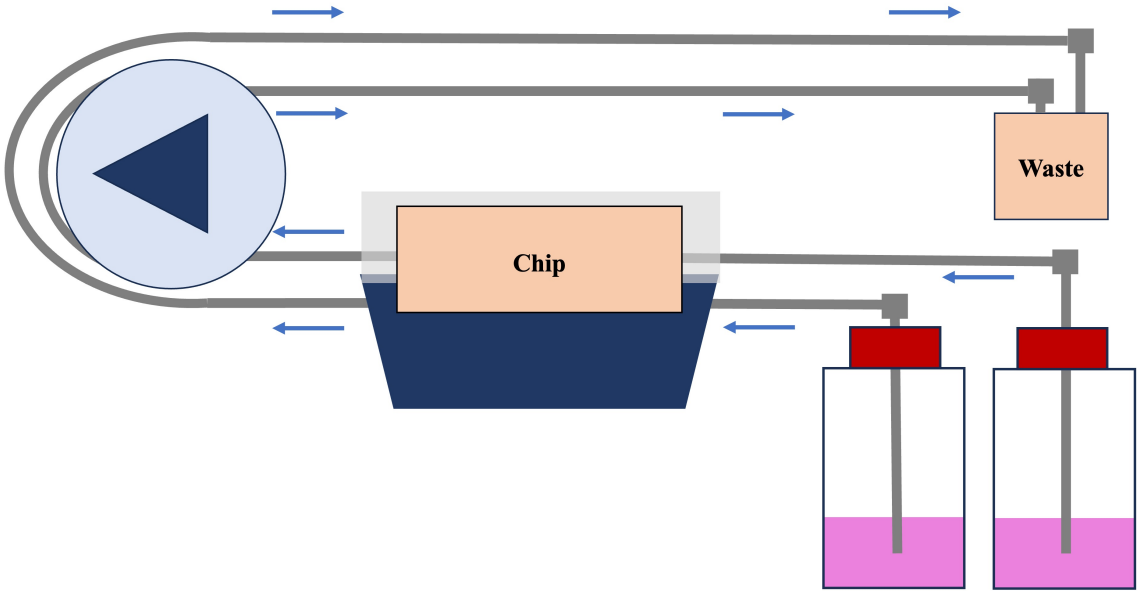

Figure 98. Diagram of the microfluidic set up reconfiguration.

Once the fibroblasts were in good conditions on the chips, HaCaT cells were introduced into the chips to initiate the fibroblast-keratinocyte co-culture. In the case of Chip 3, where syringes were connected to the inlet tubing, injecting the 100 µL solution containing 2 x 10^4 HaCaT cells proceeded without any issues. When this same procedure was repeated with Chip 4 connected to the glass vessel reservoirs, after the injection of the 100 µL the liquid did not move through the microfluidic chamber. No HaCaT cells could be observed inside the chip, indicating that the cells were moving toward the inlet tubing rather than the chip microfluidic channels. The same outcome persisted despite repeated attempts to retain the cells inside the chip by clamping the inlet tubing. The final solution employed was to manually advance the flow by moving the pins of the peristaltic pump to push the volume of the inlet tubing containing cells into the chip.

Following this seeding of keratinocytes, the chips remained without flow for two hours to facilitate cell adhesion and were connected to the microfluidic systems.

On culture DIV 8 (day 2 after seeding the HaCaT cells), a microscopic examination of the chips was conducted (Figure 99). As anticipated, Chip 3 was densely populated with keratinocytes. Conversely, Chip 4 displayed two small areas of HaCaT cell proliferation near the entrance channel. The clear demarcation of the region with HaCaT cells forming clusters provided a valuable opportunity to assess the interaction between keratinocytes and HFF fibroblasts. Figure 99B illustrates how the HaCaT cells in the central zone of the image displaced the fibroblasts by aggregating around the keratinocyte clusters, replicating the displacement phenomenon observed in the fluorescence images of subsection 6.7. Given the recurrence of this result, a reevaluation of cell distribution on the microfluidic chip became has to be considered to establish a skin model featuring two complete bilayers of keratinocytes and fibroblasts.

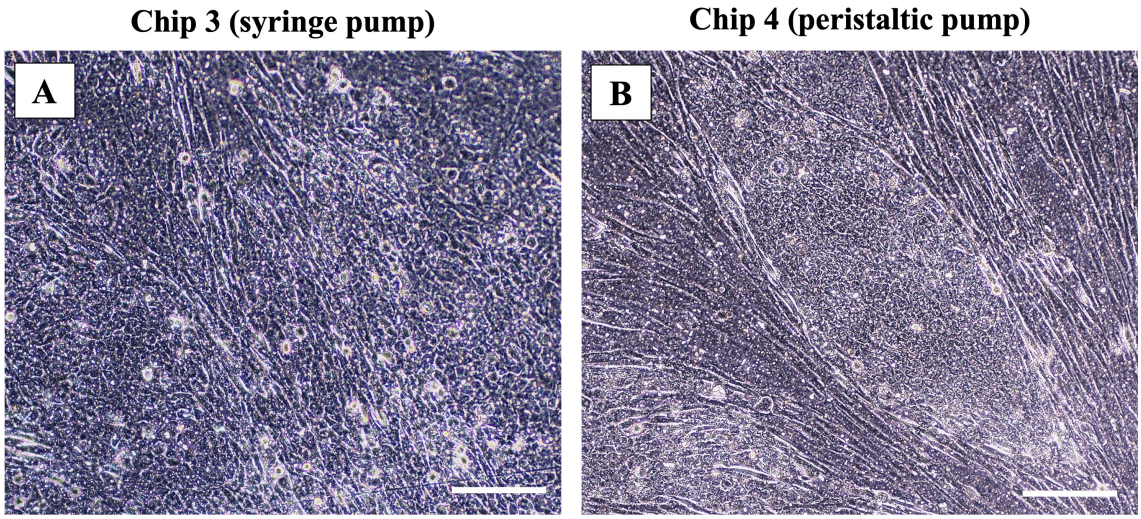

Figure 99. Comparison of HFF-HaCaT co-culture in skin-on-a-chip devices with continuous flow delivered by a syringe pump (A) and a peristaltic pump (B). Scale bars represent 100 µm.

The presence of air in the Chip 4 tubing and microfluidic chambers was also confirmed. Despite modifying the microfluidic setup of the peristaltic pump, the lower chamber was once again completely emptied, and the volume collected in the waste reservoir corresponded to a single flow instead of two flows. Since this same issue recurred with the tubing situated in the lower section inside two different peristaltic pump devices, it suggests that the failure in the chip's flow application stemmed from the operation of the peristaltic pump rather than any issue with the microfluidic chip itself.

Upon the conclusion of the three-month international stay, partial attainment of the pre-established objectives has been accomplished:

1. Jurkcat cells were cultured on the microfluidic chips using a peristaltic system and perfusion pumps in brief trials. Although the integration of this culture technique into the skin-on-a-chip model was not successful, areas for improvement have been identified to potentially recreate this model in the future. These include altering the layour of the lower compartment through which HaCaT cells would circulate, implementing a sample agitation system, and exploring alternatives to the peristaltic pump pin system to prevent mechanical cell damage during pump passage.
2. The co-culture of fibroblasts and keratinocytes was conducted in the University of Hull laboratory, following the protocol used in the CTB. The achieved results, even in the absence of fluorescence images of the culture, indicate that the co-cultures closely resemble those achieved in CTB.
3. A proof of concept was performed to compare two fibroblast-keratinocyte co-cultures: one connected to a perfusion pump and the other to a miniaturized peristaltic pump. The observed differences between the two methodologies primarily relate to the appearance of bubbles in the peristaltic system and the inability to inject volumes into the chip due to the chip's inlet tubing being connected to open reservoirs instead of syringes. As the initial fibroblast seeding was performed with the chips connected to syringes, and one of the chips was linked to the peristaltic pump, it was feasible to retain these cells within both methodologies, with less debris and cellular remnants in the chip integrated into the peristaltic microfluidic system.

6.4 CONCLUSIONS

For the design of this novel skin-on-a-chip, the brain slice-on-a-chip device was used as a reference but incorporated several modifications. Firstly, inlet and outlet ports were incorporated into the upper compartment, a feature not previously integrated. Additionally, as detailed in Chapter 5, various membranes were tested to enhance the visualization of the sample, in this case, cells, through the membrane. Ultimately, PET polymer was chosen as the membrane material, allowing the chip to be observed using a wide range of microscopes. This upgrade significantly reduces the focal length between the sample and the objective, which is particularly beneficial when employing inverted microscopes, given that the glass layer has a thinner profile than the PDMS blocks. All these innovations have led to the achievement of the following objectives with the skin-on-a-chip model:

1. A dual-chamber microfluidic chip has been successfully devised and manufactured to develop a skin-on-a-chip model, enabling the concurrent or alternating application of two parallel flows. The chosen cell distribution strategy throughout the thesis development

involved co-culturing fibroblasts and keratinocytes in the upper compartment of the chip, reserving the lower compartment for the inclusion of immune cells.

2. A fluidic characterization of the skin-on-a-chip devices was conducted to enhance understanding of their microfluidic properties. This step was needed due to the prolonged duration of the chip optimization phase, primarily attributed to a higher frequency of leaks. Calculations were performed to determine the pressure drop of the chips. This value was used to assess the functionality of the chips before cell culture within the microfluidic devices.
3. Three types of cells have been tested in the skin-on-a-chip devices: fibroblasts (which came in three different strains known as CV-1, PHF, and HFF), fibroblasts from the HaCaT cell line, and immune system cells represented by the U937 cell line. All these cell types were cultured within the microfluidic chambers of the chip, except for the U937 cell line, as the on-chip culture was found to be incompatible with the chip's sterilization methods.
4. A functional skin model based on fibroblast and keratinocyte co-culture was achieved. The state of this co-culture was evaluated using fluorescence techniques, with both cells and fluorescent markers introduced into the upper compartment of the chip via injection. The intended skin co-culture concept aimed to create two cellular bilayers. The cultures conducted in this thesis revealed that on a PET membrane, despite seeding fibroblasts on the surface, when HaCaT cells were subsequently seeded, they displaced the fibroblasts from the membrane, resulting in a mixture of the two cell types on the membrane.
5. An initial melanoma-on-a-chip model was established through the co-culture of HPF, HaCaT, and SK-MEL-28 for a proof-of-concept drug test using the injection system. Using this approach, Gemcitabine was administered in a melanoma-on-a-chip, which was then compared to another melanoma-on-a-chip that had not been exposed to the drug. This proof of concept revealed significant changes in the cell population, with a notable decrease in cell density in the chip treated with Gemcitabine.

In light of all the technological advancements achieved and the establishment of a reproducible protocol for co-culturing fibroblasts and keratinocytes in a microfluidic system, several improvements have been identified for implementing a more realistic skin-on-a-chip model. The primary goal is to establish a bilayer culture of the skin's key cell types: fibroblasts and keratinocytes. In order to obtain a proper bilayer culture, two methods could be explored. The first one involves culturing these cell types on separate sides of the membrane, with keratinocytes on top and fibroblasts below. This approach has shown promise, particularly regarding the culture of fibroblasts on the underside of the membrane. The second method aims to create a bilayer within the same compartment. This concept is the main objective, and it involves applying a

coating to the membrane surface, such as collagen, fibrin, or poly-D-lysine, to strengthen the bond between fibroblasts and the membrane. This reinforcement is intended to prevent cell detachment after fibroblast seeding on the initial monolayer of fibroblasts.

The second point of improvement involves incorporating elements of the immune system into the skin model, a significant challenge in skin models across different settings. Extensive testing with U937 cells has been conducted, but maintaining their viability inside the chip has proven challenging. Recent tests have identified the issue: ethanol residues on the surfaces of the microfluidic compartments used for autoclaving. This problem could be addressed by increasing the number of washes with alternative liquids like PBS or distilled water. Similar issues were encountered with traditional culture plates, suggesting the need for a thorough study of ethanol washes on plates before applying them to the chips.

Another potential solution is to explore alternative sterilization methods that do not require ethanol within the microfluidic channels. The current chip structure presents challenges in this regard, as the primary alternative would be autoclaving, which the PET membrane used in these chips cannot withstand. Ongoing research aims to identify alternative PET membranes capable of withstanding higher temperatures, making autoclaving feasible. While this approach may require more time and some delay in co-culture testing, it appears to be the preferred solution to address the issue of U937 cell survival. Both fibroblasts and keratinocytes are relatively undemanding in terms of culture media and surface adhesion, making this an appealing path forward.

The third area of improvement revolves around assessing co-cultures inside the chip. All tests conducted in this chapter have relied solely on fluorescence microscopy for analysis. While this method is highly useful for evaluating cell distribution within the chip, it has a temporal limitation. The fluorescence signal cannot be maintained continuously in cells, so its use is limited to studies lasting no more than 5 days without re-administering the reagents. The chip itself allows for the repeated administration of fluorescence markers, so the limitation is not related to the technology or chip construction but rather the need to use fluorescence markers for each cell type.

Using specific fluorescence markers would only allow us to determine the cell types inside the chip. It would not provide information on the state of the cells. For example, if an immune cell were present, visual observation alone would not reveal whether it is activated or producing specific metabolites of interest. The generation of analytes is crucial in disease models, like the melanoma-on-a-chip pursued in this thesis, particularly when testing the effectiveness of a drug. Therefore, it is essential to implement screening methodologies to assess the culture's state within the chip.

7 GENERAL CONCLUSIONS AND FUTURE LINES.

7.1 CONCLUSIONS

The development of a reliable protocol for the fabrication of PDMS-vinyl-glass microfluidic chips has been successfully accomplished as part of this thesis. The fabrication process exhibits sufficient versatility to adapt minor modifications depending on the chip's architecture. Three distinct OOC devices have been meticulously designed, assembled, and effectively tested.

Objective 1: Develop a fabrication methodology for microfluidic chips constructed from PDMS, vinyl, and glass that enables accurate flow compartmentalization. The new fabrication procedure must be versatile and adaptable to enable the combination of biocompatible materials while retaining the capability to recreate micrometer-scale patterns.

This doctoral thesis aimed to choose materials and a fabrication methodology for creating microfluidic chips suitable for cell culture. After evaluating various alternatives, PDMS, vinyl, and glass were chosen due to their respective chemical and mechanical characteristics. The combination of these materials resulted in a compact, biocompatible, and gas-permeable fluidic chip. The addition of vinyl as a construction material for the microfluidic geometries allowed easy and rapid layout modifications. The on-chip assembly process enabled the incorporation of new components into the chip across the three final prototypes created. These components included permeable membranes for compartmentalizing two microfluidic geometries within a single device and the use of PTFE plugs. The integration of the last element was particularly significant as it introduced a key functionality to the OOC devices in this thesis: the ability to inject volumes into the chip. This innovation provided the chips with a new method for instant reagent delivery, proving highly valuable for drug testing, fluorescence marker studies, and even cell seeding through the injection system. These advancements led to the creation of three distinct microfluidic devices: a single-chamber neuron-on-a-chip, a brain slice-on-a-chip featuring two compartments administered exclusively through the lower compartment with an integrated injection system, and finally, a dual-chamber skin-on-a-chip prototype. The latter is the most

intricate, allowing for the perfusion of dual parallel flows while retaining the integrated injection system within its design.

Objective 2: Design and manufacture a single-chamber organ-on-a-chip device suitable for invertebrate neuron culture to achieve higher maintenance over time compared to traditional culture methods. This microfluidic alternative aims to improve the culture conditions of neural networks in an in vitro model, resulting in a more stable and durable neural network.

A neuron-on-a-chip device has been successfully developed to study the formation of neural networks. This model has addressed the challenges of traditional cultures in MEAs, including achieving a higher cell density per unit area and reducing the harmful effects of melanin exposure on the culture. The neuron-on-a-chip presented in Chapter 4 has effectively mitigated these adverse factors, providing an excellent solution to enhance cell density within a specific geometric area. It also simulates a more realistic microenvironment for neurons compared to conventional MEA cultures in plates, thanks to the microfluidic system that enables continuous and renewed administration of the microfluidic chamber housing the invertebrate neurons. Furthermore, the chip constructed for this bioapplication was intentionally designed for seamless microscopic imaging, offering full compatibility with microscope stages.

These improvements have enhanced the imaging of the CNN culture and facilitated the formation of more stable neural networks in fluidic chip cultures compared to culture plates. This comparison was conducted under optimal culture conditions at 30ºC and suboptimal conditions at 37ºC. In both cases, the chip cultures exhibited a superior neural network status, confirming the effectiveness of this culture method over traditional ones.

Objective 3: Modification of the fabrication methodology to create a brain-slice-on-a-chip device capable of replicating an organotypic culture on membrane inserts incorporating a novel volume delivery system within the microfluidic device.

After successfully demonstrating the feasibility of the fabrication methodology with the neuron-on-a-chip, which allowed for the construction of microfluidic chips without any leakage issues and the maintenance of cultures for up to 21 days under optimal conditions, there was a motivation to explore more intricate microfluidic structures. This drive led to designing and fabricating a novel brain slice-on-a-chip intended to replicate the organotypic culture with membrane inserts commonly used in traditional culture methods. Additionally, since brain slices are accessible in culture plates, there was a need to conceive a procedure for delivering reagents within the chip while preserving the closed system characteristic of microfluidic platforms. To meet this requirement, two new materials were introduced into the fabrication process.

The first material was a porous polycarbonate membrane to simulate the membrane insert function. The manufacturing procedure created in this thesis involved the overlapping of vinyl

cuts, allowing the combination of two distinct layouts and the insertion of a membrane that compartmentalized two different regions on the same chip. This design resulted in a lower microfluidic compartment where the culture medium was perfused and an upper compartment, which remained flow-free, housing the brain slices without submerging them.

To address the accessibility issue, the brain slice-on-a-chip integrated a chip injection system, enabling culture analysis while administering the OGB marker through this integrated system. This was made possible by the incorporation of a second novel material, the PTFE plug, which is a self-sealing material that allowed puncturing the chip without creating contamination points.

These two novelties were employed in the final brain slice-on-a-chip prototype for mouse hippocampal slice cultures. The viability study was conducted through the fluorescence labeling of live cells. Chapter 5 results demonstrate the proper functionality of the injection system, producing clear fluorescence images within the chip and allowing the identification of the hippocampal slice cytoarchitecture after ten days of culture, despite some loss in slice thickness. A final proof-of-concept experiment was performed to address this issue by culturing a complete hemisphere within the chip, which proved to be more effective in maintaining the hippocampal cytoarchitecture.

Objective 4: Design a functional skin-on-a-chip prototype to replicate a human skin model based on keratinocyte-fibroblast co-culture and creating a melanoma-on-a-chip model with SK-MEL-28 cells. The skin-on-a-chip device must include an integrated local drug delivery system on the microfluidic chip to enable the testing of anticancer drugs.

The development of a new organ-on-a-chip to mimic a skin model introduced several upgrades to the fabrication methodology. It resulted in a skin-on-a-chip featuring two microfluidic compartments that could independently accommodate continuous flows, a capability that was not possible with the previous skin-on-a-chip device. Moreover, the PC membrane was replaced with a PET membrane to improve sample visibility. The injection system for local reagent administration, a notable innovation from the brain slice-on-a-chip, was also retained. This feature was particularly significant for the skin model, as it facilitated drug testing for potential disease models. With these three key features: the application of dual parallel flow, the new PET membrane, and the injection system for local drug delivery, the goal was to create a basic skin model comprising keratinocytes and fibroblasts. This model would allow the integration of immune system cells or melanoma cells to evaluate the effects of drug administration on the constituent cells.

The increase in chip complexity impacted the percentage of microfluidic chips experiencing leaks. This issue became more evident during the design and fabrication of the skin-on-a-chips. These devices feature two inlets, two outlets, and a permeable membrane that connects both

compartments. Maintaining pressure balance between the chip outlets is essential for ensuring proper chip operation. Failing to control this parameter can lead to incorrect assessments of the chip's fluidic behavior.

To address this challenge, two different studies were conducted to characterize the microfluidic behavior of the chip. The first study investigated how the volume perfused through a chip could fluctuate when subjected to two simultaneous flows. The goal was to determine if there was any indication of volume diffusion from one microfluidic compartment to the other. In this test, under flow conditions of 1 µL/min for a minimum of 1000 minutes and with consistent outlet tubing exit heights, the results demonstrated that the experimental flow closely matched the theoretical flow, confirming the proper functioning of the chips. The second test focused on the concept of pressure drop. Unlike the previous test, pressure drop values in each microfluidic compartment could be quantified, allowing for comparisons. While this test did not provide specific pressure drop values for each geometry within the skin-on-a-chip, it did establish a reference value to identify chip leakage. Therefore, pressure drop can serve as a metric to assess the manufacturing quality of the chips.

During the development of Chapter 6, up to seven different cell types were tested, with six of them successfully cultured on the chip. The U937 cell line was the only one that failed to survive on the skin-on-a-chip. After a series of experiments, it was determined that the cause of this failure was the ethanol-washing process, which prevented the U937 cells from thriving on the chip. This confirmed that the materials used in the chip fabrication were not incompatible with these cells.

For the other cell types, a co-culture of keratinocytes and fibroblasts was successfully achieved in the upper compartment of the chip. This co-culture was conducted in two different environments, the CTB facilities and the laboratories of the University of Hull, both yielding equivalent results. The co-culture reproducibility allowed for the creation of a melanoma-on-a-chip as a proof-of-concept, introducing the SK-MEL-28 cell line into the co-culture of keratinocytes and fibroblasts. The recreation of a melanoma model presented an ideal opportunity to compare two melanoma-on-a-chip models, administering the anticancer drug Gemcitabine in one of them. This proof-of-concept experiment significantly influenced the culture, notably reducing the number of cancer cells on the drug-treated chip compared to the untreated one. As a result, the foundation for a melanoma cancer model on an organ-on-a-chip device has been successfully established.

7.2 FUTURE LINES

Several areas for improvement and future research directions can be identified to enhance and expand the fabrication and utilization of the OOC devices developed in this thesis.

First and foremost, exploring alternative materials for chip construction is a critical avenue to pursue. While the combination of PDMS, vinyl, and glass has proven highly adaptable for designing and fabricating small-scale devices, it is now opportune to experiment with other materials. The current methodology relies heavily on manual labor, resulting in extended manufacturing times and an increased susceptibility to human errors. A significant number of chips become unusable due to manufacturing defects, and production efficiency has room for improvement. As discussed in the literature review, manufacturing processes are inherently tied to the materials employed, necessitating the exploration of new material alternatives and manufacturing techniques.

A straightforward research line already in progress within the GOFB research group involves substituting vinyl with PDMS through molding and soft lithography techniques. This transition enables manufacturing of more conventional microfluidic chips, wherein PDMS defines the microfluidic channels. This alternative holds significant advantages, given its cost-effectiveness and the suitability of layouts previously proven for culturing neurons, mouse brain slices, and human cell lines. This transition is expected to boost production capacity substantially.

Another intriguing avenue to explore is the use of thermopolymers to mitigate PDMS's capacity for absorbing hydrophobic molecules. This issue becomes more pronounced with increased PDMS in the fluidic chip composition. This alternative material selection could address a significant drawback of PDMS-vinyl-glass chips: their limited recyclability and reusability. Throughout this thesis, one significant challenge has been the availability of ready-to-use microfluidic chips, which have consumed a substantial amount of time. One potential solution that could have helped the manufacturing demand is chip reuse. Unfortunately, this has not been feasible due to PDMS's inability to withstand organic solvents, which is essential for chip reuse and remove organic remainings. Additionally, brain-slice-on-a-chip and skin-on-a-chip devices incorporate integrated membranes incompatible with organic solvents. The adoption of new materials would open the door to chip reuse procedures.

The second area for development involves the ongoing fluidic characterization of the chips. The tests conducted in section 6.1.2. represent an early stage, offering merely reference values to assess proper chip manufacturing. Due to this, it is imperative to advance the characterization tests further to obtain unique values for each chip type, allowing for establishing more precise value ranges. These ranges can then be validated using simulation software such as COMSOL, which facilitates computational fluid dynamics analysis. Progress in analyzing pressure drop in OOC devices holds particular relevance, in conjunction with the research into new materials, to observe variations in pressure drop values with identical microfluidic geometries based on the chip's constituent materials. If such variations are confirmed, fluidic characterization could serve as a valid criterion for material selection.

The final potential goal, closely aligned with the research lines of the research group where this doctoral thesis has been done, is the integration of sensors within the microfluidic platform. Throughout this thesis, all cultures performed on OOC devices were monitored and assessed through microscopic image acquisition. While this form of analysis offers a rapid means of assessing the culture's condition, evolution, and cell distribution within the culture area, it has limited capacity to detect variations in gene expression or the production of specific analytes of interest. To address this limitation, molecular screening studies involve collecting expelled liquid from the microfluidic platform's outlet, followed by molecular screening techniques. While this process is feasible, it sacrifices real-time data recording.

The significant advantage of utilizing microfluidic systems lies in their capacity for real-time sample monitoring, achieved by continuously renewing the volume within the microfluidic chambers. Moreover, the ease of adding new modules further enhances this capability. It becomes possible not only to integrate on-chip sensors for parameters like O_2, carbon dioxide, and pH to monitor the culture's status but also to incorporate a module for molecular screening. This integration would result in a comprehensive microfluidic platform housing the bioreactor and the sensing platform, enabling more precise and real-time monitoring of the culture's condition.

8 BIBLIOGRAPHY

8.1 SCIENTIFIC CONTRIBUTIONS OF THE AUTHOR RELATED TO THIS THESIS.

- Casquel, R., Holgado, M., Laguna, M. F., Hernández, A. L., Santamaría, B., Lavín, Á., Luca Tramarin, & Herreros, P. (2020). Engineering vertically interrogated interferometric sensors for optical label-free biosensing. Analytical and Bioanalytical Chemistry, 412(14). https://doi.org/10.1007/s00216-020-02411-3
- Espinosa, R. L., Garrido-Arandia, M., Romero-Sahagun, A., Herreros, P., Tramarin, L., Laguna, M. F., Díaz-Perales, A., & Holgado, M. (2020). A new optical interferometric-based in vitro detection system for the specific IgE detection in serum of the main peach allergen. Biosensors and Bioelectronics, 169. https://doi.org/10.1016/j.bios.2020.112641
- Herreros, P., Ballesteros-Esteban, L. M., Laguna, M. F., Leyva, I., Sendiña-Nadal, I., & Holgado, M. (2021). Neuronal circuits on a chip for biological network monitoring. Biotechnology Journal, 16(7). https://doi.org/10.1002/biot.202000355
- Herreros, P., Tapia-González, S., Sánchez-Olivares, L., Heras, M. F. L., & Holgado, M. (2022). Alternative Brain Slice-on-a-Chip for Organotypic Culture and Effective Fluorescence Injection Testing. International Journal of Molecular Sciences, 23(5). https://doi.org/10.3390/ijms23052549
- Murillo, A. M. M., Tomé-Amat, J., Ramírez, Y., Garrido-Arandia, M., Valle, L. G., Hernández-Ramírez, G., Tramarin, L., Herreros, P., Santamaría, B., Díaz-Perales, A., & Holgado, M. (2021). Developing an Optical Interferometric Detection Method based biosensor for detecting specific SARS-CoV-2 immunoglobulins in Serum and Saliva, and their corresponding ELISA correlation. Sensors and Actuators, B: Chemical, 345. https://doi.org/10.1016/j.snb.2021.130394
- Murillo, A. M. M., Valle, L. G., Ramírez, Y., Sánchez, M. J., Santamaría, B., Molina-Roldan, E., Ortega-Madueño, I., Urcelay, E., Tramarin, L., Herreros, P., Díaz-Perales, A., Garrido-Arandia, M., Tome-Amat, J., Hernández-Ramírez, G., Espinosa, R. L., Laguna, M. F., & Holgado, M. (2022). Integration of Multiple Interferometers in Highly Multiplexed

Diagnostic KITs to Evaluate Several Biomarkers of COVID-19 in Serum. Biosensors, 12(9). https://doi.org/10.3390/bios12090671

- Pioz, M. J., Espinosa, R. L., Laguna, M. F., Santamaria, B., Murillo, A. M. M., Hueros, Á. L., Quintero, S., Tramarin, L., Valle, L. G., Herreros, P., Bellido, A., Casquel, R., & Holgado, M. (2022). A review of Optical Point-of-Care devices to Estimate the Technology Transfer of These Cutting-Edge Technologies. Biosensors, 12(12). https://doi.org/10.3390/bios12121091
- Herreros, P., Hernández, A.L., Laguna, M.F., & Holgado, M. (to be submitted). Replication of a melanoma-on-a-chip model by cell injection for anticancer drug testing. (Tentative title).

8.2 CONSULTED REFERENCES.

Abaci, H. E., Gledhill, K., Guo, Z., Christiano, A. M., & Shuler, M. L. (2015). Pumpless microfluidic platform for drug testing on human skin equivalents. *Lab on a Chip*, *15*(3), 882–888. https://doi.org/10.1039/C4LC00999A

Agarwal, A., Goss, J. A., Cho, A., McCain, M. L., & Parker, K. K. (2013). Microfluidic heart on a chip for higher throughput pharmacological studies. *Lab on a Chip*, *13*(18), 3599–3608. https://doi.org/10.1039/c3lc50350j

Ahadian, S., Civitarese, R., Bannerman, D., Mohammadi, M. H., Lu, R., Wang, E., Davenport-Huyer, L., Lai, B., Zhang, B., Zhao, Y., Mandla, S., Korolj, A., & Radisic, M. (2018). Organ-On-A-Chip Platforms: A Convergence of Advanced Materials, Cells, and Microscale Technologies. *Advanced Healthcare Materials*, *7*(2), 1700506. https://doi.org/10.1002/ADHM.201700506

Ahmad, Z., Salman, S., Khan, S. A., Amin, A., Rahman, Z. U., Al-Ghamdi, Y. O., Akhtar, K., Bakhsh, E. M., & Khan, S. B. (2022). Versatility of Hydrogels: From Synthetic Strategies, Classification, and Properties to Biomedical Applications. *Gels*, *8*(3). https://doi.org/10.3390/GELS8030167

Ahmed, E. M. (2015). Hydrogel: Preparation, characterization, and applications: A review. *Journal of Advanced Research*, *6*(2), 105–121. https://doi.org/10.1016/J.JARE.2013.07.006

Ahmed, T. (2022). Organ-on-a-chip microengineering for bio-mimicking disease models and revolutionizing drug discovery. *Biosensors and Bioelectronics: X*, *11*, 100194. https://doi.org/10.1016/J.BIOSX.2022.100194

Alépée, N., Tornier, C., Robert, C., Amsellem, C., Roux, M. H., Doucet, O., Pachot, J., Méloni, M., & de Brugerolle de Fraissinette, A. (2010). A catch-up validation study on reconstructed human epidermis (SkinEthic RHE) for full replacement of the Draize skin irritation test.

Toxicology in Vitro : An International Journal Published in Association with BIBRA, *24*(1), 257–266. https://doi.org/10.1016/J.TIV.2009.08.024

Anava, S., Saad, Y., & Ayali, A. (2013). The role of gap junction proteins in the development of neural network functional topology. *Insect Molecular Biology*, *22*(5), 457–472. https://doi.org/10.1111/imb.12036

Attia, U. M., Marson, S., & Alcock, J. R. (2009). Micro-injection moulding of polymer microfluidic devices. *Microfluidics and Nanofluidics*, *7*(1), 1–28. https://doi.org/10.1007/S10404-009-0421-X/METRICS

Ayali, A. (2012). Editorial: Models of invertebrate neurons in culture. *Journal of Molecular Histology*, *43*(4), 379–381. https://doi.org/10.1007/S10735-012-9416-0/FIGURES/1

Ayuso, J. M., Sadangi, S., Lares, M., Rehman, S., Humayun, M., Denecke, K. M., Skala, M. C., Beebe, D. J., & Setaluri, V. (2021). Microfluidic model with air-walls reveals fibroblasts and keratinocytes modulate melanoma cell phenotype, migration, and metabolism. *Lab on a Chip*, *21*(6), 1139–1149. https://doi.org/10.1039/D0LC00988A

Azizipour, N., Avazpour, R., Rosenzweig, D. H., Sawan, M., & Ajji, A. (2020). Evolution of Biochip Technology: A Review from Lab-on-a-Chip to Organ-on-a-Chip. *Micromachines*, *11*(6), 1–15. https://doi.org/10.3390/MI11060599

Bailey, J., Thew, M., & Balls, M. (2014). An Analysis of the Use of Animal Models in Predicting Human Toxicology and Drug Safety. *Https://Doi.Org/10.1177/026119291404200306*, *42*(3), 181–199. https://doi.org/10.1177/026119291404200306

Bakmand, T., Troels-Smith, A. R., Dimaki, M., Nissen, J. D., Andersen, K. B., Sasso, L., Waagepetersen, H. S., Gramsbergen, J. B., & Svendsen, W. E. (2015). Fluidic system for long-term in vitro culturing and monitoring of organotypic brain slices. *Biomedical Microdevices*, *17*(4), 71. https://doi.org/10.1007/s10544-015-9973-6

Barré-Sinoussi, F., & Montagutelli, X. (2015). Animal models are essential to biological research: issues and perspectives. *Future Science OA*, *1*(4). https://doi.org/10.4155/FSO.15.63

Becker, H., & Gärtner, C. (2008). Polymer microfabrication technologies for microfluidic systems. *Analytical and Bioanalytical Chemistry*, *390*(1), 89–111. https://doi.org/10.1007/S00216-007-1692-2

Berggren, R., Møller, M., Moss, R., Poda, P., & Smietana, K. (2012). Outlook for the next 5 years in drug innovation. *Nature Reviews Drug Discovery*, *11*(6), 435–436. https://doi.org/10.1038/nrd3744

Beutel, A. K., & Halbrook, C. J. (2023). Barriers and opportunities for gemcitabine in pancreatic cancer therapy. *American Journal of Physiology. Cell Physiology*, *324*(2), C540–C552. https://doi.org/10.1152/AJPCELL.00331.2022

Bhatia, S. N., & Ingber, D. E. (2014). Microfluidic organs-on-chips. *Nature Biotechnology 2014 32:8*, *32*(8), 760–772. https://doi.org/10.1038/nbt.2989

Biglari, S., Le, T. Y. L., Tan, R. P., Wise, S. G., Zambon, A., Codolo, G., De Bernard, M., Warkiani, M., Schindeler, A., Naficy, S., Valtchev, P., Khademhosseini, A., & Dehghani, F. (2019). Simulating Inflammation in a Wound Microenvironment Using a Dermal Wound-on-a-Chip Model. *Advanced Healthcare Materials*, *8*(1). https://doi.org/10.1002/ADHM.201801307

Blake, A. J., Pearce, T. M., Rao, N. S., Johnson, S. M., & Williams, J. C. (2007). Multilayer PDMS microfluidic chamber for controlling brain slice microenvironment. *Lab on a Chip*, *7*(7), 842–849. https://doi.org/10.1039/b704754a

Boodaghi, M., & Shamloo, A. (2020). A comparison of different geometrical elements to model fluid wicking in paper-based microfluidic devices. *AIChE Journal*, *66*(1), e16756. https://doi.org/10.1002/AIC.16756

Brossard, R., Brouchet, T., & Malloggi, F. (2019). Replication of a Printed Volatile Mold: a novel microfabrication method for advanced microfluidic systems. *Scientific Reports 2019 9:1*, *9*(1), 1–10. https://doi.org/10.1038/s41598-019-53729-7

Cameron, N. S., Roberge, H., Veres, T., Jakeway, S. C., & John Crabtree, H. (2006). High fidelity, high yield production of microfluidic devices by hot embossing lithography: rheology and stiction. *Lab on a Chip*, *6*(7), 936–941. https://doi.org/10.1039/B600584E

Campbell, S. B., Wu, Q., Yazbeck, J., Liu, C., Okhovatian, S., & Radisic, M. (2021). Beyond Polydimethylsiloxane: Alternative Materials for Fabrication of Organ-on-a-Chip Devices and Microphysiological Systems. *ACS Biomaterials Science and Engineering*, *7*(7), 2880–2899. https://doi.org/10.1021/ACSBIOMATERIALS.0C00640/ASSET/IMAGES/MEDIUM/AB0C00640_0008.GIF

Cao, U. M. N., Zhang, Y., Chen, J., Sayson, D., Pillai, S., & Tran, S. D. (2023). Microfluidic Organ-on-A-chip: A Guide to Biomaterial Choice and Fabrication. In *International Journal of Molecular Sciences* (Vol. 24, Issue 4). MDPI. https://doi.org/10.3390/ijms24043232

Chan, M.-K., Lee, W.-B., Chan, K.-L., Ng, M.-C., & Li, L. (2019). Modeling and experimental performance analysis of a novel heating system and its application to glass hot embossing

technology. *Optics Letters, Vol. 44, Issue 14, Pp. 3454-3457*, *44*(14), 3454–3457. https://doi.org/10.1364/OL.44.003454

Chansoria, P., Narayanan, L. K., Wood, M., Alvarado, C., Lin, A., & Shirwaiker, R. A. (2020). Effects of Autoclaving, EtOH, and UV Sterilization on the Chemical, Mechanical, Printability, and Biocompatibility Characteristics of Alginate. *ACS Biomaterials Science and Engineering*, *6*(9), 5191–5201. https://doi.org/10.1021/ACSBIOMATERIALS.0C00806/SUPPL_FILE/AB0C00806_SI_001.PDF

Chen, Z., Chen, Z., Yuan, H., Yuan, H., Wu, P., Zhang, W., Juodkazis, S., Huang, H., & Cao, X. (2022). Variable focus convex microlens array on K9 glass substrate based on femtosecond laser processing and hot embossing lithography. *Optics Letters, Vol. 47, Issue 1, Pp. 22-25*, *47*(1), 22–25. https://doi.org/10.1364/OL.448344

Convery, N., & Gadegaard, N. (2019). 30 years of microfluidics. *Micro and Nano Engineering*, *2*, 76–91. https://doi.org/10.1016/J.MNE.2019.01.003

Croft, C. L., Futch, H. S., Moore, B. D., & Golde, T. E. (2019). Organotypic brain slice cultures to model neurodegenerative proteinopathies. In *Molecular Neurodegeneration* (Vol. 14, Issue 1). BioMed Central Ltd. https://doi.org/10.1186/s13024-019-0346-0

Croning, M. D. R., & Haddad, G. G. (1998). Comparison of brain slice chamber designs for investigations of oxygen deprivation in vitro. *Journal of Neuroscience Methods*, *81*(1–2), 103–111. https://doi.org/10.1016/S0165-0270(98)00023-5

Dauth, S., Maoz, B. M., Sheehy, S. P., Hemphill, M. A., Murty, T., Macedonia, M. K., Greer, A. M., Budnik, B., & Parker, K. K. (2017). Neurons derived from different brain regions are inherently different in vitro: a novel multiregional brain-on-a-chip. *Journal of Neurophysiology*, *117*(3), 1320–1341. https://doi.org/10.1152/jn.00575.2016

Daw, R., & Finkelstein, J. (2006). Lab on a chip. *Nature*, *442*(7101), 367. https://doi.org/10.1038/442367A

De Santos-Sierra, D., Sendiña-Nadal, I., Leyva, I., Almendral, J. A., Anava, S., Ayali, A., Papo, D., & Boccaletti, S. (2014). Emergence of small-world anatomical networks in self-organizing clustered neuronal cultures. *PLoS ONE*, *9*(1), 1–8. https://doi.org/10.1371/journal.pone.0085828

Debouck, G., & Metcalf, B. (2000). The impact of genomics on drug discovery. *Annual Review of Pharmacology and Toxicology*, *40*, 193–208. https://doi.org/10.1146/ANNUREV.PHARMTOX.40.1.193

Dent, S., Messersmith, H., & Trudeau, M. (2008). Gemcitabine in the management of metastatic breast cancer: A systematic review. *Breast Cancer Research and Treatment*, *108*(3), 319–331. https://doi.org/10.1007/S10549-007-9610-Z

Dixon, C., Lamanna, J., & Wheeler, A. R. (2017). Printed Microfluidics. *Advanced Functional Materials*, *27*(11), 1604824. https://doi.org/10.1002/ADFM.201604824

Dobrovolskaia, M. A., & McNeil, S. E. (2007). Immunological properties of engineered nanomaterials. *Nature Nanotechnology 2007 2:8*, *2*(8), 469–478. https://doi.org/10.1038/nnano.2007.223

Domansky, K., Sliz, J. D., Wen, N., Hinojosa, C., Thompson, G., Fraser, J. P., Hamkins-Indik, T., Hamilton, G. A., Levner, D., & Ingber, D. E. (2017). SEBS elastomers for fabrication of microfluidic devices with reduced drug absorption by injection molding and extrusion. *Microfluidics and Nanofluidics*, *21*(6), 1–12. https://doi.org/10.1007/S10404-017-1941-4/METRICS

Duval, K., Grover, H., Han, L.-H., Mou, Y., Pegoraro, A. F., Fredberg, J., & Chen, Z. (2017). Modeling Physiological Events in 2D vs. 3D Cell Culture. *Physiology*, *32*(4), 266–277. https://doi.org/10.1152/physiol.00036.2016

Eckmann, J. P., Feinerman, O., Gruendlinger, L., Moses, E., Soriano, J., & Tlusty, T. (2007). The physics of living neural networks. *Physics Reports*, *449*(1–3), 54–76. https://doi.org/10.1016/j.physrep.2007.02.014

Edmondson, R., Broglie, J. J., Adcock, A. F., & Yang, L. (2014). Three-Dimensional Cell Culture Systems and Their Applications in Drug Discovery and Cell-Based Biosensors. *ASSAY and Drug Development Technologies*, *12*(4), 207–218. https://doi.org/10.1089/adt.2014.573

Esch, E. W., Bahinski, A., & Huh, D. (2015). Organs-on-chips at the frontiers of drug discovery. *Nature Reviews Drug Discovery 2015 14:4*, *14*(4), 248–260. https://doi.org/10.1038/nrd4539

Esch, M. B., King, T. L., & Shuler, M. L. (2011). The Role of Body-on-a-Chip Devices in Drug and Toxicity Studies. *Annual Review of Biomedical Engineering*, *13*(1), 55–72. https://doi.org/10.1146/annurev-bioeng-071910-124629

Faustino, V., Catarino, S. O., Lima, R., & Minas, G. (2016). Biomedical microfluidic devices by using low-cost fabrication techniques: A review. *Journal of Biomechanics*, *49*(11), 2280–2292. https://doi.org/10.1016/J.JBIOMECH.2015.11.031

Fennema, E., Rivron, N., Rouwkema, J., van Blitterswijk, C., & De Boer, J. (2013). Spheroid culture as a tool for creating 3D complex tissues. *Trends in Biotechnology*, *31*(2), 108–115. https://doi.org/10.1016/j.tibtech.2012.12.003

Fiorini, G. S., & Chiu, D. T. (2005). Disposable microfluidic devices: Fabrication, function, and application. *BioTechniques*, *38*(3), 429–446. https://doi.org/10.2144/05383RV02/ASSET/IMAGES/LARGE/FIGURE7.JPEG

Gähwiler, B. H. (1981). Organotypic monolayer cultures of nervous tissue. *Journal of Neuroscience Methods*, *4*(4), 329–342. https://doi.org/10.1016/0165-0270(81)90003-0

Gale, B. K., Jafek, A. R., Lambert, C. J., Goenner, B. L., Moghimifam, H., Nze, U. C., & Kamarapu, S. K. (2018). A Review of Current Methods in Microfluidic Device Fabrication and Future Commercialization Prospects. *Inventions 2018, Vol. 3, Page 60*, *3*(3), 60. https://doi.org/10.3390/INVENTIONS3030060

Gao, X., Huang, Y., He, X., Fan, X., Liu, Y., Xu, H., Wu, D., & Wan, C. (2019). Mechanically Enhanced Electrical Conductivity of Polydimethylsiloxane-Based Composites by a Hot Embossing Process. *Polymers 2019, Vol. 11, Page 56*, *11*(1), 56. https://doi.org/10.3390/POLYM11010056

Gerami, A., Alzahid, Y., Mostaghimi, P., Kashaninejad, N., Kazemifar, F., Amirian, T., Mosavat, N., Ebrahimi Warkiani, M., & Armstrong, R. T. (2019). Microfluidics for Porous Systems: Fabrication, Microscopy and Applications. *Transport in Porous Media*, *130*(1), 277–304. https://doi.org/10.1007/S11242-018-1202-3/METRICS

Gourley, P. L., Copeland, R. G., Cox, J. D., Hendricks, J. K., McDonald, A. E., Peterson, S. L., & Sasaki, D. Y. (2002). Biocompatible semiconductor optoelectronics. *Journal of Biomedical Optics*, *7*(4), 546. https://doi.org/10.1117/1.1506931

Guckenberger, D. J., De Groot, T. E., Wan, A. M. D., Beebe, D. J., & Young, E. W. K. (2015). Micromilling: a method for ultra-rapid prototyping of plastic microfluidic devices. *Lab on a Chip*, *15*(11), 2364–2378. https://doi.org/10.1039/C5LC00234F

Gupta, N., Liu, J. R., Patel, B., Solomon, D. E., Vaidya, B., & Gupta, V. (2016). Microfluidics-based 3D cell culture models: Utility in novel drug discovery and delivery research. *Bioengineering & Translational Medicine*, *1*(1), 63–81. https://doi.org/10.1002/btm2.10013

Gura, T. (1997). Systems for identifying new drugs are often faulty. *Science (New York, N.Y.)*, *278*(5340), 1041–1042. https://doi.org/10.1126/SCIENCE.278.5340.1041

Hackam, D. G., & Redelmeier, D. A. (2006). Translation of research evidence from animals to humans. *JAMA*, *296*(14), 1731–1732. https://doi.org/10.1001/JAMA.296.14.1731

Hahn-Schickard, W. E., Koltay, P., Sandmaier, H., & Steger, R. (2003). *Low cost fabrication technology for microfluidic devices based on micro injection moulding ASCMICROPLAT: Fast automated detection of neonatal sepsis markers on a centrifugal microfluidic platform*

View project 3D-HiPMAS View project. https://www.researchgate.net/publication/225028680

Hájos, N., Ellender, T. J., Zemankovics, R., Mann, E. O., Exley, R., Cragg, S. J., Freund, T. F., & Paulsen, O. (2009). Maintaining network activity in submerged hippocampal slices: importance of oxygen supply. *European Journal of Neuroscience*, *29*(2), 319–327. https://doi.org/10.1111/j.1460-9568.2008.06577.x

Hájos, N., & Mody, I. (2009). Establishing a physiological environment for visualized in vitro brain slice recordings by increasing oxygen supply and modifying aCSF content. *Journal of Neuroscience Methods*, *183*(2), 107–113. https://doi.org/10.1016/j.jneumeth.2009.06.005

Halldorsson, S., Lucumi, E., Gómez-Sjöberg, R., & Fleming, R. M. T. (2015). Advantages and challenges of microfluidic cell culture in polydimethylsiloxane devices. In *Biosensors and Bioelectronics* (Vol. 63, pp. 218–231). Elsevier Ltd. https://doi.org/10.1016/j.bios.2014.07.029

Hamdallah, S. I., Zoqlam, R., Erfle, P., Blyth, M., Alkilany, A. M., Dietzel, A., & Qi, S. (2020). Microfluidics for pharmaceutical nanoparticle fabrication: The truth and the myth. *International Journal of Pharmaceutics*, *584*. https://doi.org/10.1016/J.IJPHARM.2020.119408

Hasan, M. F., & Berdichevsky, Y. (2016). Neural Circuits on a Chip. *Micromachines*, *7*(9). https://doi.org/10.3390/MI7090157

Hassan, S., Heinrich, M., Cecen, B., Prakash, J., & Zhang, Y. S. (2020). Biomaterials for on-chip organ systems. *Biomaterials for Organ and Tissue Regeneration: New Technologies and Future Prospects*, 669–707. https://doi.org/10.1016/B978-0-08-102906-0.00019-2

Hay, M., Thomas, D. W., Craighead, J. L., Economides, C., & Rosenthal, J. (2014). Clinical development success rates for investigational drugs. *Nat Biotech*, *32*(1), 40–51. https://doi.org/10.1038/nbt.2786\rhttp://www.nature.com/nbt/journal/v32/n1/abs/nbt.2786.html#supplementary-information

Henderson, V. C., Kimmelman, J., Fergusson, D., Grimshaw, J. M., & Hackam, D. G. (2013). Threats to Validity in the Design and Conduct of Preclinical Efficacy Studies: A Systematic Review of Guidelines for In Vivo Animal Experiments. *PLoS Medicine*, *10*(7). https://doi.org/10.1371/journal.pmed.1001489

Herreros, P., Ballesteros-Esteban, L. M., Laguna, M. F., Leyva, I., Sendiña-Nadal, I., & Holgado, M. (2021). Neuronal circuits on a chip for biological network monitoring. *Biotechnology Journal*, *16*(7). https://doi.org/10.1002/biot.202000355

Herreros, P., Tapia-González, S., Sánchez-Olivares, L., Heras, M. F. L., & Holgado, M. (2022). Alternative Brain Slice-on-a-Chip for Organotypic Culture and Effective Fluorescence Injection Testing. *International Journal of Molecular Sciences*, *23*(5). https://doi.org/10.3390/ijms23052549

Hirama, H., Satoh, T., Sugiura, S., Shin, K., Onuki-Nagasaki, R., Kanamori, T., & Inoue, T. (2019). Glass-based organ-on-a-chip device for restricting small molecular absorption. *Journal of Bioscience and Bioengineering*, *127*(5), 641–646. https://doi.org/10.1016/J.JBIOSC.2018.10.019

Hoarau-Véchot, J., Rafii, A., Touboul, C., & Pasquier, J. (2018). Halfway between 2D and Animal Models: Are 3D Cultures the Ideal Tool to Study Cancer-Microenvironment Interactions? *International Journal of Molecular Sciences 2018, Vol. 19, Page 181*, *19*(1), 181. https://doi.org/10.3390/IJMS19010181

Hopkins, M. M., Martin, P. A., Nightingale, P., Kraft, A., & Mahdi, S. (2007). The myth of the biotech revolution: An assessment of technological, clinical and organisational change. *Research Policy*, *36*(4), 566–589. https://doi.org/10.1016/J.RESPOL.2007.02.013

Huang, Y., Williams, J. C., & Johnson, S. M. (2012). Brain slice on a chip: Opportunities and challenges of applying microfluidic technology to intact tissues. *Lab on a Chip*, *12*(12), 2103–2117. https://doi.org/10.1039/c2lc21142d

Huh, D., Kim, H. J., Fraser, J. P., Shea, D. E., Khan, M., Bahinski, A., Hamilton, G. A., & Ingber, D. E. (2013). Microfabrication of human organs-on-chips. *Nature Protocols 2013 8:11*, *8*(11), 2135–2157. https://doi.org/10.1038/nprot.2013.137

Huh, D., Matthews, B. D., Mammoto, A., Montoya-Zavala, M., Yuan Hsin, H., & Ingber, D. E. (2010). Reconstituting organ-level lung functions on a chip. *Science (New York, N.Y.)*, *328*(5986), 1662–1668. https://doi.org/10.1126/SCIENCE.1188302

Humpel, C. (2015). Neuroscience forefront review organotypic brain slice cultures: A review. *Neuroscience*, *305*, 86–98. https://doi.org/10.1016/j.neuroscience.2015.07.086

Hwang, J., Cho, Y. H., Park, M. S., & Kim, B. H. (2019). Microchannel Fabrication on Glass Materials for Microfluidic Devices. *International Journal of Precision Engineering and Manufacturing*, *20*(3), 479–495. https://doi.org/10.1007/S12541-019-00103-2/METRICS

Iliescu, C., Taylor, H., Avram, M., Miao, J., & Franssila, S. (2012). A practical guide for the fabrication of microfluidic devices using glass and silicon. *Biomicrofluidics*, *6*(1). https://doi.org/10.1063/1.3689939

Janasek, D., Franzke, J., & Manz, A. (2006). Scaling and the design of miniaturized chemical-analysis systems. *Nature 2006 442:7101*, *442*(7101), 374–380. https://doi.org/10.1038/nature05059

Jaras, J., Navaruckiene, A., Skliutas, E., Jersovaite, J., Malinauskas, M., & Ostrauskaite, J. (2022). Thermo-Responsive Shape Memory Vanillin-Based Photopolymers for Microtransfer Molding. *Polymers*, *14*(12). https://doi.org/10.3390/polym14122460

Johnson, I. P. (2015). Age-related neurodegenerative disease research needs aging models. *Frontiers in Aging Neuroscience*, *7*(SEP), 159246. https://doi.org/10.3389/FNAGI.2015.00168/BIBTEX

Jucius, D., Lazauskas, A., Grigaliūnas, V., Guobienė, A., & Puodžiukynas, L. (2020). Hot embossing of micro-pyramids into thermoset thiol-ene film. *Polymers*, *12*(10), 1–15. https://doi.org/10.3390/POLYM12102291

Kelm, J. M., Sanchez-Bustamante, C. D., Ehler, E., Hoerstrup, S. P., Djonov, V., Ittner, L., & Fussenegger, M. (2005). VEGF profiling and angiogenesis in human microtissues. *Journal of Biotechnology*, *118*(2), 213–229. https://doi.org/10.1016/j.jbiotec.2005.03.016

Kim, J., Byun, J.-W., Choi, I., Kim, B., Jeong, H.-K., Jou, I., & Joe, E. (2013). PINK1 Deficiency Enhances Inflammatory Cytokine Release from Acutely Prepared Brain Slices. *Experimental Neurobiology*, *22*(1), 38–44. https://doi.org/10.5607/en.2013.22.1.38

Kim, P., Kwon, K. W., Park, M., Lee, S., Kim, S. M., & Suh, K. (2008). Soft Lithography for Microfluidics: a Review. *Biochip Journal*, *2(1)*.

Kimura, H., Yamamoto, T., Sakai, H., Sakai, Y., & Fujii, T. (2008). An integrated microfluidic system for long-term perfusion culture and on-line monitoring of intestinal tissue models. *Lab on a Chip*, *8*(5), 741–746. https://doi.org/10.1039/b717091b

Kola, I., & Landis, J. (2004). Can the pharmaceutical industry reduce attrition rates? *Nature Reviews Drug Discovery 2004 3:8*, *3*(8), 711–716. https://doi.org/10.1038/nrd1470

Kotz, F., Mader, M., Dellen, N., Risch, P., Kick, A., Helmer, D., & Rapp, B. E. (2020). Fused Deposition Modeling of Microfluidic Chips in Polymethylmethacrylate. *Micromachines 2020, Vol. 11, Page 873*, *11*(9), 873. https://doi.org/10.3390/MI11090873

Krassioukov, A. V., Ackery, A., Schwartz, G., Adamchik, Y., Liu, Y., & Fehlings, M. G. (2002). An in vitro model of neurotrauma in organotypic spinal cord cultures from adult mice. *Brain Research Protocols*, *10*(2), 60–68. https://doi.org/10.1016/S1385-299X(02)00180-0

Landriscina, A., Rosen, J., & Friedman, A. J. (2015). Nanotechnology, Inflammation and the Skin Barrier: Innovative Approaches for Skin Health and Cosmesis. *Cosmetics 2015, Vol. 2, Pages 177-186*, *2*(2), 177–186. https://doi.org/10.3390/COSMETICS2020177

Lanz, H. L., Saleh, A., Kramer, B., Cairns, J., Ng, C. P., Yu, J., Trietsch, S. J., Hankemeier, T., Joore, J., Vulto, P., Weinshilboum, R., & Wang, L. (2017). Therapy response testing of breast cancer in a 3D high-throughput perfused microfluidic platform. *BMC Cancer*, *17*(1), 1–11. https://doi.org/10.1186/s12885-017-3709-3

Lee, Y., Choi, J. W., Yu, J., Park, D., Ha, J., Son, K., Lee, S., Chung, M., Kim, H. Y., & Jeon, N. L. (2018). Microfluidics within a well: an injection-molded plastic array 3D culture platform. *Lab on a Chip*, *18*(16), 2433–2440. https://doi.org/10.1039/C8LC00336J

Leung, C. M., de Haan, P., Ronaldson-Bouchard, K., Kim, G. A., Ko, J., Rho, H. S., Chen, Z., Habibovic, P., Jeon, N. L., Takayama, S., Shuler, M. L., Vunjak-Novakovic, G., Frey, O., Verpoorte, E., & Toh, Y. C. (2022). A guide to the organ-on-a-chip. *Nature Reviews Methods Primers 2022 2:1*, *2*(1), 1–29. https://doi.org/10.1038/s43586-022-00118-6

Li, Q., Peer, A., Cho, I. H., Biswas, R., & Kim, J. (2018). Replica molding-based nanopatterning of tribocharge on elastomer with application to electrohydrodynamic nanolithography. *Nature Communications 2018 9:1*, *9*(1), 1–9. https://doi.org/10.1038/s41467-018-03319-4

Liao, S., He, Y., Chu, Y., Liao, H., & Wang, Y. (2019). Solvent-resistant and fully recyclable perfluoropolyether-based elastomer for microfluidic chip fabrication. *Journal of Materials Chemistry A*, *7*(27), 16249–16256. https://doi.org/10.1039/C9TA03661J

Liu, J., Pan, L., Cheng, X., & Berdichevsky, Y. (2016). Perfused drop microfluidic device for brain slice culture-based drug discovery. *Biomedical Microdevices*, *18*(3). https://doi.org/10.1007/s10544-016-0073-z

Lorusso, D., Ferrandina, G., Fruscella, E., Marini, L., Adamo, V., & Scambia, G. (2005). Gemcitabine in epithelial ovarian cancer treatment: Current role and future perspectives. *International Journal of Gynecological Cancer*, *15*(6), 1002–1013. https://doi.org/10.1111/J.1525-1438.2005.00331.X

Lu, R. X. Z., & Radisic, M. (2021). Organ-on-a-chip platforms for evaluation of environmental nanoparticle toxicity. *Bioactive Materials*, *6*(9), 2801. https://doi.org/10.1016/J.BIOACTMAT.2021.01.021

Ma, C., Peng, Y., Li, H., & Chen, W. (2021). Organ-on-a-Chip: A New Paradigm for Drug Development. In *Trends in Pharmacological Sciences* (Vol. 42, Issue 2, pp. 119–133). Elsevier Ltd. https://doi.org/10.1016/j.tips.2020.11.009

Malecha, K., Jasińska, L., Grytsko, A., Drzozga, K., Slobodzian, P., & Cabaj, J. (2019). Monolithic Microwave-Microfluidic Sensors Made with Low Temperature Co-Fired Ceramic (LTCC) Technology. *Sensors 2019, Vol. 19, Page 577*, *19*(3), 577. https://doi.org/10.3390/S19030577

Mancera-Andrade, E. I., Parsaeimehr, A., Arevalo-Gallegos, A., Ascencio-Favela, G., & Parra-Saldivar, R. (2018). Microfluidics technology for drug delivery: A review. *Frontiers in Bioscience (Elite Edition)*, *10*(1), 74–91. https://doi.org/10.2741/E809

Manz, A., Graber, N., & Widmer, H. M. (1990). Miniaturized total chemical analysis systems: A novel concept for chemical sensing. *Sensors and Actuators B: Chemical*, *1*(1–6), 244–248. https://doi.org/10.1016/0925-4005(90)80209-I

Manz, A., Miyahara, Y., Miura, J., Watanabe, Y., Miyagi, H., & Sato, K. (1990). Design of an open-tubular column liquid chromatograph using silicon chip technology. *Sensors and Actuators B: Chemical*, *1*(1–6), 249–255. https://doi.org/10.1016/0925-4005(90)80210-Q

Martins, J. P., Torrieri, G., & Santos, H. A. (2018). The importance of microfluidics for the preparation of nanoparticles as advanced drug delivery systems. *Https://Doi.Org/10.1080/17425247.2018.1446936*, *15*(5), 469–479. https://doi.org/10.1080/17425247.2018.1446936

Masato, D., Piccolo, L., Lucchetta, G., & Sorgato, M. (2022). Texturing Technologies for Plastics Injection Molding: A Review. *Micromachines 2022, Vol. 13, Page 1211*, *13*(8), 1211. https://doi.org/10.3390/MI13081211

Merrin, J. (2019). Frontiers in Microfluidics, a Teaching Resource Review. *Bioengineering 2019, Vol. 6, Page 109*, *6*(4), 109. https://doi.org/10.3390/BIOENGINEERING6040109

Michielon, E., de Gruijl, T. D., & Gibbs, S. (2022). From simplicity to complexity in current melanoma models. *Experimental Dermatology*, *31*(12), 1818–1836. https://doi.org/10.1111/EXD.14675

Mohammadi, M. H., Heidary Araghi, B., Beydaghi, V., Geraili, A., Moradi, F., Jafari, P., Janmaleki, M., Valente, K. P., Akbari, M., & Sanati-Nezhad, A. (2016). Skin Diseases Modeling using Combined Tissue Engineering and Microfluidic Technologies. *Advanced Healthcare Materials*, *5*(19), 2459–2480. https://doi.org/10.1002/ADHM.201600439

Mukherjee, P., Roy, S., Ghosh, D., & Nandi, S. K. (2022). Role of animal models in biomedical research: a review. *Laboratory Animal Research*, *38*(1). https://doi.org/10.1186/S42826-022-00128-1

Nam, Y., & Wheeler, B. C. (2011). In vitro microelectrode array technology and neural recordings. *Critical Reviews in Biomedical Engineering*, *39*(1), 45–61. https://doi.org/10.1615/CRITREVBIOMEDENG.V39.I1.40

Nascentes Melo, L. M., Kumar, S., Riess, V., Szylo, K. J., Eisenburger, R., Schadendorf, D., Ubellacker, J. M., & Tasdogan, A. (2023). Advancements in melanoma cancer metastasis models. *Pigment Cell & Melanoma Research*, *36*(2), 206–223. https://doi.org/10.1111/PCMR.13078

Nath, P., Fung, D., Kunde, Y. A., Zeytun, A., Branch, B., & Goddard, G. (2010). Rapid prototyping of robust and versatile microfluidic components using adhesive transfer tapes. *Lab on a Chip*, *10*(17), 2286–2291. https://doi.org/10.1039/C002457K

Niculescu, A. G., Chircov, C., Bîrcă, A. C., & Grumezescu, A. M. (2021). Fabrication and applications of microfluidic devices: A review. In *International Journal of Molecular Sciences* (Vol. 22, Issue 4, pp. 1–26). MDPI AG. https://doi.org/10.3390/ijms22042011

Nielsen, J. B., Hanson, R. L., Almughamsi, H. M., Pang, C., Fish, T. R., & Woolley, A. T. (2020). Microfluidics: Innovations in Materials and Their Fabrication and Functionalization. *Analytical Chemistry*, *92*(1), 150–168. https://doi.org/10.1021/ACS.ANALCHEM.9B04986

Nikonenko, I., Toni, N., Moosmayer, M., Shigeri, Y., Muller, D., & Sargent Jones, L. (2003). Integrins are involved in synaptogenesis, cell spreading, and adhesion in the postnatal brain. *Brain Research. Developmental Brain Research*, *140*(2), 185–194. https://doi.org/10.1016/S0165-3806(02)00590-4

Ofner, A., Moore, D. G., Rühs, P. A., Schwendimann, P., Eggersdorfer, M., Amstad, E., Weitz, D. A., & Studart, A. R. (2017). High-Throughput Step Emulsification for the Production of Functional Materials Using a Glass Microfluidic Device. *Macromolecular Chemistry and Physics*, *218*(2), 1600472. https://doi.org/10.1002/MACP.201600472

Olson, H., Betton, G., Robinson, D., Thomas, K., Monro, A., Kolaja, G., Lilly, P., Sanders, J., Sipes, G., Bracken, W., Dorato, M., Van Deun, K., Smith, P., Berger, B., & Heller, A. (2000). Concordance of the toxicity of pharmaceuticals in humans and in animals. *Regulatory Toxicology and Pharmacology*, *32*(1), 56–67. https://doi.org/10.1006/rtph.2000.1399

Pacifici, R., Farré, M., Pichini, S., Ortuño, J., Roset, P. N., Zuccaro, P., Segura, J., & De La Torre, R. (2001). Sweat Testing of MDMA with the Drugwipe® Analytical Device: A Controlled Study with Two Volunteers. *Journal of Analytical Toxicology*, *25*(2), 144–146. https://doi.org/10.1093/JAT/25.2.144

Pan, L. J., Tu, J. W., Ma, H. T., Yang, Y. J., Tian, Z. Q., Pang, D. W., & Zhang, Z. L. (2017). Controllable synthesis of nanocrystals in droplet reactors. *Lab on a Chip*, *18*(1), 41–56. https://doi.org/10.1039/C7LC00800G

Park, J., Lee, B. K., Jeong, G. S., Hyun, J. K., Lee, C. J., & Lee, S. H. (2015). Three-dimensional brain-on-a-chip with an interstitial level of flow and its application as an in vitro model of Alzheimer's disease. *Lab on a Chip*, *15*(1), 141–150. https://doi.org/10.1039/c4lc00962b

Pas, S. P. (2018). The rise of three-dimensional human brain cultures. In *Nature* (Vol. 553, Issue 7689, pp. 437–445). Nature Publishing Group. https://doi.org/10.1038/nature25032

Pasman, T., Grijpma, D., Stamatialis, D., & Poot, A. (2018). Flat and microstructured polymeric membranes in organs-on-chips. *Journal of The Royal Society Interface*, *15*(144). https://doi.org/10.1098/RSIF.2018.0351

Paul, S. M., Mytelka, D. S., Dunwiddie, C. T., Persinger, C. C., Munos, B. H., Lindborg, S. R., & Schacht, A. L. (2010). How to improve RD productivity: The pharmaceutical industry's grand challenge. *Nature Reviews Drug Discovery*, *9*(3), 203–214. https://doi.org/10.1038/nrd3078

Pedrosa, T. do N., Catarino, C. M., Pennacchi, P. C., Assis, S. R. de, Gimenes, F., Consolaro, M. E. L., Barros, S. B. de M., & Maria-Engler, S. S. (2017). A new reconstructed human epidermis for in vitro skin irritation testing. *Toxicology in Vitro : An International Journal Published in Association with BIBRA*, *42*, 31–37. https://doi.org/10.1016/J.TIV.2017.03.010

Perel, P., Roberts, I., Sena, E., Wheble, P., Briscoe, C., Sandercock, P., Macleod, M., Mignini, L. E., Jayaram, P., & Khan, K. S. (2007). Comparison of treatment effects between animal experiments and clinical trials: systematic review. *BMJ*, *334*(7586), 197. https://doi.org/10.1136/BMJ.39048.407928.BE

Peyrin, J. M., Deleglise, B., Saias, L., Vignes, M., Gougis, P., Magnifico, S., Betuing, S., Pietri, M., Caboche, J., Vanhoutte, P., Viovy, J. L., & Brugg, B. (2011). Axon diodes for the reconstruction of oriented neuronal networks in microfluidic chambers. *Lab on a Chip*, *11*(21), 3663–3673. https://doi.org/10.1039/c1lc20014c

Phelps, E. A., & García, A. J. (2010). Engineering more than a cell: Vascularization strategies in tissue engineering. *Current Opinion in Biotechnology*, *21*(5), 704–709. https://doi.org/10.1016/j.copbio.2010.06.005

Polini, A., Prodanov, L., Bhise, N. S., Manoharan, V., Dokmeci, M. R., & Khademhosseini, A. (2014). Organs-on-a-chip: a new tool for drug discovery.

Http://Dx.Doi.Org/10.1517/17460441.2014.886562, 335–352. https://doi.org/10.1517/17460441.2014.886562

Ponmozhi, J., Dhinakaran, S., Varga-medveczky, Z., Fónagy, K., Bors, L. A., Iván, K., & Erdő, F. (2021). Development of Skin-On-A-Chip Platforms for Different Utilizations: Factors to Be Considered. *Micromachines*, *12*(3), 1–25. https://doi.org/10.3390/MI12030294

Qi, Z. B., Xu, L., Xu, Y., Zhong, J., Abedini, A., Cheng, X., & Sinton, D. (2018). Disposable silicon-glass microfluidic devices: precise, robust and cheap. *Lab on a Chip*, *18*(24), 3872–3880. https://doi.org/10.1039/C8LC01109E

Qin, D., Xia, Y., & Whitesides, G. M. (2010). Soft lithography for micro- and nanoscale patterning. *Nature Protocols 2010 5:3*, *5*(3), 491–502. https://doi.org/10.1038/nprot.2009.234

Queval, A., Ghattamaneni, N. R., Perrault, C. M., Gill, R., Mirzaei, M., McKinney, R. A., & Juncker, D. (2010). Chamber and microfluidic probe for microperfusion of organotypic brain slices. *Lab on a Chip*, *10*(3), 326–334. https://doi.org/10.1039/b916669f

Radisic, M., & Loskill, P. (2021). Beyond PDMS and Membranes: New Materials for Organ-on-a-Chip Devices. *ACS Biomaterials Science & Engineering*, *7*(7), 2861–2863. https://doi.org/10.1021/ACSBIOMATERIALS.1C00831

Raineteau, O., Rietschin, L., Gradwohl, G., Guillemot, F., & Gähwiler, B. H. (2004). Neurogenesis in hippocampal slice cultures. *Molecular and Cellular Neuroscience*, *26*(2), 241–250. https://doi.org/10.1016/j.mcn.2004.01.003

Ramadan, Q., & Ting, F. C. W. (2016). In vitro micro-physiological immune-competent model of the human skin. *Lab on a Chip*, *16*(10), 1899–1908. https://doi.org/10.1039/c6lc00229c

Rambani, K., Vukasinovic, J., Glezer, A., & Potter, S. M. (2009). Culturing thick brain slices: an interstitial 3D microperfusion system for enhanced viability. *Journal of Neuroscience Methods*, *180*(2), 243–254. https://doi.org/10.1016/j.jneumeth.2009.03.016

Ren, K., Zhou, J., & Wu, H. (2013). Materials for microfluidic chip fabrication. *Accounts of Chemical Research*, *46*(11), 2396–2406. https://doi.org/10.1021/AR300314S

Reshetnikov, V., Ryabushkina, Y., Kovner, A., Lepeshko, A., & Bondar, N. (2020). Repeated and single maternal separation specifically alter microglial morphology in the prefrontal cortex and neurogenesis in the hippocampus of 15-day-old male mice. *NeuroReport*, 1256–1264. https://doi.org/10.1097/WNR.0000000000001544

Rimann, M., & Graf-Hausner, U. (2012). Synthetic 3D multicellular systems for drug development. *Current Opinion in Biotechnology*, *23*(5), 803–809. https://doi.org/10.1016/J.COPBIO.2012.01.011

Risueño, I., Valencia, L., Jorcano, J. L., & Velasco, D. (2021). Skin-on-a-chip models: General overview and future perspectives. *APL Bioengineering*, *5*(3), 30901. https://doi.org/10.1063/5.0046376

Ronaldson-Bouchard, K., & Vunjak-Novakovic, G. (2018). Organs-on-a-Chip: A Fast Track for Engineered Human Tissues in Drug Development. *Cell Stem Cell*, *22*(3), 310–324. https://doi.org/10.1016/J.STEM.2018.02.011

Rothbauer, M., Rosser, J. M., Zirath, H., & Ertl, P. (2019). Tomorrow today: organ-on-a-chip advances towards clinically relevant pharmaceutical and medical in vitro models. *Current Opinion in Biotechnology*, *55*, 81–86. https://doi.org/10.1016/j.copbio.2018.08.009

Russo, B., Brembilla, N. C., & Chizzolini, C. (2020). Interplay Between Keratinocytes and Fibroblasts: A Systematic Review Providing a New Angle for Understanding Skin Fibrotic Disorders. *Frontiers in Immunology*, *11*. https://doi.org/10.3389/FIMMU.2020.00648

Sanjay, S. T., Zhou, W., Dou, M., Tavakoli, H., Ma, L., Xu, F., & Li, X. J. (2018). Recent advances of controlled drug delivery using microfluidic platforms. *Advanced Drug Delivery Reviews*, *128*, 3–28. https://doi.org/10.1016/J.ADDR.2017.09.013

Scannell, J. W., Blanckley, A., Boldon, H., & Warrington, B. (2012). Diagnosing the decline in pharmaceutical R&D efficiency. *Nature Reviews Drug Discovery*, *11*(3), 191–200. https://doi.org/10.1038/nrd3681

Schetz, M., Dasta, J., Goldstein, S., & Golper, T. (2005). Drug-induced acute kidney injury. *Current Opinion in Critical Care*, *11*(6), 555–565. https://doi.org/10.1097/01.CCX.0000184300.68383.95

Seok, J., Warren, H. S., Cuenca, A. G., Mindrinos, M. N., Baker, H. V., Xu, W., Richards, D. R., McDonald-Smith, G. P., Gao, H., Hennessy, L., Finnerty, C. C., López, C. M., Honari, S., Moore, E. E., Minei, J. P., Cuschieri, J., Bankey, P. E., Johnson, J. L., Sperry, J., … Tompkins, R. G. (2013). Genomic responses in mouse models poorly mimic human inflammatory diseases. *Proceedings of the National Academy of Sciences*, *110*(9), 3507–3512. https://doi.org/10.1073/pnas.1222878110

Shah, P., Vedarethinam, I., Kwasny, D., Andresen, L., Dimaki, M., Skov, S., & Svendsen, W. E. (2011). Microfluidic bioreactors for culture of non-adherent cells. *Sensors and Actuators, B: Chemical*, *156*(2), 1002–1008. https://doi.org/10.1016/j.snb.2011.02.021

Shakeri, A., Jarad, N. A., Leung, A., Soleymani, L., & Didar, T. F. (2019). Biofunctionalization of Glass- and Paper-Based Microfluidic Devices: A Review. *Advanced Materials Interfaces*, *6*(19), 1900940. https://doi.org/10.1002/ADMI.201900940

Shen, J. X., Youhanna, S., Zandi Shafagh, R., Kele, J., & Lauschke, V. M. (2020). Organotypic and Microphysiological Models of Liver, Gut, and Kidney for Studies of Drug Metabolism, Pharmacokinetics, and Toxicity. *Chemical Research in Toxicology*, *33*(1), 38–60. https://doi.org/10.1021/ACS.CHEMRESTOX.9B00245/ASSET/IMAGES/MEDIUM/TX9B00245_0005.GIF

Shim, J. U., Cristobal, G., Link, D. R., Thorsen, T., Jia, Y., Piattelli, K., & Fraden, S. (2007). Control and measurement of the phase behavior of aqueous solutions using microfluidics. *Journal of the American Chemical Society*, *129*(28), 8825–8835. https://doi.org/10.1021/JA071820F/SUPPL_FILE/JA071820FSI20070615_031901.PDF

Shirure, V. S., & George, S. C. (2017). Design considerations to minimize the impact of drug absorption in polymer-based organ-on-a-chip platforms. *Lab on a Chip*, *17*(4), 681–690. https://doi.org/10.1039/C6LC01401A

Shoji, S., Esashi, M., & Matsuo, T. (1988). Prototype miniature blood gas analyser fabricated on a silicon wafer. *Sensors and Actuators*, *14*(2), 101–107. https://doi.org/10.1016/0250-6874(88)80057-X

Shrimal, P., Jadeja, G., & Patel, S. (2020). A review on novel methodologies for drug nanoparticle preparation: Microfluidic approach. *Chemical Engineering Research and Design*, *153*, 728–756. https://doi.org/10.1016/J.CHERD.2019.11.031

Sin, A., Chin, K. C., Jamil, M. F., Kostov, Y., Rao, G., & Shuler, M. L. (2004). The design and fabrication of three-chamber microscale cell culture analog devices with integrated dissolved oxygen sensors. *Biotechnology Progress*, *20*(1), 338–345. https://doi.org/10.1021/BP034077D

Song, M. G., Ryoo, I. G., Choi, H. Y., Choi, B. H., Kim, S. T., Heo, T. H., Lee, J. Y., Park, P. H., & Kwak, M. K. (2015). NRF2 Signaling Negatively Regulates Phorbol-12-Myristate-13-Acetate (PMA)-Induced Differentiation of Human Monocytic U937 Cells into Pro-Inflammatory Macrophages. *PLOS ONE*, *10*(7), e0134235. https://doi.org/10.1371/JOURNAL.PONE.0134235

Soum, V., Park, S., Brilian, A. I., Kwon, O. S., & Shin, K. (2019). Programmable Paper-Based Microfluidic Devices for Biomarker Detections. *Micromachines 2019, Vol. 10, Page 516*, *10*(8), 516. https://doi.org/10.3390/MI10080516

Squires, T. M., & Quake, S. R. (2005). Microfluidics: Fluid physics at the nanoliter scale. *Reviews of Modern Physics*, *77*(3), 977–1026. https://doi.org/10.1103/REVMODPHYS.77.977/FIGURES/47/MEDIUM

Stoppini, L., Buchs, P. A., & Muller, D. (1991). A simple method for organotypic cultures of nervous tissue. *Journal of Neuroscience Methods*, *37*(2), 173–182. https://doi.org/10.1016/0165-0270(91)90128-M

Sun, M., Kaplan, S. V., Gehringer, R. C., Limbocker, R. A., & Johnson, M. A. (2014). Localized drug application and sub-second voltammetric dopamine release measurements in a brain slice perfusion device. *Analytical Chemistry*, *86*(9), 4151–4156. https://doi.org/10.1021/ac5008927

Sutterby, E., Thurgood, P., Baratchi, S., Khoshmanesh, K., & Pirogova, E. (2020). Microfluidic Skin-on-a-Chip Models: Toward Biomimetic Artificial Skin. *Small*, *16*(39), 2002515. https://doi.org/10.1002/SMLL.202002515

Takayama, Y., Kotake, N., Haga, T., Suzuki, T., & Mabuchi, K. (2012). Formation of one-way-structured cultured neuronal networks in microfluidic devices combining with micropatterning techniques. *Journal of Bioscience and Bioengineering*, *114*(1), 92–95. https://doi.org/10.1016/j.jbiosc.2012.02.011

Taylor, A. M., Dieterich, D. C., Ito, H. T., Kim, S. A., & Schuman, E. M. (2010). Microfluidic Local Perfusion Chambers for the Visualization and Manipulation of Synapses. *Neuron*, *66*(1), 57–68. https://doi.org/10.1016/j.neuron.2010.03.022

Tenje, M., Cantoni, F., Porras Hernández, A. M., Searle, S. S., Johansson, S., Barbe, L., Antfolk, M., & Pohlit, H. (2020). A practical guide to microfabrication and patterning of hydrogels for biomimetic cell culture scaffolds. *Organs-on-a-Chip*, *2*, 100003. https://doi.org/10.1016/J.OOC.2020.100003

Terry, S. C., Herman, J. H., & Angell, J. B. (1979). A Gas Chromatographic Air Analyzer Fabricated on a Silicon Wafer. *IEEE Transactions on Electron Devices*, *26*(12), 1880–1886. https://doi.org/10.1109/T-ED.1979.19791

Uesugi, K., Nishiyama, K., Hirai, K., Inoue, H., Sakurai, Y., Yamada, Y., Taniguchi, T., & Morishima, K. (2020). Survival Rate of Cells Sent by a Low Mechanical Load Tube Pump: The "Ring Pump." *Micromachines 2020, Vol. 11, Page 447*, *11*(4), 447. https://doi.org/10.3390/MI11040447

Van Dam, D., & De Deyn, P. P. (2011). Animal models in the drug discovery pipeline for Alzheimer's disease. *British Journal of Pharmacology*, *164*(4), 1285–1300. https://doi.org/10.1111/J.1476-5381.2011.01299.X

Van Der Meer, A. D., & Van Den Berg, A. (2012). Organs-on-chips: Breaking the in vitro impasse. *Integrative Biology*, *4*(5), 461–470. https://doi.org/10.1039/c2ib00176d

Van Norman, G. A. (2020). Limitations of Animal Studies for Predicting Toxicity in Clinical Trials: Part 2: Potential Alternatives to the Use of Animals in Preclinical Trials. *JACC: Basic to Translational Science*, *5*(4), 387. https://doi.org/10.1016/J.JACBTS.2020.03.010

Vanzetta, I., Hildesheim, R., & Grinvald, A. (2005). Compartment-Resolved Imaging of Activity-Dependent Dynamics of Cortical Blood Volume and Oximetry. *Journal of Neuroscience*, *25*(9), 2233–2244. https://doi.org/10.1523/JNEUROSCI.3032-04.2005

Vedarethinam, I., Avaliani, N., Tønnesen, J., Hansen, J., Sabourin, D., Dimaki, M., Kokaia, M., Dufva, M., Svendsen, W. E., Emnéus, J., & Heiskanen, A. (2011). Long-term brain slice culturing in a microfluidic platform. *Proceedings of International Conference on Miniaturized Systems for Chemistry and Life Sciences*, 1560–1563.

Verpoorte, E., & De Rooij, N. F. (2003). Microfluidics meets MEMS. *Proceedings of the IEEE*, *91*(6), 930–953. https://doi.org/10.1109/JPROC.2003.813570

Victorov, I. V., Lyjin, A. A., & Aleksandrova, O. P. (2001). A modified roller method for organotypic brain cultures: free-floating slices of postnatal rat hippocampus. *Brain Research Protocols*, *7*(1), 30–37. https://doi.org/10.1016/S1385-299X(00)00059-3

Viravaidya, K., Sin, A., & Shuler, M. L. (2004). Development of a microscale cell culture analog to probe naphthalene toxicity. *Biotechnology Progress*, *20*(1), 316–323. https://doi.org/10.1021/BP0341996

Waldbaur, A., Rapp, H., Länge, K., & Rapp, B. E. (2011). Let there be chip—towards rapid prototyping of microfluidic devices: one-step manufacturing processes. *Analytical Methods*, *3*(12), 2681–2716. https://doi.org/10.1039/C1AY05253E

Walsh, D. I., Kong, D. S., Murthy, S. K., & Carr, P. A. (2017). Enabling Microfluidics: from Clean Rooms to Makerspaces. *Trends in Biotechnology*, *35*(5), 383–392. https://doi.org/10.1016/j.tibtech.2017.01.001

Weinberg, E., Kaazempur-Mofrad, M., & Borenstein, J. (2008). Concept and computational design for a bioartificial nephron-on-a-chip. *The International Journal of Artificial Organs*, *31*(6), 508–514. https://doi.org/10.1177/039139880803100606

Whitesides, G. M. (2006). The origins and the future of microfluidics. *Nature*, *442*(7101), 368–373. https://doi.org/10.1038/NATURE05058

Wlodarczyk, K. L., Carter, R. M., Jahanbakhsh, A., Lopes, A. A., Mackenzie, M. D., Maier, R. R. J., Hand, D. P., & Maroto-Valer, M. M. (2018). Rapid Laser Manufacturing of

Microfluidic Devices from Glass Substrates. *Micromachines 2018, Vol. 9, Page 409*, *9*(8), 409. https://doi.org/10.3390/MI9080409

Wu, Q., Liu, J., Wang, X., Feng, L., Wu, J., Zhu, X., Wen, W., & Gong, X. (2020). Organ-on-a-chip: Recent breakthroughs and future prospects. In *BioMedical Engineering Online* (Vol. 19, Issue 1). BioMed Central Ltd. https://doi.org/10.1186/s12938-020-0752-0

Wufuer, M., Lee, G. H., Hur, W., Jeon, B., Kim, B. J., Choi, T. H., & Lee, S. H. (2016). Skin-on-a-chip model simulating inflammation, edema and drug-based treatment. *Scientific Reports*, *6*(October), 1–12. https://doi.org/10.1038/srep37471

Wyss-Coray, T. (2016). Ageing, neurodegeneration and brain rejuvenation. *Nature 2016 539:7628*, *539*(7628), 180–186. https://doi.org/10.1038/nature20411

Yang, L., Dai, F., Tang, L., Le, Y., & Yao, W. (2017). Macrophage differentiation induced by PMA is mediated by activation of RhoA/ROCK signaling. *The Journal of Toxicological Sciences*, *42*(6), 763–771. https://doi.org/10.2131/JTS.42.763

Yeatts, A. B., Choquette, D. T., & Fisher, J. P. (2013). Bioreactors to influence stem cell fate: Augmentation of mesenchymal stem cell signaling pathways via dynamic culture systems. *Biochimica et Biophysica Acta - General Subjects*, *1830*(2), 2470–2480. https://doi.org/10.1016/j.bbagen.2012.06.007

Yi, L., Wang, X., Dhumpa, R., Schrell, A. M., Mukhitov, N., & Roper, M. G. (2015). Integrated perfusion and separation systems for entrainment of insulin secretion from islets of Langerhans. *Lab on a Chip*, *15*(3), 823–832. https://doi.org/10.1039/C4LC01360C

Zengerle, R., Ulrich, J., Kluge, S., Richter, M., & Richter, A. (1995). A bidirectional silicon micropump. *Sensors and Actuators A: Physical*, *50*(1–2), 81–86. https://doi.org/10.1016/0924-4247(96)80088-4

Zhang, X., Li, L., & Luo, C. (2016). Gel integration for microfluidic applications. *Lab on a Chip*, *16*(10), 1757–1776. https://doi.org/10.1039/C6LC00247A

Zhang, Y., Liu, J., Wang, H., & Fan, Y. (2019). Laser-induced selective wax reflow for paper-based microfluidics. *RSC Advances*, *9*(20), 11460–11464. https://doi.org/10.1039/C9RA00610A

Zhou, J., Ellis, A. V., & Voelcker, N. H. (2010). Recent developments in PDMS surface modification for microfluidic devices. *Electrophoresis*, *31*(1), 2–16. https://doi.org/10.1002/ELPS.200900475

Zhou, J., Ren, K., Zhao, Y., Dai, W., & Wu, H. (2012). Convenient formation of nanoparticle aggregates on microfluidic chips for highly sensitive SERS detection of biomolecules.

Analytical and Bioanalytical Chemistry, *402*(4), 1601–1609. https://doi.org/10.1007/S00216-011-5585-Z